ABSTRACT

Title of Dissertation: CROSS-LAYER DESIGN FOR MULTI-ANTENNA

ULTRA-WIDEBAND SYSTEMS

Wipawee Siriwongpairat, Doctor of Philosophy, 2005

Dissertation directed by: Professor K. J. Ray Liu
                          Department of Electrical and Computer Engineering

Ultra-wideband (UWB) is an emerging technology that offers great promises to satisfy the growing demand for low cost and high-speed digital wireless home networks. The enormous bandwidth available, the potential for high data rates, as well as the potential for small size and low processing power along with low implementation cost, all present a unique opportunity for UWB to become a widely adopted radio solution for future wireless home-networking technology. Nevertheless, in order for UWB devices to coexist with other existing wireless technology, the transmitted power level of UWB is strictly limited by the FCC spectral mask. Such limitation poses significant design challenges to any UWB system.

This thesis introduces various means to cope with these design challenges. Advanced technologies including multiple-input multiple-output (MIMO) coding, cooperative communications, and cross-layer design are employed to enhance the

performance and coverage range of UWB systems. First a MIMO-coding framework for multi-antenna UWB communication systems is developed. By a technique of band hopping in combination with jointly coding across spatial, temporal, and frequency domains, the proposed scheme is able to exploit all the available spatial and frequency diversity, richly inherent in UWB channels. Then, the UWB performance in realistic UWB channel environments is characterized. The proposed performance analysis successfully captures the unique multipath-rich property and random-clustering phenomenon of UWB channels. Next, a cross-layer channel allocation scheme for UWB multiband OFDM systems is proposed. The proposed scheme optimally allocates subbands, transmitted power, and data rates among users by taking into consideration the performance requirement, the power limitation, as well as the band hopping for users with different data rates. Also, an employment of cooperative communications in UWB systems is proposed to enhance the UWB performance and coverage by exploiting the broadcasting nature of wireless channels and the cooperation among UWB devices. Furthermore, an OFDM cooperative protocol is developed and then applied to enhance the performance of UWB systems. The proposed cooperative protocol not only achieves full diversity but also efficiently utilizes the available bandwidth.

Cross-Layer Design for Multi-Antenna Ultra-Wideband Systems

by

Wipawee Siriwongpairat

Dissertation submitted to the Faculty of the Graduate School of the
University of Maryland, College Park in partial fulfillment
of the requirements for the degree of
Doctor of Philosophy
2005

Advisory Committee:

     Professor K. J. Ray Liu, Chairman
     Professor Carlos A. Berenstein
     Professor Rama Chellappa
     Professor Anthony Ephremides
     Professor Steve Tretter

DEDICATION

To my parents, Sawai and Pimjai, and my sister, Wasinee, for their everlasting
and enduring support and encouragement.

To my love, Thanongsak (Kee) Himsoon, without whom I would not have come
this far and this thesis would never have been accomplished.

ACKNOWLEDGEMENTS

I owe my gratitude to all the people who have made this thesis possible and because of whom my graduate experience has been one that I will cherish forever.

First and foremost I would like to thank my advisor, Professor K. J. Ray Liu, who has given me an invaluable opportunity to do research and work on challenging and extremely interesting subjects over the past three years. He has always made himself available for help and advice; there has never been an occasion when I have knocked on his door and he has not given me time. His tireless support, advice, and discussions have greatly helped me to successfully complete this research thesis.

Thanks are due to Professor Steve Tretter, Professor Anthony Ephremides, Professor Rama Chellappa, and Professor Carlos A. Berenstein for agreeing to serve on my thesis committee and for sparing their invaluable time reviewing the manuscript.

I would like to thank Dr. Weifeng Su for his guidance. Without his extraordinary theoretical ideas and mathematical expertise, this thesis would have been a distant dream. I thank Dr. Zhu Han for his collaboration and his helpful advice, especially on cross-layer design which has been one major part of this thesis. I thank Dr. Masoud Olfat for his help and support during my early stage of research. I also thank Ahmed Sadek for many stimulating discussions and for his collaboration.

All my colleagues and friends have enriched my graduate life in many ways. I would like to thank my colleagues at the Communications and Signal Processing

TABLE OF CONTENTS

LIST OF TABLES

LIST OF FIGURES

Chapter 1

Introduction

Wireless connectivity is now making inroads into the digital home and office systems. In the near future, people will be sharing photos, video, data and voice among networked consumer electronics throughout their digital homes. Yet today's wireless personal area network (WPAN) technologies cannot meet the needs of wireless connectivity among these devices that require high bandwidth for connection and media exchange. This introduces an urgent need of a new wireless technology that is able to support multiple high data rate streams, consume very low power, and maintain low implementation cost. Ultra-wideband (UWB) is one of the emerging technologies that can fulfill these requirements. The enormous bandwidths available, the potential for the data rate, and the potential for very low cost operation makes UWB technology a viable candidate for current and future wireless applications. Nevertheless, to fulfill these expectations, UWB research and development has to cope with several design challenges that limit the performance and coverage range of UWB systems.

In this chapter, we first present an introduction of UWB and explain without resorting to too many equations the reasons why UWB is considered as an emerging

and breakthrough technology for short-range wireless communications. A brief historical background of UWB is presented. The advantages, the applications as well as the challenges of UWB technology are discussed. Then, we provide motivations of this dissertation to overcome the design challenges of UWB and point out the overall contributions. Finally, the organization of the dissertation is given and the contributions of each chapter are presented.

1.1   Introduction to UWB

In this section, we start with an overview of UWB radios, including historical development of UWB and regulatory processes. Next, we present the key benefits of UWB. Then, we discuss the application potential of UWB technology for wireless communications, and finally point out the challenges in designing UWB wireless communication systems.

1.1.1   Overview of UWB

Historically, the concept of UWB was developed in the early 1960s through research in time-domain electromagnetics where impulse measurement techniques were used to characterize the transient behavior of a certain class of microwave networks [1]. In the late 1960s, the impulse measurement techniques were applied to the design of wideband antenna elements, leading to the development of short pulse radar and communications systems. In 1973, the first UWB communications patent was awarded for the short-pulse receiver [2]. Through the late 1980s, UWB was referred to as *baseband*, *carrier-free*, or *impulse* technology. The term *ultra-wideband* was first coined in approximately 1989 by the US Department of

Defense. By 1989, UWB theory, techniques and many implementation approaches had been developed for a wide range of applications such as radar, communications, automobile collision avoidance, positioning systems, liquid level sensing and altimetry. However, much of the early work in the UWB field occurred in the military or funded by the US Government under classified programs. In late 1990s, UWB technology became more commercialized and the development of UWB technology has greatly accelerated. For further interesting and informative review of UWB history, the interested reader is referred to [3].

A substantial change in UWB history occurred in February 2002 when the federal communications commission (FCC) issued UWB rulings that provided the first radiation limitations for UWB transmission, and also permitted the operation of UWB devices on an unlicensed basis [4]. According to the FCC rulings, UWB is defined as any transmission scheme that occupies a fractional bandwidth of greater than 0.2, or a signal bandwidth of more than 500 MHz. The fractional bandwidth is defined as B/f_c, where $B \triangleq f_H - f_L$ represents the -10 dB bandwidth and $f_c \triangleq (f_H + f_L)/2$ denotes the center frequency. Here, f_H and f_L are the upper frequency and the lower frequency, respectively, measured at -10 dB below the peak emission point. Based on [4], UWB systems with $f_c > 2.5$ GHz need to have a -10 dB bandwidth of at least 500 MHz, whereas UWB systems with $f_c < 2.5$ GHz need to have fractional bandwidth of at least 0.2. The FCC has mandated that UWB radio transmission can legally operate in the range from 3.1 GHz to 10.6 GHz, with the power spectral density (PSD) satisfied a specific spectral mask assigned by the FCC. In particular, Fig. 1.1 illustrates the UWB spectral mask for indoor communications under Part 15 of the FCC's rules [4]. According to the spectral mask, the PSD of UWB signal measured in 1 MHz bandwidth must
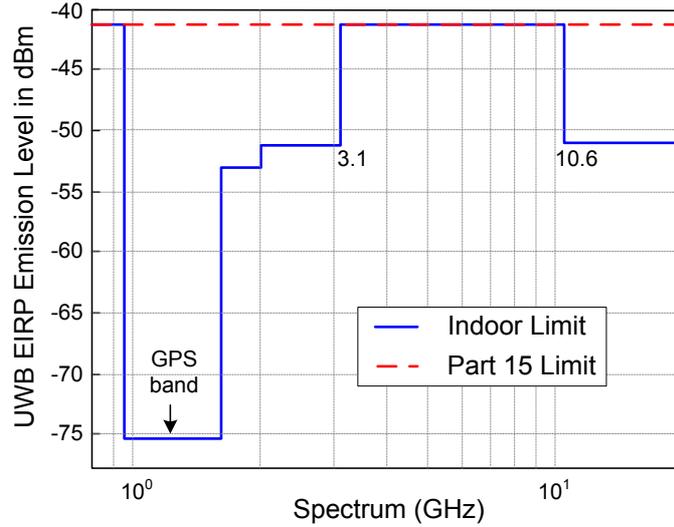
Figure 1.1: UWB spectral mask for indoor communication systems.

not exceed -41.3 dBm, which complies with the Part 15 general emission limits to successfully control radio interference. For particularly sensitive bands, such as the global positioning system (GPS) band (0.96 - 1.61 GHz), the PSD limit is much lower. As depicted in Fig. 1.2, such ruling allows the UWB devices to overlay existing narrowband systems, while ensuring sufficient attenuation to limit adjacent channel interference. Although only the US permits operation of UWB devices currently, regulatory efforts are under way in many countries, especially in Europe and Japan [5]. Market drivers for UWB technology are many even at this early stage, and are expected to include new applications in the next few years.

1.1.2 Advantages of UWB

Due to the ultra wideband nature, UWB radios come with unique benefits that have been attractive for the radar and communications applications. The key advantages of UWB can be summarized as [6]
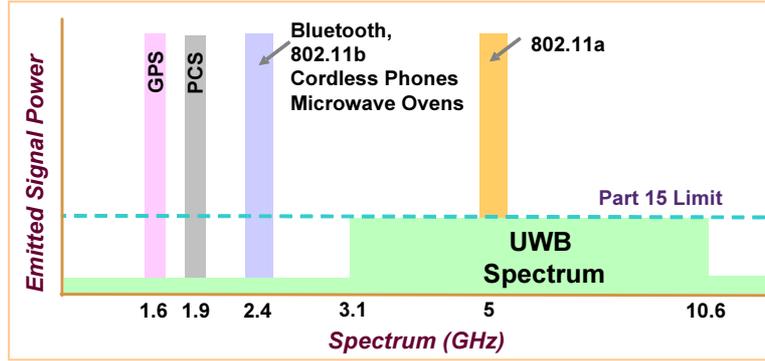
Figure 1.2: Spectrum of UWB and existing narrowband systems.

- Potential for high data rates

- Extensive multipath diversity

- Potential small size and processing power along with low equipment cost

- High precision ranging and localization at the centimeter level

The extremely large bandwidth occupied by UWB gives the potential of very high theoretical capacity, yielding very high data rates. This can be seen by considering Shannon's capacity equation [7],

$$C = B \log \left(1 + \frac{S}{N} \right), \tag{1.1}$$

where C is the maximum channel capacity, B is the signal bandwidth, S is the signal power, and N is the noise power. The Shannon's equation shows that the capacity can be improve by increasing the signal bandwidth or by increasing the signal power. Moreover, it shows that increasing channel capacity requires linear increases in bandwidth while similar channel capacity increases would require exponential increases in power. Thus, from Shannon's equation we can see that UWB system has a great potential for high speed wireless communications.

Conveying information with ultra-short duration waveforms, UWB signals have low susceptibility to multipath interference. Multipath interference occurs when a modulated signal arrives at a receiver from different paths. The combining of signals at the receiver can result in the distortion of the received signal. The ultra-short duration of UWB waveforms gives rise to a fine resolution of reflected pulses at the receiver. As a result, UWB transmissions can resolve many paths, and are thus rich in multipath diversity.

The low complexity and low cost of UWB systems arises from the carrier-free nature of the signal transmission. Specifically, due to its ultra wide bandwidth, the UWB signal may span frequency commonly used as carrier frequency. This eliminates the needs for an additional radio frequency (RF) mixing stage as required in conventional radio technology. Such omission of up/down-conversion processes and RF components allows the entire UWB transceiver to be integrated with a single CMOS implementation. Single chip CMOS integration of UWB transceiver contributes directly to low cost, small size, and low power.

The ultra-short duration of UWB waveforms gives rise to the potential ability to provide high precision ranging and localization. Together with good material penetration properties, UWB signals offer opportunities for short range radar applications such as rescue and anti-crime operations, as well as in surveying and in the mining industry.

1.1.3 UWB Applications

UWB technology can enable a wide variety of applications in wireless communications, networking, radar imaging, and localization systems. For wireless communications, the use of UWB technology under the FCC guidelines [4] offers

significant potential for the deployment of two basic communications systems:

- High data rate short range communications - high data rate wireless personal area networks

- Low data rate and location tracking - sensor, positioning, and identification networks

The high data rate WPANs can be defined as networks with a medium density of active devices per room (5-10) transmitting at the data rates ranging from 100 Mbps to 500 Mbps within a distance of 20 m. The ultra wide bandwidth of UWB enables various WPAN applications such as high-speed wireless universal serial bus (WUSB) connectivity for personal computers (PCs) and PC peripherals, high-quality real-time video and audio transmission, file exchange among storage systems, and cable replacement for home entertainment systems.

Recently, the IEEE 802.15.3 standard task group has established the 802.15.3a study group [8] to define a new physical layer concept for high data rate WPAN applications. Major efforts of this study group is to standardize UWB wireless radios for indoor WPAN transmissions. The goal for the IEEE 802.15.3a standard is to provide a higher speed physical layer for the existing approved 802.15.3 standard for applications which involve imaging and multimedia. The work of the 802.15.3a study group also includes standardizing the channel model to be used for UWB system evaluation.

Alternatively, UWB transmission can trade a reduced in data rate for increased in transmission range. Under the low rate operation mode, UWB technology could be beneficial and potentially used in sensor, positioning, and identification networks. A sensor network comprises a large number of nodes spread over a geographical area to be monitored. Depending on specific application, the sensor

nodes can be static or mobile. Key requirements for sensor networks operating in challenging environments include low-cost, low-power and multi-functionality. With its unique properties of low complexity, low cost, low power, UWB technology is well suited to sensor network applications [9]. Moreover, due to the fine time resolution of UWB signal, UWB based sensing has the potential to improve the resolution of conventional proximity and motion sensors. The low rate transmission combined with accurate location tracking capabilities offers an operational mode also known as as low data rate and location tracking.

Recently, the IEEE established the 802.15.4 study group to define a new physical layer concept for low data rate applications utilizing UWB technology at the air interface. The study group addresses new applications which require only moderate data throughput, but require long battery life such as low-rate wireless personal area networks, sensors and small networks.

1.1.4 UWB Transmission Schemes

Although the FCC has regulated spectrum and transmitted power levels for UWB, there is currently no standard for UWB transmission scheme. Various pulse generation techniques have been proposed to use the 7.5 GHz license-free UWB spectrum. Generally, UWB transmission approaches can be categorized into two main approaches, namely single-band and multiband approaches. Fig. 1.3 illustrates the UWB signals in time-domain and frequency domains when single-band and multiband approaches are employed.

A traditional UWB technology is based on single-band systems employing carrier-free or impulse radio communications [10]- [15]. Impulse radio refers to the generation of a series of impulse-like waveforms, each with duration in the
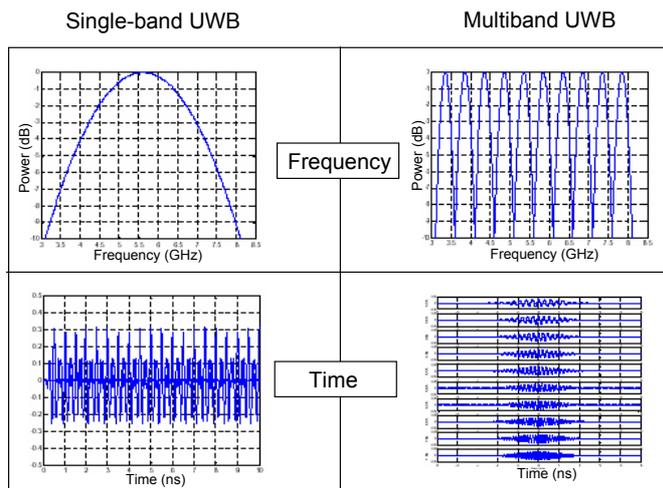
Figure 1.3: UWB transmission approaches: single band and multiband approaches.

order of hundreds of pico-seconds. Each pulse occupies a several gigahertz bandwidth that must adhere to the spectral mask requirements. The information is directly modulated into the sequence of pulses. Typically, one pulse carries the information for one bit. Data could be modulated using either pulse amplitude modulation (PAM) or pulse position modulation (PPM). Multiple users can be supported via the use of time hopping or direct sequence spreading approaches. This type of transmission does not require the use of additional carrier modulation as the pulse will propagate well in the radio channel. The technique is therefore a baseband signal approach. However, the single band system faces a challenging problem in building RF and analog circuits, and in designing a low complexity receiver that can capture sufficient multipath energy.

Recently, multiband approaches were proposed in [16]- [19]. Instead of using the entire UWB frequency band to transmit information, multiband technique divides the UWB frequency band from 3.1 GHz to 10.6 GHz into several smaller bands, referred to as subbands. Each subband occupies bandwidth of at least 500

9

MHz in compliance with the FCC regulations [4]. By interleaving the transmitted symbols across subbands, multiband approaches can still maintain the transmitted power as if the large GHz bandwidth is utilized. The advantage is that multiband approaches allow the information to be processed over a much smaller bandwidth, thereby reducing overall design complexity as well as improving spectral flexibility and worldwide compliance. The current leading proposal for the IEEE 802.15.3a WPAN standard [8] is based on *multiband orthogonal frequency division multiplexing* (multiband OFDM), which utilizes a combination of OFDM and time-frequency interleaving [18]. The OFDM technique is efficient at collecting multipath energy in highly dispersive channels, as is the case for most UWB channels [19]. Moreover, OFDM allows for each subband to be divided into a set of orthogonal narrowband channels (with much larger symbol period duration). The major difference between multiband OFDM and traditional OFDM schemes is that the multiband OFDM symbols are not continually sent on one frequency-band; instead, they are interleaved over different subbands across both time and frequency. Multiple access of multiband approach is enabled by the use of suitably designed frequency-hopping sequences over the set of subbands. A frequency synthesizer can be utilized to perform frequency hopping. By using proper time-frequency codes, multiband system provides both frequency diversity and multiple access capability [19].

There are many trade-offs in the UWB approaches described above. The single-band approach benefits from a coding-gain achieved through the use of time-hopping (TH) or direct sequence (DS) spreading, exploits the Shannon's principals to a greater degree than the multiband approach, has greater precision for position location, and realizes better spectrum efficiency. However, it has less flexibility

with regard to foreign spectral regulation and may be too broadband if foreign governments choose to limit their UWB spectral allocations to smaller ranges than authorized by the FCC. On the other hand, the multiband approach has the main advantage on the ability for more fine-grained control of the transmit PSD so as to maximize the average transmitted power while meeting the spectral mask. It allows for peaceful coexistence with flexible spectral coverage and is easier to adopt to different worldwide regulatory environments. Moreover, processing over smaller bandwidth eases the requirement on analog-to-digital converter sampling rates and, consequently, facilitates greater digital processing. Furthermore, in the UWB multiband OFDM approach, due to the increased length of the OFDM symbol period, the modulation method can successfully reduce the effects of intersymbol-interference (ISI). Nevertheless, this robust multipath tolerance comes at the price of increased transceiver complexity, the need to combat inner carrier interference (ICI), and tighter linear constraint on amplifying circuit elements.

1.1.5   Challenges for UWB

While UWB technology has several attractive properties that make it a promising technology for future short-range wireless communications and many other applications, there also remain some challenges that must be overcome to fulfill these expectations.

The transmitted power level of UWB signals is strictly limited in order for UWB devices to peacefully coexist with other wireless systems. Such strict power limitation poses significant challenges for designing UWB systems. One major challenge is to achieve the desired performance at adequate transmission range using limited transmitted power. Another challenge is to design UWB waveform that efficiently

utilize the bandwidth and power allowed by the FCC spectral mask. Moreover, to ensure that the transmitted power level satisfies the spectral mask, adequate characterization and optimization of transmission techniques (e.g., adaptive power control, duty cycle optimization) may be required.

The ultra-short duration of UWB pulses leads to a large number of resolvable multipath components at the receiver. Particularly, the received UWB signal contains many delayed and scaled replicas of the transmitted pulses. Additionally, each of the resolvable pulses undergoes a different channel fading. These make multipath energy capture a challenging problem in UWB system design. For example, if a RAKE receiver [7] is used to collect the multipath energy, a large number of fingers is needed to achieve desired performance.

Design challenges also exist in the areas of modulation and coding techniques that are suitable for UWB systems. Originally, UWB radio has been used for military applications where multiuser transmission and achieving high multiuser capacity are not major concerns. However, these issues become very important in commercial applications such as high-speed wireless home networks. Effective coding and modulation schemes are thus necessary to improve UWB multiuser capacity as well as system performance.

One design challenge is the impact of narrowband interference on UWB receivers. Specifically, the UWB frequency band overlaps with that for the IEEE 802.11a wireless local area networks (WLANs). The signals from 802.11a devices represent in-band interference for the UWB receiver front-end.

Other design challenges include scalable system architectures and spectrum flexibility. UWB potential applications include both high rate applications (e.g. images and video), and lower rate applications (e.g. computer peripheral support).

Thus it is necessary that the UWB transceiver can support a wide range of data rates. Furthermore, the unlicensed nature of the UWB spectrum makes it essential for UWB devices to coexist with other devices that share the same spectrum. However, it is challenging to design UWB systems with spectrum flexibility that allow UWB devices to coexist effectively with other wireless technologies and to meet potentially different regulatory requirements in different regions of the world.

1.2 Motivations

As discussed in the previous section, strict limitation on transmitted power level poses significant design challenges for any UWB systems. Moreover, the design and implementation of UWB receiver that is able to capture sufficient multipath energy are complicated. The major contribution of this dissertation is to cope with these design challenges for UWB systems by exploiting advanced technologies such as multiple-input multiple output (MIMO), cooperative communications, and cross-layer design.

MIMO communication systems have been well known for their great potential to play a significant role in the design of the next-generation broadband wireless communications due to the advantages such systems can offer. By employing multiple transmit and receive antennas and taking advantage of a large number of propagation paths between the transmit and receive antennas, the adverse effects of the wireless propagation environment can be greatly reduced. It has been shown that MIMO systems offer a large potential capacity increase and performance improvement compared with single antenna systems. A considerable number of MIMO modulation and coding methods have been proposed, for example, in [20]- [34]. The rich scattering multipath channel in UWB indoor environment

provides an ideal transmission scenario for MIMO implementation. In addition, the GHz center frequency of UWB radio relaxes the requirements on the spacing between antenna array elements. Consequently, the combination of UWB and MIMO technology will become a viable and cost-efficient method to achieve the very high data rate requirement for future short range wireless applications. In this thesis, we will develop a general MIMO coding framework for UWB communications, and provide performance analysis to quantify the coding and diversity advantages of UWB-MIMO systems regardless of specific coding schemes.

In order to implement an efficient UWB system, it is also critical to comprehend the characteristics of the propagation channel. Several channel measurements established important differences between UWB channels and narrowband wireless channels, especially with respect to fading statistics and time-of-arrival of multipath components. In particular, the channel measurements showed multipath arrivals in clusters rather than in a continuum, as is common for narrowband channels. Although the fine time resolution of UWB results in a large number of resolvable multipath components at the receiver, these components occur at random and tend to have very low power. As a result, the performance improvement with the multipath diversity order may not be as much as that in narrowband systems. Furthermore, several experiments show that the UWB performances are related to clustering property of UWB channels. Although performance of UWB systems has been investigated in the literature (see for example [6], [35]- [40] and references therein), none of the existing analysis is insightful in revealing the effect of such multipath clustering phenomenon. This motivates us to devise an analytical performance of single antenna and multi-antenna UWB systems in realistic UWB channel environments that takes into account the clustering property

of UWB channels. This result will allow us to investigate the effects of the channel characteristics on the performance of UWB systems as well as the performance tradeoff between the diversity and coding advantages. Moreover, it can lead to further code design that is effective for UWB system.

Since many applications enabled by UWB are expected to be in portable devices, low power consumption becomes a fundamental requirement. The low transmitted power of UWB emissions not only ensures long life-time for the energy-limited devices, but also reduces co-channel interference. In addition, UWB systems are expected to support an integration of multimedia traffic, such as voice, image, data, and video streams. This requires a cross layer algorithm that is able to allocate the available resources to a variety of users with different service rates in an effective way. Most of the existing resource allocation schemes for UWB systems (see [41]- [47] and references therein) are based on single-band impulse radio technology. On the other hand, most research efforts on multiband UWB systems have been devoted to the physical layer issues [16]- [18], [48]- [49]. Some of the key issues in multiband UWB systems that remain largely unexplored are resource allocations such as power control and channel allocation. The current multiband proposal divides the subbands into groups, each comprising 2-3 subbands. A set of certain time-frequency codes is used to interleave the data within each band group [18]. This strategy lacks of the ability to allocate subbands optimally since the available subbands are not assigned to each user according to its channel condition. Moreover, in the multiband OFDM proposal [18], the transmitted power of each user is equally distributed among its assigned subbands without any power adaptation to the channel variations. This calls for an adaptive optimization of the subband assignment and power control to improve the performance of multiband

UWB systems.

Another significant design challenge for UWB systems is to improve the coverage ranges. Due to the limitation on the spectral mask, UWB transmitted power confines applications to relatively short ranges. Currently, the coverage of UWB systems is at most 10 meters at the data rate of 110 Mbps. At the high data rate of 480 Mbps, the coverage reduces to less than 3 meters [18], [19]. Such small coverage may be inadequate for some applications, e.g. those in warehouse, industrial, or even residential environments. To fully exploit the benefits of UWB technology, it is therefore greatly necessary to develop efficient techniques to enhance the performances and coverage ranges of UWB systems. To this date, limited works have been proposed to improve the coverage of UWB systems. One alternative is to utilize UWB-MIMO systems [50]- [58]. Nevertheless, in some applications, installing multiple antennas in UWB devices might be difficult due to cost or space limitations.

Recently, cooperative communications has emerged as a new communication paradigm that provides a new kind of diversity, namely cooperative diversity, by exploring the broadcast nature of the wireless channels. The basic principle of cooperative communications is that when a user has some information to transmit, other users in the network are willing to cooperate and help relay the information to the destination. In this way, the cooperation system is able to achieve diversity via forming a virtual antenna array, and hence provide significant gain in fading wireless environments. The research works in [59]- [66] have proved the significant potential of cooperative diversity in wireless networks. Current UWB technology, on the other hand, relies on a non-cooperative transmission, in which the diversity can be obtained only from MIMO coding or information repetition at the transmit-

ter [19], [50]- [58]. Furthermore, many UWB devices are expected to be in home and office environments; most of these devices are not in active mode simultaneously, but they can be utilized as relays to help the active devices. Additionally, due to the time division multiple access (TDMA) mechanism of the medium access control (MAC) layer and the network structure of the IEEE 802.15.3a WPAN standard [8], the cooperative protocols can be adopted in UWB WPANs. These facts motivate us to introduce the concept of cooperative diversity in UWB systems as an alternative approach to improve the UWB performance and coverage without the requirement of additional antennas or network infrastructures. In this thesis, we will first use the existing cooperative protocol to enhance the performance of UWB systems. Then, we will further develop a more efficient cooperative protocol for general OFDM and UWB multiband OFDM systems.

1.3   Dissertation Overview and Contributions

In this dissertation, we develop a cross-layer framework with an aim to enhance the performance of UWB systems. The organization of this dissertation is given as follows.

In Chapter 2, we give the basic mathematical background. First, we provide the fundamental UWB wireless communications. We begin with an overview of UWB radios with emphasis on physical layer issues including channel modeling, signal modeling and transceiver design. Next, we present the MAC layer protocol for UWB systems, and discuss the resource allocation issues as well as summarize the references on cross-layer design for UWB systems. Then, we present mathematical background for MIMO wireless communications. Diversity and coding gains are discussed. Finally, we describe a general background for considering coopera-

tive diversity in wireless networks. The fundamental background provided in this chapter will be used in developing our main contributions and results contained in Chapter 3-7.

In Chapter 3, we present our proposed MIMO coding framework for UWB communication systems. We develop a general framework to analyze the performance of UWB-MIMO systems regardless of specific coding schemes. We also propose a combination of space-time-frequency coding and hopping multiband OFDM modulation to fully exploit all of the available spatial and frequency diversities, richly inherent in UWB environments. Moreover, we provide performance analysis and quantify the diversity as well as the coding advantages of UWB-MIMO systems under Nakagami-m channel model. Our analysis reveals that the maximum achievable diversity gain of UWB-MIMO systems slightly depends on the severity of the fading, i.e., the diversity advantage obtained in Nakagami fading with arbitrary parameter m is almost the same as that obtained in Rayleigh fading which is equivalent to Nakagami-m fading with m=1.

In Chapter 4, we provide a novel performance analysis for UWB systems that successfully captures the unique multipath-rich property and multipath-clustering phenomenon of UWB channels. We characterize pairwise error probability and outage probability for UWB systems employing multiband OFDM based on the cluster arrival rate, the ray arrival rate within a cluster, and the cluster and ray decay factors. Furthermore, an approximation technique is established, which allows us to obtain closed-form performance formulations that provide insightful understanding of the effect of channel characteristics on the performances of UWB systems. Finally, we characterize the effect of random-clustering phenomenon on the performance of UWB-MIMO systems. The theoretical results reveal that re-

gardless of the clustering behavior of UWB channels, the diversity gain can be improved by increasing the number of jointly encoded subcarriers, the number of jointly encoded OFDM symbols, or the number of antennas. The coding gain on the other hand, depends heavily on the clustering property of UWB channels.

In Chapter 5, we develop a cross layer multiuser UWB multiband OFDM scheme to obtain the optimal subband and power allocation strategy. Optimization criteria involve minimization of power consumption under the constraints on the packet error rate, the data rate, and the FCC limit. To ensure the system feasibility in variable channel conditions, an algorithm that jointly manages the rate assignment of UWB devices, subband allocation, and power control is proposed. A computationally inexpensive suboptimal approach is also developed to reduce the complexity of the problem, which is found to be NP hard. Simulation results show that the proposed algorithm achieves comparable performances to those of the complex optimal full search approach, and it can save up to 61% of transmitted power compared to the current multiband scheme in the standard proposal. Moreover, the proposed algorithm can obtain the feasible solutions adaptively when the initial system is not feasible for the rate requirements of the users.

In Chapter 6, an employment of cooperative communications in UWB is proposed to enhance the performance and the coverage of UWB by exploiting the broadcasting nature of wireless channels and the cooperation among UWB devices. Symbol-error-rate (SER) performance analysis and optimum power allocation are provided for cooperative UWB multiband OFDM systems with decode-and-forward cooperative protocol. To capture the multipath-clustering phenomenon of UWB channels, the SER performance is characterized in terms of the cluster and the ray arrival rates. From the established SER formulation, an optimum power

allocation is determined based on two different objectives, namely minimizing the overall transmitted power and maximizing the system coverage. Furthermore, an improved cooperative UWB multiband OFDM scheme is proposed to take advantage of unoccupied subbands.

In Chapter 7, we propose an OFDM cooperative protocol that not only achieves full diversity but also efficiently utilizes available bandwidth. The proposed protocol exploits limited feedback from the destination terminal (central node) such that each relay is able to help forward information of multiple sources in one OFDM symbol. To specify how relay-source pairs should be assigned, we propose a practical relay-assignment scheme, in which the relays are fixed at optimum locations. We provide outage probability analysis of the proposed protocol in wireless indoor environment. Moreover, a lower bound on the outage probability of any relay-assignment schemes is established, and the performance of the proposed relay-assignment schemes is analyzed. Finally, we exploit the proposed protocol to enhance the performance of UWB systems.

In Chapter 8, we draw conclusions and discuss some possible future directions.

Chapter 2

Background and Related Literature

This chapter summarizes mathematical background and literature that relate to the problems studied in this dissertation. The wireless indoor channel models for UWB systems are considered in Section 2.1. Section 2.2 introduces a general UWB physical layer system models which includes channel models, signal models, and transceiver design. Section 2.3 describes the MAC layer protocols for UWB WPANs and then provides relevant concepts as well as summarizes references on cross-layer design for UWB systems. Section 2.4, describes mathematical background and surveys important results from the MIMO wireless communications literature. Section 2.5 introduces the concept of cooperative diversity for wireless network and summarizes references on cooperative communications.

2.1 UWB Channel Models

The analysis and design of UWB communication systems requires an accurate channel model to determine the achievable performance, to design efficient modulation and coding schemes, and to develop associated signal processing algorithms. The signal propagating through a wireless channel consists of multiple reflections caused by objects in the environment. The multipath components are characterized by different delays and attenuations. For narrowband signal with bandwidth less than the coherence bandwidth of the propagation channel, the multipath components arrive continuously, and severe multipath fading can be observed. When a large number of multipath components are observed at the receiver within its resolution time, the central limit theorem is commonly invoked to model the amplitude of the received signal as Rayleigh distributed. The Rayleigh fading is therefore extensively used for channel models in many narrowband systems.

In UWB systems, on the other hand, the ultra large bandwidth of UWB signals significantly increases the ability of the receiver to resolve the multipath components. This characteristic of UWB systems can give rise to two major effects which make UWB channels different from that of narrowband systems. These two effects are as follows.

1. The number of multipath components arrived at the receiver within the period of an ultra short waveform is much smaller as the duration becomes shorter. Consequently, the channel fading is not as severe as that in narrowband channels, and Rayleigh fading may not perfectly match to the amplitude of the received signal. In addition, a large number of resolvable multipath components can be observed at the receiver.

2. Since the multipath components can be resolved on a very fine time duration, the time of arrival of the multipath components may not be continuous. In other words, there are empty delay bins (bins containing no energy) between the arriving multipath components. In UWB systems, the channel measurements showed multipath arrivals in clusters rather than in a continuum, as is common for narrowband channels. Particularly, due to the very fine resolution of UWB waveforms, different objects or walls in a room could contribute different clusters of multipath components.

A reliable channel model, which captures such important characteristics of UWB channel, is therefore critical for the analysis and design of UWB systems. Recently, the IEEE 802.15.3a standards task group formed a subgroup to establish a common channel model for UWB systems. Three main indoor channel models considered in the standard are as follows.

2.1.1 Tap-delay line fading model

A simple model for characterization of UWB channel is the tap-delay line fading model [67], [68] in which the received signal is a sum of the replicas of the transmitted signal, being related to the reflecting, scattering, and/or deflecting objects via which the signal propagates. Such tap-delay line fading model allows frequency selectivity of UWB channels to be taken into consideration. The channel impulse response under tap-delay fading model can be described as [7]

$$h(t) = \sum_{l=0}^{L-1} \alpha(l)\delta(t - \tau_l), \tag{2.1}$$

where $\alpha(l)$ is the multipath gain coefficient of the lth path, L denotes the number of resolvable multipath components, and τ_l represents the path delay of the lth path.

In conventional narrowband systems, it is well established that the amplitude of the lth path, $|\alpha(l)|$, is modeled as a Rayleigh random variable with a probability density function (PDF) [7]

$$p_{|\alpha(l)|}(x) = \left(\frac{x}{\Omega_l}\right) \exp\left(-\frac{x^2}{\Omega_l}\right), \tag{2.2}$$

where $\Omega_l = \mathrm{E}\left[|\alpha(l)|^2\right]$ denotes the average power of the lth path. Here, $p_X(x)$ represents the PDF of x, $\mathrm{E}[\cdot]$ stands for the expectation operation. In UWB systems, the number of components falling within each delay bin is much smaller, which leads to a change in the statistics. Various alternative distributions have been used in the literature.

- Lognormal distribution: It has been suggested in [69], [70]. The lognormal distribution is given by [7]

$$p_{|\alpha(l)|}(x) = \frac{20/\ln 10}{x\sqrt{2\pi\Omega_l}} \exp\left(\frac{(10\log_{10}(x^2) - \mu_l)^2}{2\Omega_l}\right), \tag{2.3}$$

  where Ω_l is the variance of the local mean $|\alpha(l)|$ and μ_l is the mean of $|\alpha(l)|$ in dB. The lognormal distribution has the advantage that the fading statistics of the small-scale statistics and the large-scale variations have the same form; the superposition of lognormal variables can also be well approximated by a lognormal distribution. The drawback is that it is difficult to obtain insightful performance analysis, especially for MIMO system, under lognormal fading model.

- Nakagami distribution: It has been suggested in [67] that amplitude of multipath coefficient can be modeled by Nakagami-m distribution [71]:

$$p_{|\alpha(l)|}(x) = \frac{2}{\Gamma(m)} \left(\frac{m}{\Omega_l}\right)^m x^{2m-1} \exp\left(-\frac{m}{\Omega_l}x^2\right), \tag{2.4}$$

where $\Gamma(\cdot)$ denotes the Gamma function, $m \geq 1/2$ is the Nakagami fading parameter, and Ω_l is the mean-square value of the fading amplitude. The fading parameter, m, describes the severity of the fading. The smaller the m, the more severe the fading, with $m = 1$ and $m = \infty$ corresponding to the Rayleigh fading and non-fading channel, respectively. The advantage of Nakagami-m statistics is that they can model a wide range of fading conditions by adjusting their fading parameters. In fact, Nakagami-m distributions with large value m are similar to the log-normal distributions. Furthermore, if the amplitude is Nakagami-distributed, then the power is Gamma-distributed which enables closed-form performance formulation.

Although the tap-delay line fading model is able to capture the frequency selectivity, it does not reflect the clustering characteristic of UWB channels. To capture the clustering property, an approach that modeled the multipath arrival times using a statistically random process based on the Poisson process has been considered. Specifically, the multipath arrival times τ_l can be characterized by a Poisson process with a constant arrival rate λ as

$$P_r(\tau_l - \tau_{l-1} > t) = \exp(-\lambda t). \tag{2.5}$$

In other words, the inter-arrival time of multipath components is exponentially distributed, i.e., given a certain arrival time τ_{l-1} for the previous time, the PDF for the arrival of path l can be written as

$$p_{\tau_l}(\tau_l | \tau_{l-1}) = \lambda \exp[-\lambda(\tau_l - \tau_{l-1})], \; l > 0. \tag{2.6}$$

Two mathematical models that reflect this clustering is the $\Delta - K$ model [72] and the SalehValenzuela (S-V) model [73].

2.1.2 $\Delta - K$ model

The $\Delta - K$ was first introduced for the outdoor environment, and popularized for the indoor scenario by [72]. The $\Delta - K$ model defines two states, state A where the arrival rate of paths is λ, and state B where the rate is $K\lambda$. The model starts in state A. If a path arrives at time t, then a transition is made to state B for a minimum of time λ. If no path arrives during that time, the model reverts to state A; otherwise, it remains in state B. The $\Delta - K$ model was used for UWB channels in [74], [75]. Note that both the number of clusters and the duration of the clusters become random variables in this model. Specifically, the number of clusters is a random variable, whose realization is determined by how often system enters into state B. In addition, the clusters are strictly separated from each other; the duration between two clusters is determined by the parameter Δ.

2.1.3 SalehValenzuela (S-V) model

The S-V model [73] was first introduced for wideband indoor channel. In S-V model, the multipath arrivals were grouped into two different categories: a cluster arrival and a ray arrival within a cluster. This model requires four main parameters, namely, the cluster arrival rate, the ray arrival rate within a cluster, the cluster decay factor, and the ray decay factor. The channel impulse response of S-V model is modeled by

$$h(t) = \sum_{c=0}^{C} \sum_{l=0}^{L} \alpha(c,l)\delta(t - T_c - \tau_{c,l}), \tag{2.7}$$

where $\alpha(c,l)$ denotes the gain of the lth multipath component in the cth cluster, C is the total number of cluster, and L is the total number of rays within each cluster. The time duration T_c represents the delay of the cth cluster, and $\tau_{c,l}$ is
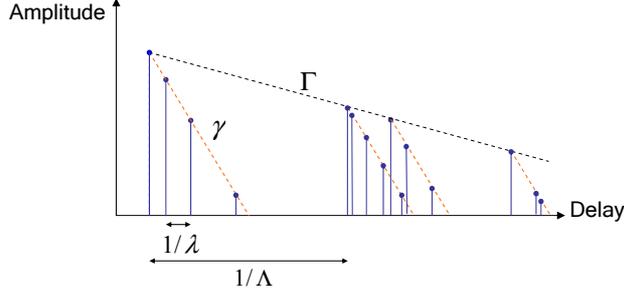
Figure 2.1: Principle of the Saleh-Valenzuela fading model.

the delay of the lth path in the cth cluster relative to the cluster arrival time. By definition, we have $\tau_{c,0} = 0$. The cluster arrivals and the path arrivals within each cluster are modeled by Poisson processes

$$p_{T_c}(T_c|T_{c-1}) = \lambda \exp[-\Lambda(T_c - T_{c-1})], \ c > 0; \qquad (2.8)$$

$$p_{\tau_{c,l}}(\tau_{c,l}|\tau_{c,l-1}) = \lambda \exp[-\lambda(\tau_{c,l} - \tau_{c,l-1})], \ l > 0, \qquad (2.9)$$

where Λ is the cluster arrival rate, and λ (where $\lambda > \Lambda$) is the ray arrival rate, i.e., the arrival rate of path within each cluster. The path amplitude $|\alpha(c, l)|$ follows the Rayleigh distribution, whereas the phase $\angle\alpha(c, l)$ is uniformly distributed over $[0, 2\pi)$. Specifically, the multipath gain coefficient $\alpha(c, l)$ is modeled as zero-mean, complex Gaussian random variable with variance [68]

$$\Omega_{c,l} = \mathrm{E}\left[|\alpha(c, l)|^2\right] = \Omega_{0,0} \exp\left(-\frac{T_c}{\Gamma} - \frac{\tau_{c,l}}{\gamma}\right), \qquad (2.10)$$

where $\Omega_{0,0}$ is the mean energy of the first path of the first cluster, Γ is the cluster decay factor, and γ is the ray decay factor; this reflects the exponential decay of each cluster, as well as the decay of the total cluster power with delay. The four main parameters can be changed for different environments. They provide great flexibility to model very different environments. Fig. 2.1 illustrates the different parameters in the S-V model.

Table 2.1: Multipath channel model parameters

Parameters	CM 1	CM 2	CM 3	CM 4
Λ (1/ns)	0.0233	0.4	0.0667	0.0667
λ (1/ns)	2.5	0.5	2.1	2.1
Γ	7.1	5.5	14	24
γ	4.3	6.7	7.9	12

The channel model adopted in the IEEE 802.15.3a standard [8] is based on the S-V model. Although the path amplitude $|\alpha(c,l)|$ may follow the lognormal distribution [68], the Nakagami distribution [67], or the Rayleigh distribution [80], the lognormal distribution is adopted in the standard. Four set of channel model (CM) parameters for different measurement environments were defined, namely CM1, CM2, CM3, and CM4. CM1 describes a line-of-sight (LOS) scenario with a separation between transmitter and receiver of less than 4m. CM2 describes the same range, but for a non-LOS situation. CM3 describes a non-LOS scenario for distances between transmitter and receiver of 4-10m. CM4 describes an environment with strong delay dispersion, resulting in a delay spread of 25ns. Table 2.1 provides the model parameters of CM1-CM4. Note that the total average received power of the multipath realizations is typically normalized to unity in order to provide a fair comparison with other systems.

2.2 UWB Physical Layer Design

As discuss in the previous chapter, the UWB signals are categorized into single-band and multiband signals. This subsection describes the signal model for both single-band and multiband approaches.
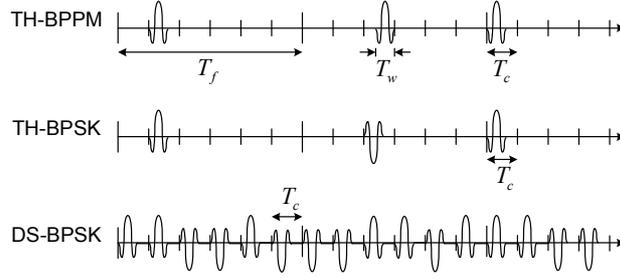
Figure 2.2: UWB signals with various modulation and multiple access techniques

2.2.1 Single-Band Approaches

The single-band UWB signal is implemented by directly modulating a sequence of impulse-like waveforms that occupies several gigahertz bandwidth. Continuous pulse transmission will lead to strong lines in the spectrum of the transmitted signal. The regularity of these energy spikes may interfere with other communication systems over short distances. In order to minimize potential interference from UWB transmissions and to make the spectrum of the UWB transmission more noise-like, a randomizing technique is applied to the transmitted signal. The two commonly used approaches are TH and DS spreading. Fig. 2.2 illustrates an example of TH-UWB and DS-UWB signals.

The TH-UWB utilizes low duty cycle pulses, where the time spreading between the pulses is used to provide time multiplexing of users. The uth user's transmitted waveform can be described as [10]- [12]

$$\tilde{x}_u(t) = \sqrt{E_u} \sum_{k=-\infty}^{\infty} a_u(k)\tilde{w}\left(t - kT_f - c_u(k)T_c - b_u(k)T_d\right), \qquad (2.11)$$

where $\tilde{w}(t)$ is the transmitted monocycle of duration T_w, and T_f is the frame interval with $T_f \gg T_w$. The monocycle is normalized to have unit energy, and each frame is transmitted with energy E_u. To accommodate the TH sequences in multiple access environments, T_f is further divided into N_c segments of T_c seconds

29

where $N_c T_c \leq T_f$. The TH sequence of the uth user is denoted by $\{c_u(k)\}$, $0 \leq c_u(k) \leq N_c - 1$. The modulation delay is represented by T_d and the data sequence is either $\{a_u(k)\}$ or $\{b_u(k)\}$, depending on the modulation techniques. In BPPM, the data is conveyed by the positions of the pulses, whence $a_u(k) = 1$ for all k and $b_u(k) \in \{0, 1\}$. BPSK on the other hand, alternates the polarities of the pulses in response to the information. Accordingly, the data sequence is $a_u(k) \in \{-1, 1\}$ whereas $b_u(k) = 0$ for all k.

In contrast to TH approach, DS-UWB employs a train of high duty cycle pulses whose polarities follow pseudo-random code sequences. Specifically, each user in the system is assigned a pseudo-random sequence which controls pseudo-random inversions of the UWB pulse train. A data bit is then used to modulate this sequence of UWB pulses. The transmitted DS-BPSK signal model can be described as [13], [15]

$$\tilde{x}_u(t) = \sqrt{\frac{E_u}{N_c}} \sum_{k=-\infty}^{\infty} d_u(k) \sum_{n_c=0}^{N_c-1} c_u(n_c) \tilde{w}(t - kT_f - n_c T_c), \qquad (2.12)$$

where $d_u(k) \in \{-1, 1\}$ is the data, $\{c_u(n_c)\}_{n_c=0}^{N_c-1} \in \{-1, 1\}$ represents the spreading sequence, and $T_c \geq T_w$ denotes the hop period. The factor $\sqrt{1/N_c}$ is introduced such that the sequence of N_c monocycles has unit energy, and hence the transmitted energy per frame is E_u.

2.2.2 Multiband Approaches

As opposed to the conventional single-band approach in which a single bandwidth is used for all data transmission, the multiband approach divides the available UWB frequency band into smaller subbands and uses multiple carrier frequencies to transmit the information. In order to efficiently capture the multipath
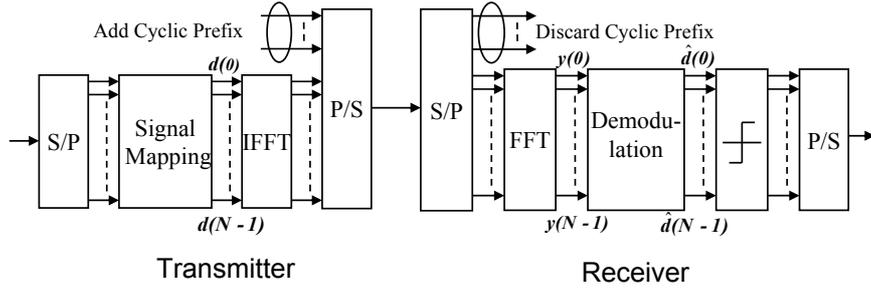
Figure 2.3: Transmitter and receiver of an OFDM system.

energy, which is richly inherent in UWB environment, OFDM technique has been used to modulate the information in each subband. Different bit rates are achieved by using different channel coding, frequency spreading, or time spreading rates.

Consider a UWB multiband OFDM system with N subcarriers and the subband bandwidth of BW. Let $d_k(n)$ denotes the complex coefficient to be transmitted in subcarrier n during the k^{4h} OFDM symbol period. The coefficient $d_k(n)$ can by data symbols, pilots, or training symbols. The baseband signal is constructed in the similar way to the conventional OFDM system, as shown in Fig. 2.3. Particularly, each OFDM symbol $x_k(t)$ is constructed using an inverse Fourier transform:

$$x_k(t) = \sum_{n=0}^{N-1} d_k(n) \exp(\mathbf{j}2\pi n\Delta f t) \tag{2.13}$$

where $\Delta f = BW/N$ is the frequency spacing between the adjacent subcarreirs. The resulting waveform has a duration of $T_{FFT} = 1/\Delta f$. The cyclic prefix of length T_{CP} is appended in order to mitigate the effects of multipath interference and to transform the multipath linear convolution into a circular one. Also, the guard interval of length T_{GI} is added at the end of the OFDM block. The guard interval is used to provide more flexibility in the implementation. For instance, it can be used to provide sufficient time for switching between bands, to relax the analog transmit and receive filters, to relax filter specifications for adjacent

31
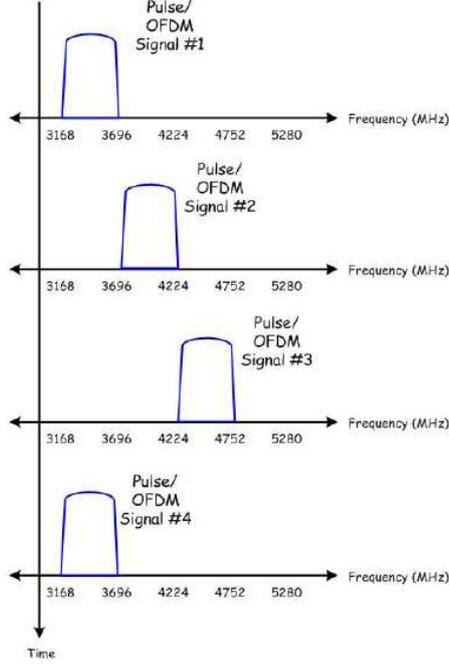
Figure 2.4: A transmitted UWB multiband OFDM signal.

channel rejection, or to help reduce peak-to-average power ratio (PARP). The symbol duration becomes $T_{SYM} = T_{FFT} + T_{CP} + T_{GI}$. The complex baseband signal $x_k(t)$ is modulated to the RF signal with carrier frequency f_k. The RF transmitted signal can be modeled as

$$s(t) = \sum_k \text{Re} \left\{ x_k(t - k\, T_{SYM}) \exp(\mathbf{j}2\pi f_k t) \right\}, \tag{2.14}$$

The carrier frequency, f_k, specifies subband, in which the signal is transmitted during the kth OFDM symbol duration. These carrier frequency sequences are based on time-frequency codes, which are uniquely assigned to different users so as to minimize the multiple access interference. Fig. 2.4 depicts an example of the transmitted UWB multiband OFDM signal.
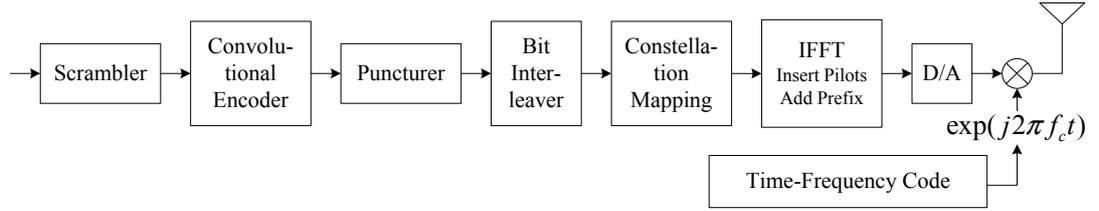
Figure 2.5: Single-antenna UWB multiband-OFDM transmitter

2.2.3 Transceiver Design

In this subsection, we describe a single-antenna transceiver architecture that uses UWB multiband-OFDM scheme. We consider the multiband OFDM approach as proposed in the IEEE 802.15.3a standard proposal [18]. The OFDM has 128 subcarriers, and the bandwidth of each subband is 528 MHz. Different pattern of band switching is assigned to different users in order to gain frequency diversity while minimize the multi-user interference. The structure of the UWB multiband-OFDM transmitter is shown in Fig. 2.5, which includes scrambler, channel encoder, interleaver, and so on.

- *Scrambling*: In each data packet, a standard preamble shall be added prior to the header to aid receiver algorithms related synchronization, carrier-offset recovery, and channel estimation. The standard preamble consists of three distinct portions: packet synchronization sequence, frame synchronization sequence, and the channel estimation sequence [8]. The scrambler is used to make data more random to eliminate long runs of ones and zeros as well as repetitive patterns.

- *Channel Encoding*: At the transmitter, the data bit stream is encoded with the convolutional code. The convolutional encoder uses the rate $R = 1/3$ industry-standard generator polynomials, $g_0 = 133_8, g_1 = 145_8$, and $g_2 =$
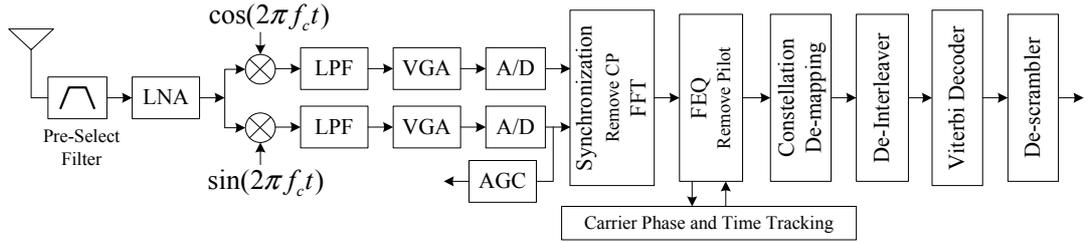
Figure 2.6: Single-antenna UWB multiband-OFDM receiver

175_8. Additional coding rates are generated by puncturing the convolutional code, i.e., omitting some of the encoded bits in the transmitter and inserting a dummy zero metric into the convolutional decoder in place of the omitted bits.

- *OFDM Modulation*: The output of the puncturer is interleaved, mapped into a sequence of quadrature phase shift keying (QPSK) samples and parallelized by a serial-to-parallel (S/P) converter. Each sample is subsequently modulated onto one of 128 subcarriers, 12 pilot samples are inserted to facilitate coherent reception, and 10 subcarriers are dedicated to guard subcarriers to relax the specs on transmit and receive filters. After performing a 128-point inverse fast Fourier transform (IFFT), a cyclic prefix is added so as to preserve orthogonality between subcarriers and allow the receiver to efficiently capture multipath energy.

- *D/A Converting*: The samples are serialized by a parallel-to-serial (P/S) converter and pass through a digital-to-analog (D/A) converter. The resulting analog signal is up-converted to a specified frequency band, passed through a power-amplifier (PA), and finally transmitted.

The corresponding receiver structure is shown in Fig. 2.6. First, the received signal is passed through a pre-select filter, amplified with a low-noise amplifier

(LNA), down-converted to baseband, scaled in amplitude by voltage gain amplifier (VGA), and digitized by an analog-to-digital (A/D) converter . After synchronization and removing the cyclic extension, a 128-point fast Fourier transform (FFT) is carried out. The samples containing information are extracted and sent to a P/S converter. Subsequently, the estimated transmitted bit sequence is reconstructed, and then de-interleaved. Next, a maximum likelihood decoding is performed at a Viterbi decoder. Finally, the output of the decoder is descrambled, resulting an estimated sequence of binary data.

2.3 UWB MAC Layer and Cross-Layer Design

In this section, we first present the MAC layer protocol for UWB WPANs, and then summarize the research work on MAC layer as well as cross layer design for UWB systems.

The MAC layer for UWB WPANs will be based on the MAC layer specification in the IEEE 802.15.3 standard [77], which is designed to support ad-hoc networking and provide multimedia capabilities. The UWB devices with high rate WPAN functionality are communicating on a centralized and connection-oriented networking topology called piconet. The piconet corresponds to collocated cluster of different UWB devices that form their own network. One piconet comprises UWB devices that are associated via a piconet coordinator (PNC). The PNC is responsible for the task of maintaining piconet operation including transmitting beacons that carry piconet parameter information which allows new devices to join the piconet as well as allocate resources for channel access to existing devices in the piconet. The UWB devices and the PNC are communicating via the channels allocated by the PNC. Note that unlike the cellular systems in which the base
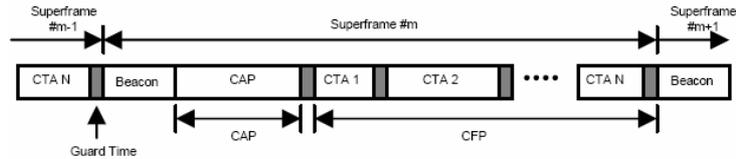
Figure 2.7: A superframe structure in for UWB WPAN specified in the IEEE 802.15.3 standard

station and mobiles have different characteristics, the UWB devices and the PNC have the same communication properties. So there is no uplink/downlink concept in the UWB piconet.

The 802.15.3 MAC adheres to a TDMA superframe structure, as shown in Fig. 2.7. The superframe consists of three major components:

- A beacon

- An optional contention access period (CAP)

- A contention free period (CFP)

The beacon frame is transmitted by the PNC at the beginning of each superframe. It lets all devices know about the specific information for controlling a piconet. The CAP is used for short data frame, command frames, and nondelay critical applications such as asynchronous data frames. The medium access mechanism during the CAP is collision sense multiple access/collision avoidance (CSMA/CA) with short request to send and clear to send (RTS/CTS) messages. The remaining period in the superframe is CFP. The CFP comprises channel time allocation (CTA) periods which are assigned by the PNC through a beacon frame. During each CTA period, one device can transmit several frames to its destination without collision. Each frame transmission is followed by an acknowledgement (ACK) frame, which can be no-acknowledgement (No-ACK), immediate-acknowledgement

(Imm-ACK) or delayed acknowledgement (Dly-ACK). If the transmitted frame is received correctly, an Imm-ACK is transmitted from the destination. On the other hand, if the frame is not received successfully, then no acknowledgement will be transmitted which corresponds to the No-ACK case. The Dly-ACK is used only for directed stream data frame, i.e. isochronous connections. The relative duration of CAP and CFP can be dynamically adjusted on a per-frame basis as required by traffic demands.

To set up a piconet, a device which is capable of acting as a PNC sends the beacon on an empty channel. Other devices join the piconet by following the association process. When a device has data to be sent on a regular basis, it makes a CTA request to the PNC. If the resources are available, the PNC allocates the required number of CTAs for the device and informs the device in a subsequent beacon. The device can then communicate with the destination during these time slots on a peer-to-peer basis. A similar disassociation process is followed when a device leaves the network.

The layered architecture of communication systems has been key the success to the development of wireless systems. Traditionally, the resources are managed within each layer. For instance, in physical layer, the transmitted power and/or modulation are optimally allocated to maximize the spectral efficiency and minimize the co-channel interferences. Access to the radio medium, on the other hand, is traditionally considered a problem of the MAC layer. However, it has recently become evident that optimizing within layers is insufficient to obtain the performance necessary to satisfy the growing demand in the next-generation wireless services. This is primarily due to the interaction of links through interference, which implies that a change in power allocation or medium access on one link

can induce changes in capacities of all links and consequently changes in the performance of the entire system. This calls for network protocols and designs that takes into consideration the optimization across the layers, the so called cross-layer design.

To this date, most of the research efforts on UWB systems have been devoted to the transmission issues at the physical layer. Research work on resource management and cross-layer design is still limited. The existing related work is summarized as follows. In [42], [43], the radio resource sharing problem was formulated as a joint rate and power assignment problem that is central in multiuser UWB networks. The authors also proposed suboptimal algorithms that dynamically assign the transmission rate and transmitted power of each node. The proposed radio resource sharing mechanism performs a handshaking procedure to establish a communication link. Specifically, the mechanism relies on two handshakes between the sender and its neighbors to obtain the required information for link rate and power assignments. Later in [44], a radio resource allocation problem was also formulated to allocate transmitted power and data rate of each node such that the system throughput is maximized. Different from [42], [43], the algorithms in [44] always reserved a specific amount of channel capacity for best effort traffic. In [45], the authors proposed an algorithm which optimizes transmission efficiency of mobile UWB users by adapting the error protection to both channel status and quality of service (QoS) constraints. Performance in the case of a slowly time-varying UWB channel was discussed. In [46], the authors discussed a joint scheduling, routing, and power allocation problem with an objective to maximize the total utility of UWB system. Later in [47], a joint scheduling and resource control algorithm was also proposed to allocate for transmitted power and data rate for each UWB node

in WPANs. Different from [46], the algorithm in [47] provides explicit QoS support while optimizing resource allocation.

2.4 MIMO Wireless Communications

In conventional RF technology, MIMO has been well known for its effectiveness of improving system performance in fading environments. Space-time (ST) coded MIMO systems [20]- [24] have been proposed for narrowband communications, where the fading channel is frequency-non-selective. The main concept is the joint processing in time as well as in space via the use of multiple transmit and receive antennas, so as to achieve both spatial and temporal diversity. When the fading channel is frequency-selective, space-frequency (SF) coded MIMO-OFDM systems [25]- [30] have been shown to be an efficient approach to make benefits of spatial and frequency diversity. Recently, space-time-frequency (STF) codes [31]- [34] have also been proposed for MIMO-OFDM systems. By utilizing some proper STF coding and modulation techniques, STF coded MIMO systems can exploit all of the spatial, temporal and frequency diversity, and hence promise to yield high spectral efficiency and remarkable performance improvement.

In a point-to-point MIMO system, multiple antennas are deployed at both transmitter and receiver, as shown in Fig. 2.8. At the transmitter, the data sequence is divided into blocks. Each block is encoded into a codeword matrix $\mathbf{D}$. Each column of $\mathbf{D}$ contains a sequence of symbols that will be sent from each transmit antenna over a series of time slot or frequency tones (depending on the underlined modulation scheme, e.g. single carrier or multi-carrier). These symbol streams are modulated with a pulse shaping function, translated to the passband via parallel RF chains, and then simultaneously transmitted over all transmit an-
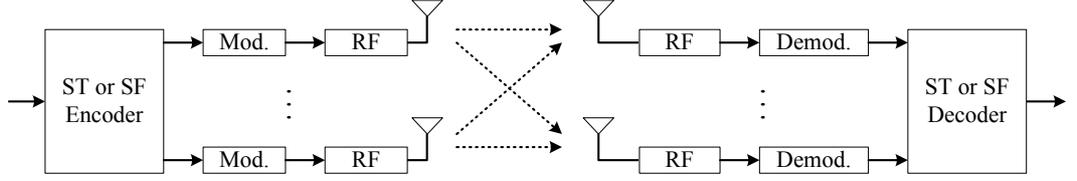
Figure 2.8: A point-to-point MIMO communication system.

tennas. After down conversion, matched-filtering and demodulation processes, the receiver jointly decodes the received signals across all receive antennas.

The design of matrix $\mathbf{D}$ is originally studied for flat fading channels. In this case, the row and column indices of $\mathbf{D}$ indicate the dimensions of space and time, and hence $\mathbf{D}$ is termed ST code. For a MIMO system with N_t transmit and N_r receive antennas, $\mathbf{D}$ is an $K \times N_t$ matrix whose $(k, i)^{th}$ element, denoted by $d_i(k)$, represents the symbol transmitted at transmit antenna i over time slot k. Here, K represents the number of time slots for one codeword transmission. The MIMO channel is described by an $N_t \times N_r$ matrix $\mathbf{A}$. The $(i, j)^{th}$ component of $\mathbf{A}$, denoted by α_{ij}, is the channel fading coefficient from the ith transmit to the jth receive antenna. The received signal at each receive antenna is a noisy superposition of the N_t transmitted signals degraded by the channel fading. Consider the case when the channels are quasi-static, i.e., they remain constant during the transmission of an entire codeword. The received signal can be described as an $K \times N_r$ matrix

$$\mathbf{Y} = \sqrt{\frac{E}{N_t}} \mathbf{D} \mathbf{A} + \mathbf{Z},$$

where $\mathbf{Z}$ is the matrix of additive complex Gaussian noises, each with zero mean and variance $N_0/2$ per dimension. For normalization purposes, the fading coefficient for each transmit-receive link is assumed to have unit variance, and the ST code satisfies the energy constraint $\mathrm{E}\left[\|\mathbf{D}\|^2\right] = KN_t$. Here, $\mathrm{E}\left[\mathbf{X}\right]$ and $\|\mathbf{X}\|$ denote

the expectation and Frobenius norm[1] of $\mathbf{X}$ [76], respectively. The factor $\sqrt{1/N_t}$ ensures transmit energy identical to single antenna transmission. Assuming that the channel state information is perfectly known at the receiver, the receiver performs maximum likelihood decoding by choosing the codeword $\hat{\mathbf{D}}$ that minimizes the square Euclidean distance between the hypothesized and actual received signal matrices, i.e.

$$\hat{\mathbf{D}} = \arg\min_{\mathbf{D}} \|\mathbf{Y} - \sqrt{\frac{E}{N_t}}\mathbf{DA}\|^2.$$

The upper bound of the average pairwise error probability (PEP) between $\mathbf{D}$ and $\hat{\mathbf{D}}$ is of the form [20], [21]

$$P\left(\mathbf{D} \to \hat{\mathbf{D}}\right) \leq \left[G_c \frac{\rho}{4N_t}\right]^{-G_d},$$

where $\rho = E/N_0$ is the average signal-to-noise ratio (SNR) at each receive antenna. The quantities G_d and G_c depend on the distribution of channel fading coefficients and the structure of $\mathbf{D}$. They characterize the performance of ST coded MIMO system as follows. The exponent G_d determines the slope of the error probability curve plotted as a function of SNR (measured in dB). The factor G_c displaces the performance curve rather than alternating its slope. The minimum values of G_d and G_c over all pairs of distinct codewords are called diversity gain and coding gain, respectively.

In wideband system, the channel fading is frequency selective. To exploit the additional frequency diversity in wideband MIMO communications, SF code incorporating with OFDM modulation has been introduced. The strategy of SF

---

[1]The Frobenius norm of an $M \times N$ matrix $\mathbf{X} = (x_{mn})$, is defined as [76]

$$\|\mathbf{X}\|^2 = tr\left(\mathbf{X}^{\mathcal{H}}\mathbf{X}\right) = tr\left(\mathbf{X}\mathbf{X}^{\mathcal{H}}\right) = \left(\sum_{m=0}^{M-1}\sum_{n=0}^{N-1}|x_{mn}|^2\right).$$

coding is to distribute the symbols across space (transmit antenna) and frequency (OFDM tones). The codeword $\mathbf{D}$ in this case represents SF codeword of size $N \times N_t$, where N is the number of OFDM tones. Note that the design of SF code is restricted to one OFDM symbol duration (T seconds), and the MIMO channel is normally assumed constant over a period of T. The performance criteria for SF coded MIMO-OFDM can be characterized in a similar fashion as that of ST system.

2.5   Cooperative Communications

Cooperative diversity has recently emerged as a promising alternative to combat fading in wireless channels. The basic idea is that users or nodes in a wireless network share their information and transmit cooperatively as a virtual antenna array, thus providing diversity without the requirement of additional antennas at each node.

In [60], the authors proposed various cooperative strategies including fixed relaying, selection relaying, and incremental relaying schemes for single relay scenarios and analyzed their outage probability. The fixed relaying protocols include amplify-and-forward (AF) and decode-and-forward (DF) protocols. With the AF protocol, the relays simply amplify and forward the information, whereas with the DF protocol, the relays decode the received information and then forward the decoded symbols to the destination. In selection relaying protocol, the relay decides whether to forward the received information from the source by applying a threshold test on the measured channel state information between the source and the relay. With incremental relaying protocol, limited feedback from the destination is employed in the form of automatic repeat request, and the relay forwards the source
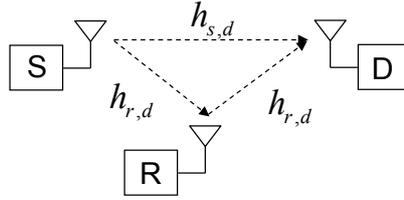
Figure 2.9: A simplified cooperation model.

information only when the information is not successfully captured at the destination via direct transmission. In [59], the authors extended the DF cooperation in [60] to the case of multiple relays where they proposed distributed space-time coding. In [61], [62], a similar concept, called user cooperation diversity, was proposed for code division multiple access (CDMA) systems in which orthogonal codes are used to mitigate multiple access interference. The work in [61], [62] assumes full channel state information at the cooperating nodes that utilize beamforming, while the protocols in [60] assumes no channel information at the transmitters since beamforming requires high complexity radios and has not been demonstrated for the distributed case. In [63], a coded cooperation is proposed to achieve diversity by incorporating error control coding into cooperation. The scheme in [63] does not use beamforming but assumes full channel state information at the transmitter. In [64], the authors introduced a concept of multihop diversity in which each relay combines the signals received from all of the previous transmissions. Later in [65], the authors provided SER performance analysis and optimum power allocation for decode-and-forward cooperation systems with two users. The SER performance analysis of a class of multinode cooperative protocols was presented in [66].

Consider a cooperation strategy for a wireless network, which can be a mobile ad hoc network or a cellular network. Each user (or node) in the network can be a source node that sends information to its destination, or it can be a relay node

that helps transmit the other user's information. Under the cooperation strategy in [60], the signal transmission involves two phases. In Phase 1, each source sends information to its destination, and the information is also received by other users in the network. In Phase 2, each relay may forward the source information to the destination or remain idle. In both phases, all users transmit signals through orthogonal channels by using TDMA, FDMA, or CDMA scheme [59]- [62]. Fig. 2.9 illustrates a simplified cooperation model in which S, R, and D denote source, relay, and destination, respectively.

Chapter 3

MIMO Coding Framework

To enhance the data rates and the transmission ranges of UWB systems, the employment MIMO scheme to UWB has gained considerable interest recently. In conventional RF technology, MIMO has been well known for its effectiveness of improving system performance in fading environments. Most UWB applications are in rich scattering indoor environment, which provides an ideal transmission scenario for MIMO implementation. In addition, the GHz center frequency of UWB radio relaxes the requirements on the spacing between antenna array elements. Consequently, the combination of UWB and MIMO technology will become a viable and cost-efficient method to achieve the very high data rate requirement for future short range wireless applications. To this date, UWB-MIMO technology has been well documented for the traditional single-band UWB system [50]- [55]. On the other hand, research for multi-antenna multiband UWB systems is still largely unexplored, thus offering limited resources in handling the benefits and challenges of UWB-MIMO communications.

In this chapter, we develop a general framework to characterize the performance of UWB-MIMO systems with multiband OFDM. A combination of STF

coding and hopping multiband UWB transmission is introduced to exploit all of the available spatial and frequency diversities. In the performance evaluation, we do not impose any restriction on the delays or the average powers of the multipath components, and the proposed framework is applicable for any channel models. Since Nakagami-m statistics can be used to model a wide range of fading conditions, we evaluate the theoretical performances of UWB systems by using the tap-delay line Nakagami-m fading model, as it can provide some insightful understanding of UWB systems [13], [55]- [56]. We quantify the average pairwise error probability as well as the diversity and the coding advantages, regardless of specific coding schemes. It turns out that the maximum achievable diversity is the product of the number of transmit and receive antennas, the number of multipath components, and the number of jointly encoded OFDM symbols. An interesting result is that the diversity advantage does not depend on the fading parameter m. The diversity gain obtained under Nakagami fading with arbitrary m parameter is almost the same as that obtained in Rayleigh fading, which is equivalent to Nakagami-m fading with $m = 1$. Simulation results confirm the theoretical expectation of considerable performance improvement, gained from adopting STF codes in multiband system.

An outline of this chapter is as follows. In Section 3.1, we present the multiband UWB-MIMO system model, including the signal modulation, channel model, receiver description, and detection technique. The performance analysis of a peer-to-peer multi-antenna multiband UWB system is presented in Section 3.2. In Section 3.3 simulation results are presented to support the theoretical analysis.
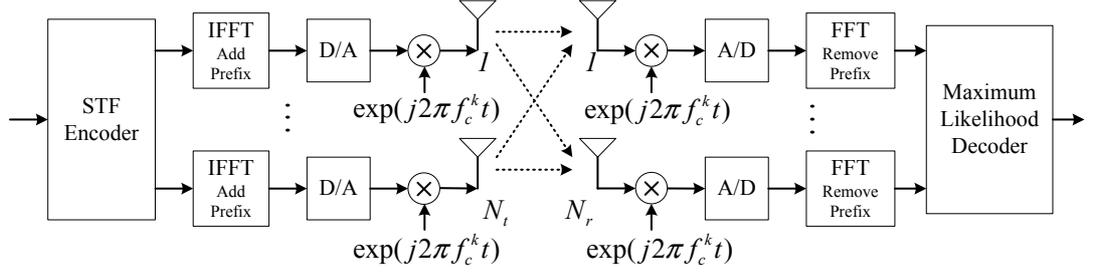
Figure 3.1: Multiband UWB-MIMO system.

3.1 Multiband UWB-MIMO System Model

Consider a UWB multiband OFDM system with fast band-hopping rate, i.e., the signal is transmitted on a frequency-band during one OFDM symbol interval, then moved to a different frequency-band at the next interval.

3.1.1 Transmitter Description

We consider a peer-to-peer UWB multiband OFDM system with N_t transmit and N_r receive antennas, as shown in Fig. 3.1. The information is encoded across N_t transmit antennas, N OFDM subcarriers, and K OFDM blocks.

At the transmitter, the coded information sequence from a channel encoder is partitioned into blocks of N_b bits. Each block is mapped onto a $KN \times N_t$ STF codeword matrix

$$\mathbf{D} = \left[\begin{array}{cccc} \mathbf{D}_0^T & \mathbf{D}_1^T & \cdots & \mathbf{D}_{K-1}^T \end{array} \right]^T, \tag{3.1}$$

where

$$\mathbf{D}_k = \left[\begin{array}{cccc} \mathbf{d}_1^k & \mathbf{d}_2^k & \cdots & \mathbf{d}_{N_t}^k \end{array} \right], \tag{3.2}$$

in which $\mathbf{d}_i^k = \left[d_i^k(0)\ d_i^k(1)\ \cdots\ d_i^k(N-1) \right]^T$ for $i = 1,\ 2, \ldots,\ N_t$ and $k = 0, 1, \ldots,$ $K-1$. The symbol $d_i^k(n)$, $n = 0,\ 1, \ldots,\ N-1$, represents the complex symbol to be

transmitted over subcarrier n by transmit antenna i during the kth OFDM symbol period. The matrix $\mathbf{D}$ is normalized to have average energy $\mathrm{E}\left[\|\mathbf{D}\|^2\right] = KNN_t$. At the kth OFDM block, the transmitter applies N-point IFFT over each column of the matrix $\mathbf{D}_k$, yielding an OFDM symbol of length T_{FFT}. In order to mitigate the effect of inter-symbol interference, a cyclic prefix of length T_{CP} is added to the output of the IFFT processor.

After adding the cyclic prefix and guard interval, the OFDM symbol is passed through a digital-to-analog converter, resulting in an analog baseband OFDM signal of duration $T_{SYM} = T_{FFT} + T_{CP} + T_{GI}$. The baseband OFDM signal to be transmitted by the ith transmit antenna at the kth OFDM block can be expressed as

$$x_i^k(t) = \sqrt{\frac{E}{N_t}} \sum_{n=0}^{N-1} d_i^k(n) \exp\left\{(\mathbf{j}2\pi n\Delta f)(t - T_{CP})\right\}, \qquad (3.3)$$

where $t \in [T_{CP},\ T_{FFT} + T_{CP}]$, $\mathbf{j} \triangleq \sqrt{-1}$, and $\Delta f = 1/T_{FFT} = BW/N$ is the frequency separation between two adjacent subcarriers. The factor $\sqrt{E/N_t}$ guarantees that the average energy per transmitted symbol is E, independent of the number of transmit antennas. In the interval $[0,\ T_{CP}]$, $x_i^k(t)$ is a copy of the last part of the OFDM symbol, and $x_i^k(t)$ is zero in the interval $[T_{FFT} + T_{CP},\ T_{SYM}]$.

The complex baseband signal $x_i^k(t)$ is filtered, up-converted to an RF signal with a carrier frequency f_c^k, and finally sent from the ith transmit antenna. The transmitted multiband OFDM signal at transmit antenna i over K OFDM symbol periods is given by

$$s_i(t) = \sum_{k=0}^{K-1} \mathrm{Re}\left\{x_i^k(t - k\,T_{SYM})\exp(\mathbf{j}2\pi f_c^k t)\right\}. \qquad (3.4)$$

The carrier frequency f_c^k specifies the subband, in which the signal is transmitted during the kth OFDM symbol period. The carrier frequency can be changed from
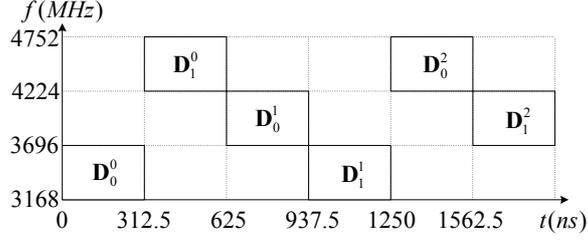
Figure 3.2: Time-frequency representation of multiband UWB symbols with $K = 2$ and fast band-hopping rate.

one OFDM block to another, so as to enable the frequency diversity while minimize the multiple access interference. The band hopping rate depends on the channel environment and the desired data rates. Since the signals from all transmit antennas share the same subband, f_c^k is identical for every transmit antenna. Note that the transmissions from all of the N_t transmit antennas are simultaneous and synchronous. Fig. 3.2 illustrates a time-frequency representation of the transmitted signal, which is based on a time-frequency code that has been proposed for the IEEE 802.15.3a standard [19]. In this example, the STF coding is performed across $K = 2$ consecutive OFDM blocks, and the superscript τ of $\mathbf{D}_k^\tau$ represents the index of STF codewords. Since N_b information bits are transmitted in KT_{SYM} seconds, the transmission rate (without channel coding) is $R = N_b/(KT_{SYM})$.

3.1.2 Channel Model

We consider a tap-delay line Nakagami-m fading channel model with L taps. At the kth OFDM block, the channel impulse response from the ith transmit antenna to the jth receive antenna can be described as

$$h_{ij}^k(t) = \sum_{l=0}^{L-1} \alpha_{ij}^k(l)\delta(t - \tau_l), \tag{3.5}$$

where $\alpha_{ij}^k(l)$ is the multipath gain coefficient, L denotes the number of resolvable paths, and τ_l represents the path delay of the lth path. The amplitude of the lth path, $|\alpha_{ij}^k(l)|$, is modeled as a Nakagami-m random variable with PDF given in (2.4) and average power $\Omega_l = \mathrm{E}\left[|\alpha_{ij}^k(l)|^2\right]$. The powers of the L paths are normalized such that $\sum_{l=0}^{L-1} \Omega_l = 1$. We assume that the time delay τ_l and the average power Ω_l are the same for every transmit-receive link. From (3.5), the channel frequency response is given by

$$H_{ij}^k(f) = \sum_{l=0}^{L-1} \alpha_{ij}^k(l) \exp(-\mathbf{j}2\pi f\tau_l). \tag{3.6}$$

3.1.3   Receiver Processing

The signal received at each receive antenna is a superposition of the N_t transmitted signals corrupted by additive white Gaussian noise. Assume that the receiver perfectly synchronizes to the band switching pattern. The received RF signal at each receive antenna is down-converted to a complex baseband signal, matched to the pulse waveform, and then sampled before passing through an OFDM demodulator. After the OFDM modulator discards the cyclic prefix and performs an N-point FFT, a maximum-likelihood detection is jointly performed across all N_r receive antennas. The choice of prefix length greater than the duration of the channel impulse response, i.e., $T_{CP} \geq \tau_{L-1}$, ensures that the interference between OFDM symbols is eliminated. Effectively, the frequency-selective fading channel decouples into a set of N parallel frequency-non-selective fading channels, whose fading coefficients are equal to the channel frequency response at the center frequency of the subcarriers. Therefore, the received signal at the nth subcarrier at

receive antenna j during the kth OFDM symbol duration can be expressed as

$$y_j^k(n) = \sqrt{\frac{E}{N_t}} \sum_{i=1}^{N_t} d_i^k(n) H_{ij}^k(n) + z_j^k(n), \qquad (3.7)$$

where

$$H_{ij}^k(n) = \sum_{l=0}^{L-1} \alpha_{ij}^k(l) \exp\left[-\mathbf{j}2\pi n \Delta f \tau_l\right] \qquad (3.8)$$

is the frequency response of the channel at subcarrier n between the ith transmit and the jth receive antenna during the kth OFDM block. In (3.7), $z_j^k(n)$ represents the noise sample at the nth subcarrier. We model $z_j^k(n)$ as complex Gaussian random variable with zero mean and a two-sided power spectral density of $N_0/2$.

For subsequent performance evaluation, we provide a matrix representation of (3.7) as follows. Based on the formulation in [34], we rewrite the received signal at receive antenna j in the matrix form as

$$\mathbf{Y}_j = \sqrt{\frac{E}{N_t}} \mathbf{S}_D \mathbf{H}_j + \mathbf{Z}_j, \qquad (3.9)$$

where $\mathbf{S}_D$ is a $KN \times KNN_t$ data matrix of a form

$$\mathbf{S}_D = \begin{bmatrix} \mathbf{S}_1 & \mathbf{S}_2 & \cdots & \mathbf{S}_{N_t} \end{bmatrix}, \qquad (3.10)$$

in which $\mathbf{S}_i$ is a $KN \times KN$ diagonal matrix whose main diagonal comprises the information to be sent from transmit antenna i. We format $\mathbf{S}_i$ as

$$\mathbf{S}_i = diag\left(\left[(\mathbf{d}_i^0)^T (\mathbf{d}_i^1)^T \cdots (\mathbf{d}_i^{K-1})^T\right]^T\right), \qquad (3.11)$$

where $diag(\mathbf{x})$ is a diagonal matrix with the elements of $\mathbf{x}$ on its main diagonal. The $KNN_t \times 1$ channel vector $\mathbf{H}_j$ is of a form

$$\mathbf{H}_j = \begin{bmatrix} \mathbf{H}_{1j}^T & \mathbf{H}_{2j}^T & \cdots & \mathbf{H}_{N_tj}^T \end{bmatrix}^T, \qquad (3.12)$$

where $\mathbf{H}_{ij} = \begin{bmatrix} H_{ij}^0(0) & \cdots & H_{ij}^0(N-1) & \cdots & H_{ij}^{K-1}(0) & \cdots & H_{ij}^{K-1}(N-1) \end{bmatrix}^T$. The received signal $\mathbf{Y}_j$ of size $KNN_r \times 1$ is given by $\mathbf{Y}_j = \begin{bmatrix} (\mathbf{y}_j^0)^T & (\mathbf{y}_j^1)^T & \cdots & (\mathbf{y}_j^{K-1})^T \end{bmatrix}^T$, in

which $\mathbf{y}_j^k$ is an $N \times 1$ vector whose n^{th} element is $y_j^k(n)$. The noise vector $\mathbf{Z}$ has the same form as $\mathbf{Y}$ by replacing $y_j^k(n)$ with $z_j^k(n)$.

We assume that the receiver has perfect knowledge of the channel state information, while the transmitter has no channel information. The receiver exploits a maximum likelihood decoder, where the decoding process is jointly performed on N_r receive signal vectors. The decision rule can be stated as

$$\hat{\mathbf{D}} = \arg \min_{\mathbf{D}} \sum_{j=1}^{N_r} \| \mathbf{Y}_j - \sqrt{\frac{E}{N_t}} \mathbf{S}_D \mathbf{H}_j \|^2. \tag{3.13}$$

3.2 Performance Analysis

In this section, we first present a general framework to analyze the performance of multiband MIMO coding for UWB communication systems. Then, we derive the average PEP of the proposed system under the Nakagami-m frequency-selective fading channel model. Finally, we quantify the performance criteria in terms of diversity order and coding gain, and determine the maximum achievable diversity advantage for such systems.

Suppose that $\mathbf{D}$ and $\hat{\mathbf{D}}$ are two distinct STF codewords. The PEP, denoted by P_e, is defined as the probability of erroneously decoding the STF codeword $\hat{\mathbf{D}}$ when $\mathbf{D}$ is transmitted. Let $\mathbf{S}_D$ and $\mathbf{S}_{\hat{D}}$ be two data matrices, related to the STF codewords $\mathbf{D}$ and $\hat{\mathbf{D}}$, respectively. Following the computation steps as in [7], the PEP conditioned on the channel matrix is given by

$$P_e|_{\mathbf{H}_j} = \mathrm{Q}\left(\sqrt{\frac{\rho}{2N_t} \sum_{j=1}^{N_r} \| (\mathbf{S}_D - \mathbf{S}_{\hat{D}}) \mathbf{H}_j \|^2} \right), \tag{3.14}$$

where $\rho = E/N_0$ is the average SNR at each receive antenna, and $\mathrm{Q}(x)$ is the Gaussian error function, $\mathrm{Q}(x) = \frac{1}{\sqrt{2\pi}} \int_x^\infty \exp(-\frac{s^2}{2}) ds$. The average PEP can be

obtained by calculating the expected value of the conditional PEP with respect to the distribution of $\gamma \triangleq \sum_{j=1}^{N_r} \left\| (\mathbf{S}_D - \mathbf{S}_{\hat{D}}) \, \mathbf{H}_j \right\|^2$, i.e.,

$$P_e = \int_0^\infty Q\left(\sqrt{\frac{\rho}{2N_t}} s \right) p_\gamma(s) ds, \tag{3.15}$$

where $p_\gamma(s)$ represents the PDF of γ.

For convenience, let us denote an $N_t N_r L K \times 1$ channel vector

$$\mathbf{a} = \left[\mathbf{a}_1^T, \ \mathbf{a}_2^T \ \cdots \ \mathbf{a}_{N_r}^T \right]^T, \tag{3.16}$$

where $\mathbf{a}_j$ contains the multipath gains from all transmit antennas to the jth receive antenna. The $N_t L K \times 1$ vector $\mathbf{a}_j$ is formatted as

$$\mathbf{a}_j = \left[(\mathbf{a}_{1j}^0)^T \ \cdots (\mathbf{a}_{N_t j}^0)^T \ \cdots \ (\mathbf{a}_{1j}^{K-1})^T \ \cdots (\mathbf{a}_{N_t j}^{K-1})^T \right]^T, \tag{3.17}$$

in which

$$\mathbf{a}_{ij}^k = \left[\alpha_{ij}^k(0) \ \alpha_{ij}^k(1) \ \cdots \ \alpha_{ij}^k(L-1) \right]^T. \tag{3.18}$$

According to (3.8) and (3.17), we can express (3.12) as

$$\mathbf{H}_j = (\mathbf{I}_{KN_t} \otimes \mathbf{W}) \mathbf{a}_j, \tag{3.19}$$

where $\otimes$ denotes the Kronecker product [76], $\mathbf{I}_M$ represents an $M \times M$ identity matrix, and $\mathbf{W}$ is an $N \times L$ Fourier matrix, defined as

$$\mathbf{W} = \begin{pmatrix} 1 & 1 & \cdots & 1 \\ \omega^{\tau_0} & \omega^{\tau_1} & \cdots & \omega^{\tau_{L-1}} \\ \vdots & \vdots & \ddots & \vdots \\ \omega^{(N-1)\tau_0} & \omega^{(N-1)\tau_1} & \cdots & \omega^{(N-1)\tau_{L-1}} \end{pmatrix}, \tag{3.20}$$

in which $\omega = \exp(-\mathbf{j} 2\pi \Delta f)$. As a consequence, γ can be expressed as

$$\gamma = \sum_{j=1}^{N_r} \left\| (\mathbf{S}_D - \mathbf{S}_{\hat{D}}) \, (\mathbf{I}_{KN_t} \otimes \mathbf{W}) \mathbf{a}_j \right\|^2. \tag{3.21}$$

We can see from (3.21) that the distribution of γ depends on the joint distribution of the multipath gain coefficients, $\alpha_{ij}^k(l)$.

In the sequel, we evaluate the average PEP of multi-antenna multiband UWB systems with $|\alpha_{ij}^k(l)|$ being Nakagami-m distributed. First, we analyze the performance of a system with independent fading. Such assumption allows us to characterize the performances of UWB systems with the diversity and the coding advantages. The performance of independent fading system also provides us a benchmark for subsequent performance comparisons. Then, we investigate the performance of a more realistic system, where the multipath gain coefficients are allowed to be correlated.

3.2.1 Independent Fading

Due to the band hopping, the K OFDM symbols in each STF codeword are sent over different subbands. With an ideal band hopping, we assume that the signal transmitted over K different frequency-bands undergo independent fading. We also assume that the path gains $\alpha_{ij}^k(l)$ are independent for different paths and different pairs of transmit and receive antennas, and that each transmit and receive link has the same power delay profile, i.e., $\mathrm{E}\left[|\alpha_{ij}^k(l)|^2\right] = \Omega_l$. The correlation matrix of $\mathbf{a}_j$ is given by

$$\mathrm{E}\left[\mathbf{a}_j \mathbf{a}_j^{\mathcal{H}}\right] = \mathbf{I}_{KN_t} \otimes \boldsymbol{\Omega}, \tag{3.22}$$

where $(\cdot)^{\mathcal{H}}$ denotes conjugate transpose operation, and $\boldsymbol{\Omega} = diag(\Omega_0, \Omega_1, \cdots, \Omega_{L-1})$ is an $L \times L$ matrix formed from the power of the L paths. Since the matrix $\boldsymbol{\Omega}$ is diagonal, we can define $\boldsymbol{\Omega}^{\frac{1}{2}} = diag\left(\sqrt{\Omega_0} \ \sqrt{\Omega_1} \cdots \ \sqrt{\Omega_{L-1}}\right)$ such that $\boldsymbol{\Omega} = \boldsymbol{\Omega}^{\frac{1}{2}} \boldsymbol{\Omega}^{\frac{1}{2}}$. Let $\mathbf{q}_j = (\mathbf{I}_{KN_t} \otimes \boldsymbol{\Omega}^{\frac{1}{2}})^{-1} \mathbf{a}^j$, then it is easy to see that the elements of $\mathbf{q}_j$ are identically independent distributed (iid) Nakagami-m random variables with normalized

power $\Omega = 1$. Substitute $\mathbf{a}_j = (\mathbf{I}_{KN_t} \otimes \mathbf{\Omega}^{\frac{1}{2}})\mathbf{q}_j$ into (3.21), and apply the property of Kronecker product, $(\mathbf{A}_1 \otimes \mathbf{B}_1)(\mathbf{A}_2 \otimes \mathbf{B}_2) = (\mathbf{A}_1\mathbf{A}_2) \otimes (\mathbf{B}_1\mathbf{B}_2)$ ([76] p.251), resulting in

$$\gamma = \sum_{j=1}^{N_r} \left\| (\mathbf{S}_D - \mathbf{S}_{\hat{D}}) \, (\mathbf{I}_{KN_t} \otimes \mathbf{W}\mathbf{\Omega}^{\frac{1}{2}})\mathbf{q}_j \right\|^2 = \sum_{j=1}^{N_r} \mathbf{q}_j^{\mathcal{H}} \mathbf{\Psi} \mathbf{q}_j, \qquad (3.23)$$

where

$$\mathbf{\Psi} = (\mathbf{I}_{KN_t} \otimes \mathbf{W}\mathbf{\Omega}^{\frac{1}{2}})^{\mathcal{H}}(\mathbf{S}_D - \mathbf{S}_{\hat{D}})^{\mathcal{H}}(\mathbf{S}_D - \mathbf{S}_{\hat{D}})(\mathbf{I}_{KN_t} \otimes \mathbf{W}\mathbf{\Omega}^{\frac{1}{2}}). \qquad (3.24)$$

Since $\mathbf{\Psi}$ is a Hermitian matrix of size $KN_tL \times KN_tL$, it can be decomposed into $\mathbf{\Psi} = \mathbf{V}\mathbf{\Lambda}\mathbf{V}^{\mathcal{H}}$, where $\mathbf{V} \triangleq [\mathbf{v}_1 \cdots \mathbf{v}_{KN_tL}]$ is a unitary matrix, and $\mathbf{\Lambda} = diag\{\lambda_1(\mathbf{\Psi}), \ldots, \lambda_{KN_tL}(\mathbf{\Psi})\}$ is a diagonal matrix whose diagonal elements are the eigenvalues of $\mathbf{\Psi}$. After some manipulations, we arrive at

$$\gamma = \sum_{j=1}^{N_r} \sum_{n=1}^{KN_tL} \lambda_n(\mathbf{\Psi})|\beta_{j,n}|^2, \qquad (3.25)$$

where $\beta_{j,n} \triangleq \mathbf{v}_n^{\mathcal{H}}\mathbf{q}_j$. Since $\mathbf{V}$ is unitary and the components of $\mathbf{q}_j$ are iid, $\{\beta_{j,n}\}$ are independent random variables, whose magnitudes are approximately Nakagami-$\tilde{m}$ distributed with parameter ([71] p.25)

$$\tilde{m} = \frac{KLN_tm}{KLN_tm - m + 1} \qquad (3.26)$$

and average power $\Omega = 1$. Hence, the PDF of $|\beta_{j,n}|^2$ approximately follows Gamma distribution ([78] p. 24)

$$p_{|\beta_{j,n}|^2}(x) = \frac{1}{\Gamma(\tilde{m})} \left(\frac{\tilde{m}}{\Omega}\right)^{\tilde{m}} x^{\tilde{m}-1} \exp\left(-\frac{\tilde{m}}{\Omega}x\right). \qquad (3.27)$$

Now, the average PEP can be obtained by substituting (3.25) into (3.14), and averaging (3.14) with respect to the distribution of $|\beta_{j,n}|^2$. To this end, we resort to an alternate representation of Q function [78], $Q(x) = \frac{1}{\pi} \int_0^{\pi/2} \exp(-\frac{x^2}{2\sin^2\theta})d\theta$ for

$x \geq 0$. This allows us to express (3.14) in term of the moment generating function (MGF) of γ, denoted by $\phi_\gamma(s)$, as

$$P_e = \frac{1}{\pi} \int_0^{\pi/2} \phi_\gamma \left(-\frac{\rho}{4N_t \sin^2 \theta} \right) d\theta. \tag{3.28}$$

Due to the fact that $\phi_{|\beta_{j,n}|^2}(s) = \left(1 - \frac{\Omega}{\tilde{m}} s \right)^{-\tilde{m}}$, and $|\beta_{j,n}|^2$ are independent, (3.28) can be written as

$$P_e = \frac{1}{\pi} \int_0^{\pi/2} \prod_{n=1}^{KLN_t} \left(1 + \frac{\rho}{4N_t \sin^2 \theta} \frac{\Omega}{\tilde{m}} \lambda_n(\boldsymbol{\Psi}) \right)^{-\tilde{m}N_r} d\theta. \tag{3.29}$$

At high SNR, the average PEP in (3.29) can be upper bounded by

$$P_e \leq \prod_{n=1}^{rank(\boldsymbol{\Psi})} \left(\frac{\rho}{4N_t} \frac{\Omega}{\tilde{m}} \lambda_n(\boldsymbol{\Psi}) \right)^{-\tilde{m}N_r}, \tag{3.30}$$

where $rank(\boldsymbol{\Psi})$ and $\{\lambda_n(\boldsymbol{\Psi})\}_{n=1}^{rank(\boldsymbol{\Psi})}$ are the rank and nonzero eigenvalues of matrix $\boldsymbol{\Psi}$, respectively. In this case, the exponent $\tilde{m}N_r rank(\boldsymbol{\Psi})$ determines the slope of the performance curve plotted as a function of SNR, whereas the product $\frac{\Omega}{\tilde{m}} \left(\prod_{n=1}^{rank(\boldsymbol{\Psi})} \lambda_n(\boldsymbol{\Psi}) \right)^{1/rank(\boldsymbol{\Psi})}$ displaces the curve. Therefore, the performance merits of STF coded multiband UWB system can be quantified by the minimum values of these two quantities over all pairs of distinct codewords as the diversity gain

$$G_d = \min_{\mathbf{D} \neq \hat{\mathbf{D}}} \tilde{m}N_r rank(\boldsymbol{\Psi}), \tag{3.31}$$

and the coding gain

$$G_c = \min_{\mathbf{D} \neq \hat{\mathbf{D}}} \frac{\Omega}{\tilde{m}} \left(\prod_{n=1}^{rank(\boldsymbol{\Psi})} \lambda_n(\boldsymbol{\Psi}) \right)^{\frac{1}{rank(\boldsymbol{\Psi})}}. \tag{3.32}$$

We note that (3.30) can also be derived from the Chernoff bound of the Q function.

In order to quantify the maximum achievable diversity gain, we calculate the rank of $\boldsymbol{\Psi}$ as follows. According to (4.11) and the rank property, we have

$$rank(\boldsymbol{\Psi}) = rank \left((\mathbf{S}_D - \mathbf{S}_{\hat{D}})(\mathbf{I}_{KN_t} \otimes \mathbf{W}\Omega^{1/2}) \right). \tag{3.33}$$

Observe that the size of $\mathbf{S}_D - \mathbf{S}_{\hat{D}}$ is $KN \times KNN_t$, whereas the size of $\mathbf{W}\Omega^{1/2}$ is $N \times L$. Therefore, the rank of matrix $\mathbf{\Psi}$ becomes $rank(\mathbf{\Psi}) \leq \min\{KN, KLN_t\}$. Hence, the maximum achievable diversity gain is

$$G_d^{max} = \min\{\tilde{m}KLN_tN_r, \tilde{m}KNN_r\}. \tag{3.34}$$

Note that the diversity gain in (3.34) depends on the parameter $\tilde{m}$ which is close to one for any fading parameter m. Indeed, for multiband UWB-MIMO systems,

$$\tilde{m} = (1 - \frac{1}{KLN_t} + \frac{1}{KLN_tm})^{-1} \approx 1. \tag{3.35}$$

For example,

- With $N_t = 2$, $K = 2$, $L = 10$, $m = 2$; $\tilde{m} = 1.01 \approx 1$.

- With $N_t = 2$, $K = 2$, $L = 10$, $m = 10$; $\tilde{m} = 1.02 \approx 1$.

- With $N_t = 2$, $K = 2$, $L = 20$, $m = 10$; $\tilde{m} = 1.01 \approx 1$.

In this case, the maximum achievable diversity gain is well approximated by

$$G_d^{max} = \min\{KLN_tN_r, KNN_r\}. \tag{3.36}$$

The result in the analysis above is somewhat surprising since the diversity gain of multiband UWB-MIMO system does not depend on the fading parameter m. The reason behind this is that $\beta_{j,n}$ in (3.25) is a normalized summation of KLN_t independent Nakagami random variables. When KLN_t is large enough, $\beta_{j,n}$ behaves like a complex Gaussian random variable, and hence the channel is like Rayleigh fading. Since the ultra-wide bandwidth results in a large number of multipath components, the effect of KLN_t on the diversity gain dominates the effect of fading parameter m, and $\tilde{m}$ is close to one for any m. This implies that the diversity

advantage does not depend on the severity of the fading. The diversity gain obtained under Nakagami fading with arbitrary m parameter is almost the same as that obtained in Rayleigh fading channels.

We emphasize here the major difference between the use of STF coding in the conventional OFDM systems and in the multiband OFDM systems. For STF coding in the conventional OFDM systems, the symbols are continuously transmitted in the same frequency-band. In this case, the temporal diversity relies on the temporal correlation of the channel, and hence the system performance depends on the time varying nature of the propagation channel [34]. In contrast, the diversity advantage in (3.36) reveals that by the use of band switching, the STF coded multiband UWB is able to achieve the diversity gain of $\min\{KLN_tN_r, KNN_r\}$, regardless of the channel time-correlation property.

It is worth noting that the proposed theoretical framework incorporates the analysis for ST or SF coded UWB systems as special cases. In case of single-carrier frequency-non-selective channel, i.e., $N = 1$ and $L = 1$, the performance of STF coded UWB system is similar to that of ST coded UWB system. In case of $K = 1$, i.e., when the coding is performed over one OFDM block, the STF coded UWB system performance is the same as that of SF coded scheme. The maximum achievable diversity reduces to $\min\{LN_tN_r, NN_r\}$. This reveals that as long as the K OFDM symbols are sent on different frequency-bands, coding across K OFDM blocks can offer the diversity advantage of K times larger than that from SF coding approach.

3.2.2 Correlated Fading

In this section, we investigate the performance of STF coded multiband UWB systems in correlated fading scenarios. From (3.21), we know that γ can be expressed as

$$\gamma = \mathbf{a}^{\mathcal{H}} \Big\{ \mathbf{I}_{N_r} \otimes \big[(\mathbf{I}_{KN_t} \otimes \mathbf{W}^{\mathcal{H}})(\mathbf{S}_D - \mathbf{S}_{\hat{D}})^{\mathcal{H}}$$
$$(\mathbf{S}_D - \mathbf{S}_{\hat{D}}) \, (\mathbf{I}_{KN_t} \otimes \mathbf{W}) \big] \Big\} \, \mathbf{a}. \tag{3.37}$$

To simplify the analysis, we assume that the channel correlation matrix, $\mathbf{R}_A = \mathrm{E}\big[\mathbf{a}\mathbf{a}^{\mathcal{H}}\big]$ is of full rank. Since $\mathbf{R}_A$ is positive definite Hermitian symmetric, it has a symmetric square root $\mathbf{U}$ such that $\mathbf{R} = \mathbf{U}^{\mathcal{H}}\mathbf{U}$, where $\mathbf{U}$ is also of full rank [76]. Let $\mathbf{q} = \mathbf{U}^{-1}\mathbf{a}$, then it follows that $\mathrm{E}\big[\mathbf{q}\mathbf{q}^{\mathcal{H}}\big] = \mathbf{I}_{KLN_tN_r}$, i.e., the components of $\mathbf{q}$ are uncorrelated. Substituting $\mathbf{a} = \mathbf{U}\mathbf{q}$ into (3.37), we have

$$\gamma = \mathbf{q}^{\mathcal{H}}\mathbf{\Phi}\mathbf{q}, \tag{3.38}$$

where $\mathbf{\Phi} = \mathbf{U}^{\mathcal{H}}\big\{\mathbf{I}_{N_r} \otimes \big[(\mathbf{I}_{KN_t} \otimes \mathbf{W}^{\mathcal{H}})(\mathbf{S}_D - \mathbf{S}_{\hat{D}})^{\mathcal{H}}(\mathbf{S}_D - \mathbf{S}_{\hat{D}})(\mathbf{I}_{KN_t} \otimes \mathbf{W})\big]\big\}\mathbf{U}$. Accordingly, performing an eigenvalue decomposition of the $KLN_tN_r \times KLN_tN_r$ Hermitian symmetric matrix $\mathbf{\Phi}$ results in $\mathbf{\Phi} = \mathbf{V}\mathbf{\Lambda}\mathbf{V}^{\mathcal{H}}$. Therefore, we can express (3.38) as

$$\gamma = \sum_{n=1}^{KLN_tN_r} \lambda_n(\mathbf{\Phi})|\beta_n|^2, \tag{3.39}$$

where $\beta_n \triangleq \mathbf{v}_n^{\mathcal{H}}\mathbf{q}$, $\mathbf{v}_n$'s and $\lambda_n(\mathbf{\Phi})$'s are the eigenvectors and the eigenvalues of matrix $\mathbf{\Phi}$. From (3.15) and (3.39), the PEP can be obtained by averaging the conditional PEP with respect to the joint distribution of $\{|\beta_n|^2\}$, i.e.

$$P_e = \int_0^\infty \cdots \int_0^\infty \mathrm{Q}\left(\sqrt{\frac{\rho}{2N_t}\sum_{n=1}^{M}\lambda_n(\mathbf{\Phi})s_n}\right)$$

$$p_{|\beta_1|^2\cdots|\beta_M|^2}(s_1,\ldots,s_M) \, ds_1 \, \cdots \, ds_M, \tag{3.40}$$
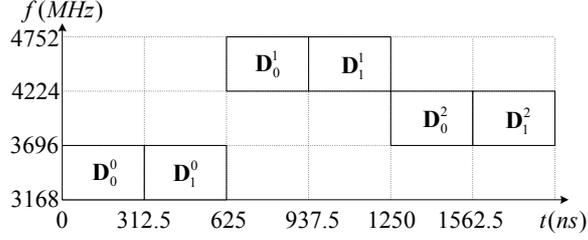
Figure 3.3: Time-frequency representation of multiband UWB symbols with $K = 2$ and slow band-hopping rate.

where $M = KLN_tN_r$. In general, β_n's for different n are not independent, and the closed-form solution for (3.40) is difficult, if not possible, to determine. In what follows, we will discuss two special cases where the average PEP in (3.40) can be further simplified.

Special case 1: *Constant fading*

We consider the situation when the MIMO channel stays constant over K OFDM blocks. This corresponds to the case when the modulated OFDM signal is transmitted continually over the same subband for entire K OFDM symbol periods. Fig. 3.3 illustrates such multiband signal with one of the time-frequency codes in the IEEE 802.15.3a standard proposal [19]. In this example, the STF coding is applied across $K = 2$ OFDM blocks and two OFDM symbols are sent on one subband before the band switching.

In this case, (3.21) can be re-expressed as

$$\gamma = \sum_{j=1}^{N_r} \left\| (\mathbf{C}_D - \mathbf{C}_{\hat{D}}) \left(\mathbf{I}_{N_t} \otimes \mathbf{W} \right) \tilde{\mathbf{a}}_j \right\|^2, \tag{3.41}$$

where $\mathbf{C}_D = \begin{bmatrix} \mathbf{C}_0^T & \mathbf{C}_1^T & \cdots & \mathbf{C}_{K-1}^T \end{bmatrix}^T$ is a $KN \times N_tN$ matrix, and $\mathbf{C}_k = \begin{bmatrix} diag(\mathbf{d}_1^k) & \cdots & diag(\mathbf{d}_{N_t}^k) \end{bmatrix}$. The channel vector $\tilde{\mathbf{a}}_j$ of size $LN_t \times 1$ is given by $\tilde{\mathbf{a}}_j = \begin{bmatrix} \mathbf{a}_{1j}^T & \mathbf{a}_{2j}^T & \cdots & \mathbf{a}_{N_tj}^T \end{bmatrix}^T$ in which $\mathbf{a}_{ij}$ is defined in (3.18). Since the path gains $\mathbf{a}_{ij}^k$'s are the same for every

k, $0 \leq k \leq K-1$, the time superscript index k is omitted to simplify the notations. Following the steps given previously, we can show that the average PEP is of a form similar to (3.40) with M replaced by LN_tN_r and $\{\lambda_n(\tilde{\mathbf{\Phi}})\}_{n=1}^{LN_tN_r}$ being the eigenvalues of the matrix $\tilde{\mathbf{\Phi}} = \tilde{\mathbf{U}}^{\mathcal{H}}\{\mathbf{I}_{N_r} \otimes [(\mathbf{I}_{N_t} \otimes \mathbf{W}^{\mathcal{H}})(\mathbf{C}_D - \mathbf{C}_{\hat{D}})^{\mathcal{H}}(\mathbf{C}_D - \mathbf{C}_{\hat{D}})(\mathbf{I}_{N_t} \otimes \mathbf{W})]\}\tilde{\mathbf{U}}$. Here, $\tilde{\mathbf{U}}$ is a symmetric square root of $\tilde{\mathbf{R}}_A = \mathrm{E}[\tilde{\mathbf{a}}\tilde{\mathbf{a}}^{\mathcal{H}}]$, in which $\tilde{\mathbf{a}} = [\tilde{\mathbf{a}}_1^T \ \tilde{\mathbf{a}}_2^T \ \cdots \ \tilde{\mathbf{a}}_{N_r}^T]^T$.

With a further assumption that the path gains are independent for every transmit-receive link, the average PEP can be obtained in a similar fashion to that derived in Section 3.2.1 as

$$P_e \leq \left[\prod_{n=1}^{rank(\mathbf{\Theta})} \left(\frac{\rho}{4N_t}\frac{\Omega}{\tilde{m}}\lambda_n(\mathbf{\Theta})\right)\right]^{-\tilde{m}N_r}, \tag{3.42}$$

where $\lambda_n(\mathbf{\Theta})$'s are the nonzero eigenvalues of the matrix $\mathbf{\Theta} = (\mathbf{I}_{N_t} \otimes \mathbf{W}^{\mathcal{H}})(\mathbf{C}_D - \mathbf{C}_{\hat{D}})^{\mathcal{H}}(\mathbf{C}_D - \mathbf{C}_{\hat{D}})(\mathbf{I}_{N_t} \otimes \mathbf{W})$. Observe that the maximum rank of $(\mathbf{C}_D - \mathbf{C}_{\hat{D}})(\mathbf{I}_{N_t} \otimes \mathbf{W})$ is $\min\{LN_t, KN\}$. In typical multiband OFDM systems, the number of subcarriers, N is larger than LN_t, hence the maximum achievable diversity gain of this system is LN_tN_r. Based on this observation, we can conclude that when K OFDM symbols are sent on one subband prior to band switching, coding across K OFDM blocks does not offer any additional diversity advantage compared to the coding scheme within one OFDM block.

Special case 2: *Fading parameter $m = 1$*

With $m = 1$, Nakagami is equivalent to Rayleigh distribution, and the path gain coefficients can be modeled as complex Gaussian random variables. Recall that for Gaussian random variables, uncorrelated implies independent. Thus, $\{|\beta_n|^2\}$ in (3.39) becomes a set of iid Rayleigh random variables. By using of MGF of γ,

the average PEP in (3.40) is given by

$$P_e = \frac{1}{\pi} \int_0^{\pi/2} \prod_{n=1}^{KLN_tN_r} \left(1 + \frac{\rho}{4N_t \sin^2 \theta} \lambda_n(\mathbf{\Phi}) \right)^{-1} d\theta. \qquad (3.43)$$

where $\mathbf{\Phi}$ is defined in (3.38). The PEP above can be upper-bounded by

$$P_e \leq \left[\prod_{n=1}^{KLN_tN_r} \left(\frac{\rho}{4N_t} \lambda_n(\mathbf{\Phi}) \right) \right]^{-1} \qquad (3.44)$$

at high SNR. Therefore, the diversity gain and the coding gain for this system are defined respectively as

$$G_d = \min_{\mathbf{D} \neq \hat{\mathbf{D}}} N_r rank(\mathbf{\Phi}), \qquad (3.45)$$

and

$$G_c = \min_{\mathbf{D} \neq \hat{\mathbf{D}}} \left(\prod_{n=1}^{rank(\mathbf{\Phi})} \lambda_n(\mathbf{\Phi}) \right)^{\frac{1}{rank(\mathbf{\Phi})}}. \qquad (3.46)$$

3.3 Simulation Results

To support the theoretical analysis given in the preceding sections, we perform simulations for multi-antenna multiband UWB systems employing various STF codes. Following the IEEE 802.15.3a standard proposal, our simulated multiband UWB system has $N = 128$ subcarriers and the bandwidth of each subband is $BW = 528$ MHz. Thus, the OFDM symbol is of duration $T_{FFT} = 128/(528$ MHz$) = 242.42$ ns. After adding the cyclic prefix of length $T_{CP} = 60.61$ ns and the guard interval of length $T_{GI} = 9.47$ ns, the symbol duration becomes $T_{SYM} = 312.5$ ns.

We simulated the STF coded multiband UWB systems in Nakagami-m fading environment. We employed the stochastic tapped-delay-line channel model in (3.5), where the path amplitudes $|\alpha_{ij}^k(l)|$ are Nakagami-m distributed and the phases
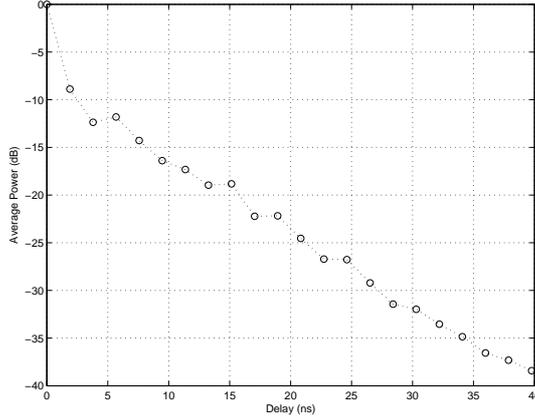
Figure 3.4: Power delay profile based on statistical channel model in [79].

$\angle \alpha_{ij}^k(l)$ are chosen uniformly from $[0, 2\pi)$. The path gain coefficients $\alpha_{ij}^k(l)$ for different i, j, and l are generated independently. The power delay profile, used to specify the path delays τ_l's and powers Ω_l's, follows the statistical model in [79], which is based on an extensive propagation study in residential environments. Fig. 3.4 shows the power delay profile of the simulated channel. Note that in our simulations, we normalize the total average power of the L paths to unity, i.e. $\sum_{l=0}^{L-1} \Omega_l = 1$.

In our simulations, the STF codeword $\mathbf{D} = \begin{bmatrix} \mathbf{D}_0^T & \mathbf{D}_1^T & \cdots & \mathbf{D}_{K-1}^T \end{bmatrix}^T$ in (4.40) is further simplified as

$$\mathbf{D}_k = \begin{bmatrix} \mathbf{G}_{k,1}^T & \mathbf{G}_{k,2}^T & \cdots & \mathbf{G}_{k,P}^T & \mathbf{0}_{(N-P\Upsilon N_t) \times N_t}^T \end{bmatrix}, \qquad (3.47)$$

in which Υ is a fixed integer ($\Upsilon \in \{1, 2, \ldots, L\}$), $P = \lfloor N/(\Upsilon N_t) \rfloor$, and $\mathbf{0}_{m \times n}$ stands for an $m \times n$ all-zero matrix. The code matrix $\mathbf{G}_{k,p}$ for $p = 1, 2, \ldots, P$ and $k = 0, 1, \ldots, K-1$ is of size $\Upsilon N_t \times N_t$. The code matrices $\{\mathbf{G}_{k,p}\}_{k=0}^{K-1}$ for each p are jointly designed, whereas the matrices $\mathbf{G}_{k,p}$ and $\mathbf{G}_{k',p'}$ with $p \neq p'$ are designed independently. Such code structures are able to provide the maximum achievable diversity, while enable low computational complexity [34].

63

Let us consider a system with two transmit antennas. Based on the repetition STF code in [34], $\mathbf{G}_{k,p}$ is given by

$$\mathbf{G}_{k,p} = (\mathbf{I}_{N_t} \otimes \mathbf{1}_{\Upsilon \times 1}) \begin{pmatrix} x_{p,1} & x_{p,2} \\ -x_{p,2}^* & x_{p,1}^* \end{pmatrix}, \qquad (3.48)$$

where $\mathbf{1}_{m \times n}$ denotes an $m \times n$ all-one matrix, and $x_{p,i}$'s are selected from BPSK or QPSK constellations. Note that $\mathbf{G}_{k,p}$ is the same for all k's. We also exploit a full-rate STF code [34], in which $\mathbf{G}_{k,p}$ is

$$\mathbf{G}_{k,p} = \sqrt{N_t} \begin{pmatrix} \mathbf{x}_{p,1}^k & \mathbf{0}_{\Upsilon \times 1} \\ \mathbf{0}_{\Upsilon \times 1} & \mathbf{x}_{p,2}^k \end{pmatrix}. \qquad (3.49)$$

In (4.48), $\mathbf{x}_{p,i}^k$ is a column vector of length Υ, whose elements are specified as follows. For notation convenience, we omit the subscript p and denote $\mathcal{L} = K\Upsilon N_t$. Let $\mathbf{s} = [s_1\ s_2\ \cdots\ s_{\mathcal{L}}]$ be a vector of BPSK or QPSK symbols. The $1 \times \mathcal{L}$ matrix $\mathbf{x} \triangleq \left[(\mathbf{x}_1^0)^T\ (\mathbf{x}_2^0)^T\ \ldots\ (\mathbf{x}_1^{K-1})^T\ (\mathbf{x}_2^{K-1})^T \right]$ is given by

$$\mathbf{x} = \frac{1}{\sqrt{K}}\ \mathbf{s}\ \mathbf{V}(\theta_1, \theta_2, \ldots, \theta_{\mathcal{L}}), \qquad (3.50)$$

in which $\mathbf{V}$ is a Vandermonde matrix[1] with $\theta_l = \exp(\mathbf{j}(4l-3)\pi/(2\mathcal{L}))$ for $\mathcal{L} = 2^s (s \geq 1)$ and $\theta_l = \exp(\mathbf{j}(6l-1)\pi/(3\mathcal{L}))$ for $\mathcal{L} = 2^s \cdot 3^t (s \geq 0, t \geq 1)$ [34]. We note that when $K = 1$, the repetition-coded and full-rate STF codes are reduced to those proposed for SF coding in [28]- [30], respectively. Unless specified otherwise, we apply a random permutation technique [30] so as to reduce the correlation in the channel frequency response among different subcarriers. This permutation strategy allows us to achieve larger coding advantage, and hence improve the system performance. Note that our simulation results are based on

---

[1]A Vandermonde matrix with variables θ_1, θ_2, $\ldots$, $\theta_{\mathcal{L}}$ is a $\mathcal{L} \times \mathcal{L}$ matrix whose l^{th} ($l = 1, 2, \ldots, \mathcal{L}$) row is defined as $[\theta_1^{l-1}\ \theta_2^{l-1}\ \cdots\ \theta_{\mathcal{L}}^{l-1}]$.
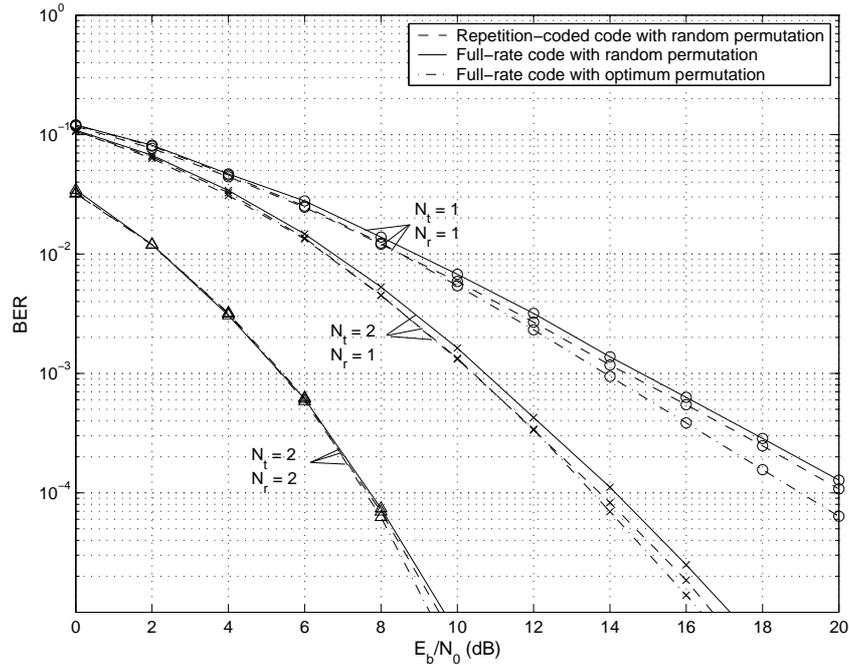
Figure 3.5: Performance of multiband UWB with different coding schemes ($K = 1$).

the uncoded information. The performance can be further improved by the use of channel coding, such as convolutional and Reed-Solomon codes [19].

In what follows, we present the average bit error rate (BER) curves of multiband UWB systems as functions of the average SNR per bit (E_b/N_0) in dB. In every case, the curves with circles ('o'), crosses ('x') and triangles ('△') show the performances of the systems with single transmit and single receive antennas, two transmit and one receive antennas, and two transmit and two receive antennas, respectively.

First, we consider the performance of coding approach over one OFDM block ($K = 1$). We utilize both repetition-coded and full-rate STF codes, each with spectral efficiency of 1 bit/s/Hz (omitting the prefix and guard interval). We use QPSK constellation for the repetition code and BPSK for the full-rate STF code. Both systems achieve the data rate (without channel coding) of 128 bits/(312.5 ns)
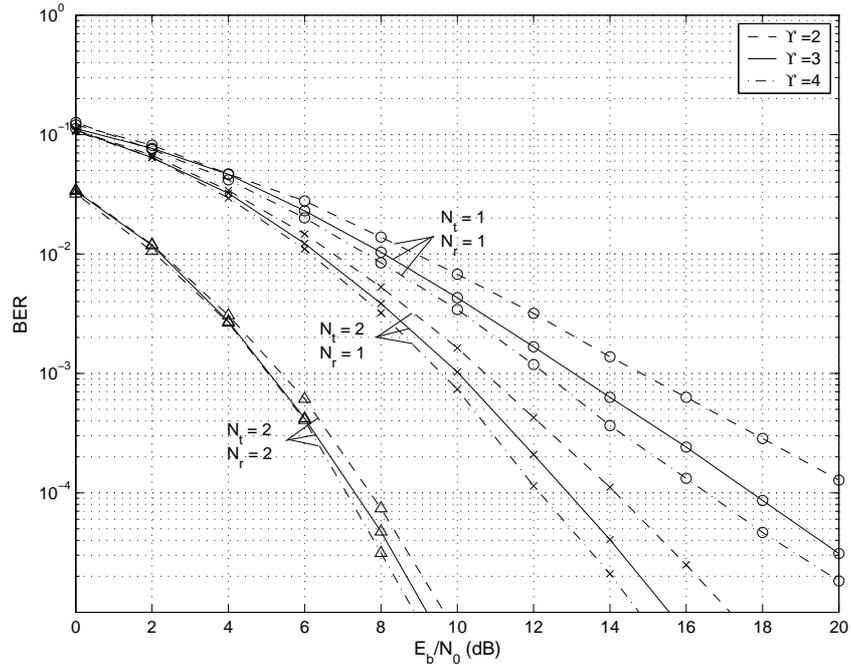
Figure 3.6: Performance of multiband UWB with different diversity orders.

= 409.6 Mbps. Fig. 3.5 depicts the performances of the STF coded UWB system with $\Upsilon = 2$. We observe that regardless of particular STF coding scheme, the spatial diversity gained from multi-antenna architecture does improve the system performance significantly. In addition, the performance can be further improved with the choice of STF codes and permutation schemes. In Fig. 3.6, we compare the performance of multiband UWB system with different frequency diversity orders. Here, we employ the full-rate code with $\Upsilon = 2$, 3, and 4. We can see that by increasing the number of jointly encoded subcarriers, the system performance can be improved. This observation is in accordance with our theoretical result in (3.30). Therefore, with a properly designed STF code, we can effectively exploit both spatial and frequency diversities in UWB environment.

Second, we compare the performances of STF coded multiband UWB system,
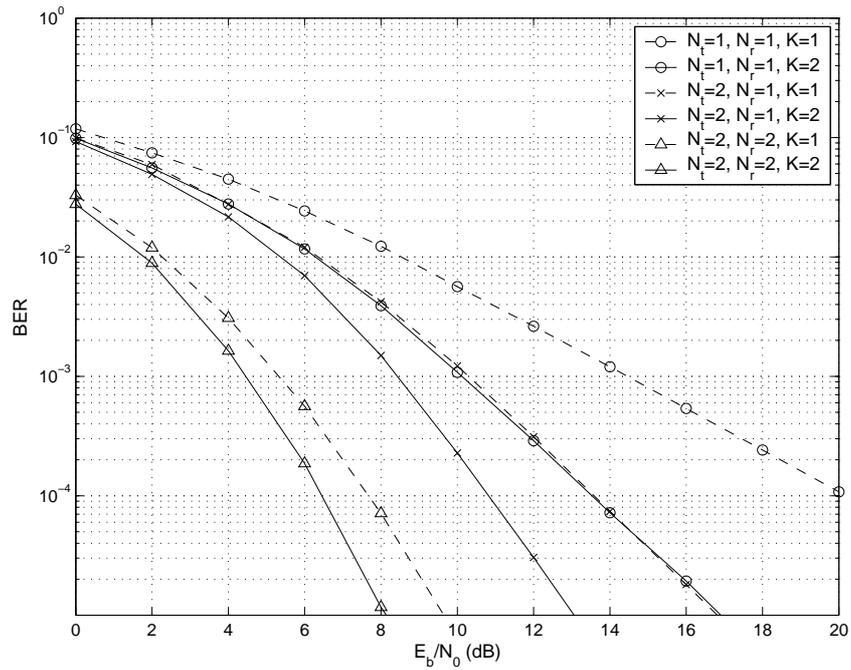
(a) Repetition codes, 0.5 bit/s/Hz
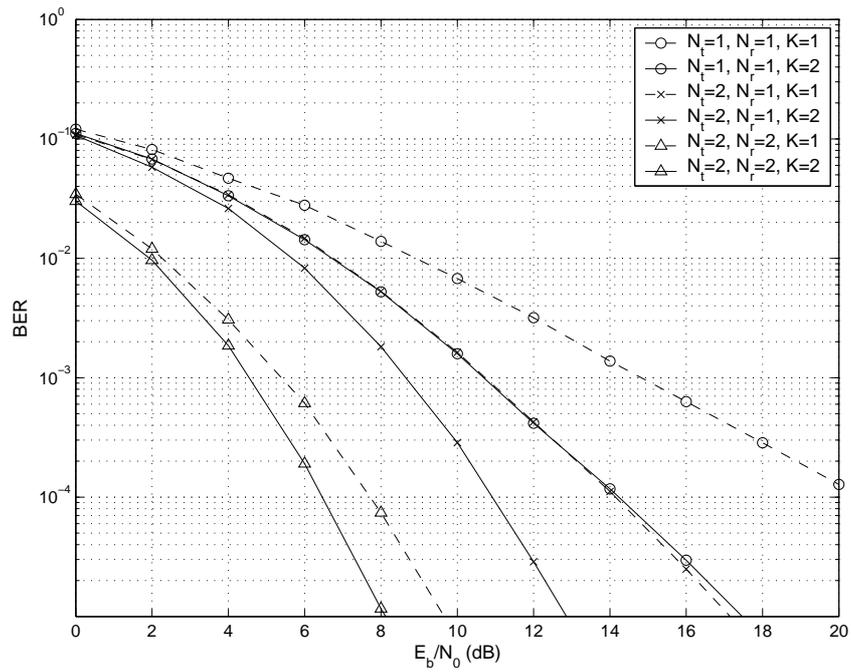
(b) Full-rate codes, 1 bit/s/Hz

Figure 3.7: Performance of multiband UWB with different time spreading factors.

in which the coding is performed over one and two OFDM blocks ($K = 1, 2$). We consider a scenario when two consecutive OFDM symbols are transmitted over different subbands, for instance, when the multiband signal has a time-frequency representation as in Fig. 3.2. The performances of the repetition and full-rate STF coded UWB systems with $\Upsilon = 2$ are shown in Figs. 3.7 (a) and 3.7 (b), respectively. The repetition code is constructed from BPSK constellation for $K = 1$ and QPSK for $K = 2$. Thus, the spectral efficiency of the resulting codes is 0.5 bit/s/Hz. The full-rate STF codes are generated from BPSK constellation for both $K = 1$ and 2, and their spectral efficiency is 1 bit/s/Hz. From both figures, it is apparent that by jointly coding over multiple OFDM blocks, STF coded UWB system has a BER performance curve that is steeper than that of UWB system without jointly encoding, i.e., the diversity advantage increases with the number of jointly encoded OFDM blocks. Such achieved improvement results from the band hopping rather than the temporal diversity. Hence, by coding across multiple OFDM blocks, the diversity order of STF coded band-hopping UWB increases significantly regardless of the temporal correlation of the channel. This supports our analytical results in the previous section that the diversity order of a STF coded multiband UWB system with fast band-hopping rate is increasing with K.

Finally, we compare the performance of multiband systems with different band-hopping rates. Fig. 3.8 depicts the performance of full-rate STF coded UWB system with $\Upsilon = 2$ and $K = 2$. Each STF codeword is transmitted during two OFDM block periods. We consider the cases when the two consecutive OFDM symbols are sent on different subband (fast band-hopping rate), and when they are continually transmitted on the same frequency-band (slow band-hopping rate). From Fig. 3.8, we observe the performance degradation when the band-hopping
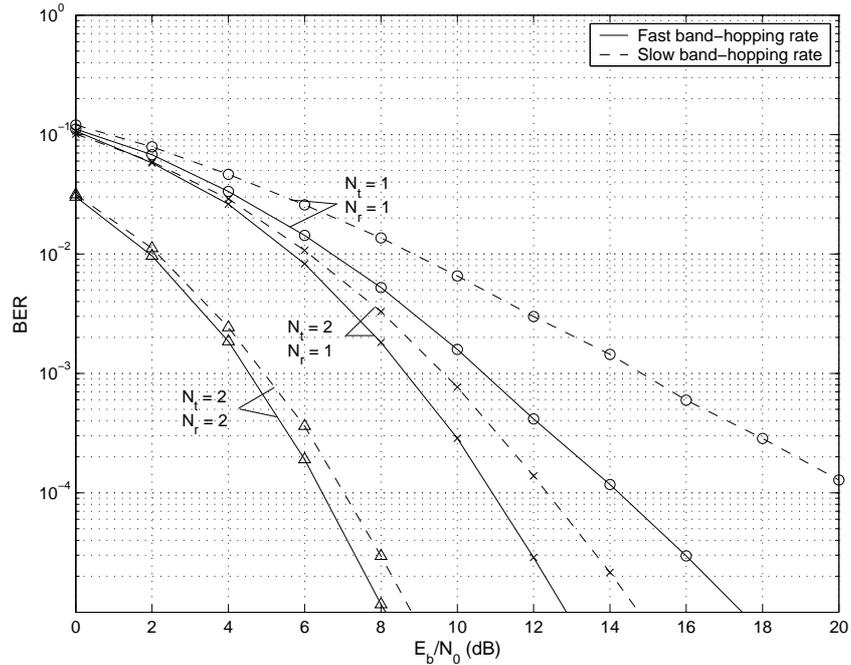
Figure 3.8: Performance of multiband UWB with different hopping rates.

rate decreases, which corresponds to the results in (3.30) and (3.42) that coding over multiple OFDM blocks will offer the additional diversity advantage when the STF coding is applied together with fast band-hopping scheme, i.e., the K OFDM symbols in each STF codeword are transmitted on various frequency-bands.

3.4   Chapter Summary

In conventional OFDM systems with N_t transmit and N_r receive antennas, STF coding across K OFDM blocks can lead to a maximum achievable diversity order of TLN_tN_r, where L is the number of resolvable paths and T is the rank of the temporal correlation matrix of the channel ($T \leq K$). In this chapter, we propose a multiband MIMO coding framework for UWB systems. By a technique of band

hopping in combination with jointly coding across spatial, temporal and frequency domains, the proposed scheme is able to exploit all available spatial and multipath diversities, richly inherent in UWB environments. From the theoretical results, we can draw some interesting conclusions as follows. First, the effect of Nakagami fading parameter m on the diversity gain is insignificant, and the diversity advantages obtained in Nakagami-m fading and Rayleigh fading channels are almost the same. Second, the maximum achievable diversity advantage of multiband UWB-MIMO system is KLN_tN_r. In contrast to the conventional OFDM, the factor K comes from the band hopping approach, which is regardless of the temporal correlation of the channel. The simulation results show that the employment of STF coding and band hopping techniques is able to increase the diversity advantage significantly, thereby considerably improving the system performance. In case of single-antenna system, increasing the number of jointly encoded OFDM blocks from one to two yields the performance improvement of 6 dB at a BER of 10^{-4}. By increasing also the number of transmit antennas from one to two, the proposed STF coded multiband UWB system has a total gain of 9 dB at a BER of 10^{-4}.

Chapter 4

Performance Characterization under Realistic Channel Scenarios

The ultra-wide bandwidth of UWB gives rise to important differences between UWB and narrowband channels, especially with respect to the number of resolvable paths and arrival times of multipath components [68]. In particular, the large bandwidth of UWB waveform considerably increases the ability of a receiver to resolve different reflections in UWB channels. As a result, the received signal contains a significant number of resolvable multipath components. Additionally, due to the fine time resolution of UWB waveform, the multipath components tend to occur in cluster rather than in a continuum, as is common for narrowband channels.

In recent years, performance analysis of UWB systems has been an area of considerable interest. There is a large number of papers dealing with the performance of UWB systems over additive white Gaussian noise (AWGN) as well as fading channels. For example, the performance of single-user time-hopping UWB system over multipath channel corrupted by AWGN was analyzed in [35]. The au-

thors in [36] evaluated the bit error probability of a time-hopping UWB system in AWGN channel with the presence of multiuser interference. Later in [39], the authors analyzed the average BER performance of multiuser direct-sequence UWB system over log-normal fading channel. The authors in [37] derived an explicit symbol error probability expression for UWB system employing RAKE receiver in multipath log-normal fading channels. In [40], the BER of time-hopping system in multipath Rayleigh fading channels was discussed. More recently, channel capacity and error probability performance of single-band multi-antenna UWB system over multipath Nakagami-m fading channels was analyzed in [56]. Further, the authors in [58] provided closed-form expressions for the average error probability of multiband UWB system under Nakagami-m fading channels.

Although a clustering phenomenon has been observed in several large data sets of UWB channel measurements [8], it has not been taken into consideration for the analysis due to the fact that random clustering behavior introduces the difficulty in evaluating the analytical performance. In fact, most of the existing works are based on the stochastic tapped-delay-line (STDL) models [7] used in conventional narrowband/wideband systems. However, performance analysis in STDL models is basically an extension of that for narrowband systems. More importantly, it does not reflect the multipath-rich nor random-clustering characteristics of UWB channels. To the best of our knowledge, none of the existing analysis is insightful in revealing the effect of the unique clustering characteristic on UWB system performances. In order to implement an efficient UWB system, it is vital to capture the behavior of UWB channels, which has been characterized by the S-V model [73].

In this chapter, we analyze the performance of the UWB systems employing multiband OFDM [18] by taking into account the multipath-rich and random-

clustering characteristics of UWB channels. Using the S-V model, we characterize the UWB performance in terms of cluster arrival rate, ray arrival rate, and cluster and ray decay factors. Two performance criteria we consider are PEP and outage probability. First, we provide an exact PEP formulation for single-antenna multiband UWB systems. Then, we establish an approximation approach, which allows us to obtain a closed-form PEP formulation and an explicit outage probability expression. It turns out that the uncoded UWB multiband OFDM system cannot gain from the multipath-clustering property of UWB channels. On the other hand, jointly encoding the data across subcarriers yields performance improvement, which strongly depends on cluster and ray arrival rates. Finally, we generalize the performance results to STF coded UWB-MIMO systems. The theoretical analysis reveals that the diversity gain does not severely rely on the clustering phenomenon of UWB channels, whereas the coding gain is in terms of both multipath arrival rates and decay factors. Simulation results are provided to support the theoretical analysis.

An outline of this chapter is as follows. A brief description of the channel model and system model under consideration are given in Section 4.1. In Section 4.2, the PEP and outage probability analysis is provided. First, an approximation technique is established and a new closed-form PEP formulation is obtained. Then, we present closed-form expressions for the probability density function (PDF) and outage probability of the combined signal-to-noise ratio over S-V fading scenarios. In Section 4.3, we characterize the performance of UWB-MIMO systems. Simulation results are presented in Section 4.4.

4.1 System Model

We consider a peer-to-peer UWB multiband OFDM system. Within each subband, the information is modulated using OFDM with N subcarriers. The channel model is based on the S-V model as described in (2.7). The path amplitude $|\alpha(c,l)|$ may follow the log-normal distribution [68], the Nakagami distribution [67], or the Rayleigh distribution [80], whereas the phase $\angle\alpha(c,l)$ is uniformly distributed over $[0, 2\pi)$. For analytical tractability and in order to obtain insight understanding of the UWB systems, we consider the scenario that the path amplitude $|\alpha(c,l)|$ is modeled as Rayleigh distribution [68], [80]. Specifically, the multipath gain coefficients $\alpha(c,l)$ are modeled as zero-mean, complex Gaussian random variables with variances $\Omega_{c,l}$ as specified in (2.10). The powers of the multipath components are normalized such that $\sum_{c=0}^{C} \sum_{l=0}^{L} \Omega_{c,l} = 1$. The channel parameters corresponding to different fading scenarios are specified in [68]. From (2.7), the channel frequency response is given by

$$H(f) = \sum_{c=0}^{C} \sum_{l=0}^{L} \alpha(c,l) \exp\left(-\mathbf{j}2\pi f(T_c + \tau_{c,l})\right). \qquad (4.1)$$

With the choice of cyclic prefix length greater than the duration of the channel impulse response, OFDM allows for each UWB subband to be divided into a set of N orthogonal narrowband channels. At the transmitter, an information sequence is partitioned into blocks. Each block is mapped onto an $N \times 1$ matrix $\mathbf{D} = [d(0)\ d(1)\ \cdots\ d(N-1)]^T$, where $d(n)$, $n = 0,\ 1,\ldots,\ N-1$, represents the complex channel symbol to be transmitted over subcarrier n. Suppose the information is jointly encoded across M ($1 \leq M \leq N$) subcarriers. Particularly, the data matrix $\mathbf{D}$ is a concatenation of $P = \lfloor N/M \rfloor$ data matrices as follows:

$$\mathbf{D} = \left[\ \mathbf{D}_0^T\ \ \mathbf{D}_1^T\ \ \cdots\ \ \mathbf{D}_{(P-1)}^T\ \ \mathbf{0}_{(N-PM)\times 1}\ \right]^T, \qquad (4.2)$$

74

where $\mathbf{D}_p$ is an $M \times 1$ data matrix defined as $\mathbf{D}_p = [d_p(0) \ d_p(1) \ \cdots \ d_p(M-1)]^T$ with $d_p(n) \triangleq d(p \ M + n)$ for $p = 0, 1, \ldots, P-1$, and $\mathbf{0}_{m \times n}$ stands for an $m \times n$ all-zero matrix. The data matrices $\mathbf{D}_p$ are independently designed for different p, and each data symbol $d_p(n)$ is normalized to have unit energy, i.e., the data matrix satisfies the energy constraint $\mathrm{E}\left[\|\mathbf{D}_p\|^2\right] = M$ for all p. The transmitter applies N-point IFFT to the matrix $\mathbf{D}$, appends a cyclic prefix and guard interval, up-converts to RF, and then sends the modulated signal at each subcarrier.

At the receiver, after matched filtering, removing the cyclic prefix, and applying FFT, the received signal at the nth subcarrier is given by

$$y(n) = \sqrt{E_s} \ d(n) \ H(n) + z(n), \tag{4.3}$$

where E_s is the average transmitted energy per symbol, $H(n)$ is the channel frequency response at the nth subcarrier, and $z(n)$ denotes the noise sample at the nth subcarrier. We model $z(n)$ as complex Gaussian random variable with zero mean and variance N_0. The channel frequency response can be specified as

$$H(n) = \sum_{c=0}^{C} \sum_{l=0}^{L} \alpha(c,l) \exp\left(-\mathbf{j}2\pi n \Delta f (T_c + \tau_{c,l})\right), \tag{4.4}$$

where $\Delta f = 1/T$ is the frequency separation between two adjacent subcarriers, and T is the OFDM symbol period. We assume that the channel state information $H(n)$ is known at the receiver, but not at the transmitter.

4.2   Performance Analysis

In this section, we present at first a general framework to analyze the PEP performance of UWB multiband OFDM systems. Then, using the S-V model, we characterize the average PEP of UWB systems in terms of multipath arrival rates

and decay factors. Finally, an outage probability formulation of UWB systems in S-V fading channel is provided.

4.2.1 Average PEP Analysis

For subsequent performance evaluation, we format the received signal in (4.3) in a vector form as

$$\mathbf{Y}_p = \sqrt{E_s} \, X(\mathbf{D}_p) \, \mathbf{H}_p + \mathbf{Z}_p, \tag{4.5}$$

where $X(\mathbf{D}_p) = diag\big(d_p(0), \, d_p(1), \ldots, \, d_p(M-1)\big)$ is an $M \times M$ diagonal matrix with the elements of $\mathbf{D}_p$ on its main diagonal. In (4.5), the channel matrix $\mathbf{H}_p$, the received signal matrix $\mathbf{Y}_p$, and the noise matrix $\mathbf{Z}_p$ are of the same forms as $\mathbf{D}_p$ by replacing d with H, y and z, respectively. The receiver exploits a maximum likelihood decoder, where the decoding process is jointly performed within each data matrix $\mathbf{D}_p$, and the decision rule can be stated as

$$\hat{\mathbf{D}}_p = \arg\min_{\mathbf{D}_p} \|\mathbf{Y}_p - \sqrt{E_s} \, X(\mathbf{D}_p) \, \mathbf{H}_p\|^2. \tag{4.6}$$

Suppose that $\mathbf{D}_p$ and $\hat{\mathbf{D}}_p$ are two distinct data matrices. Since the data matrices $\mathbf{D}_p$ for different p are independently en/decoded, for simplicity, the PEP can be defined as the probability of erroneously decoding the matrix $\hat{\mathbf{D}}_p$ when $\mathbf{D}_p$ is transmitted. Following the computation steps as in [7], the average PEP, denoted as P_e, is given by

$$P_e = \mathrm{E}\left[\mathrm{Q}\left(\sqrt{\frac{\rho}{2} \|\mathbf{\Delta}_p \, \mathbf{H}_p\|^2} \right) \right], \tag{4.7}$$

where $\rho = E_s/N_0$ is the average SNR, $\mathbf{\Delta}_p = X(\mathbf{D}_p) - X(\hat{\mathbf{D}}_p)$, and $\mathrm{Q}(x) = \frac{1}{\sqrt{2\pi}} \int_x^\infty \exp(-\frac{s^2}{2}) ds$ is the Gaussian error function. Denoting

$$\eta = \left\| \mathbf{\Delta}_p \, \mathbf{H}_p \right\|^2, \tag{4.8}$$

and using an alternate representation of Q function [81], $Q(x) = \frac{1}{\pi} \int_0^{\pi/2} \exp(-\frac{x^2}{2\sin^2\theta}) d\theta$ for $x \geq 0$, the average PEP in (4.7) can be expressed as

$$P_e = \frac{1}{\pi} \int_0^{\pi/2} \mathcal{M}_\eta \left(-\frac{\rho}{4\sin^2\theta}\right) d\theta, \tag{4.9}$$

where $\mathcal{M}_\eta(s) = \mathrm{E}[\exp(s\eta)]$ represents the MGF of η [81]. From (4.9), we can see that the remaining problem is to obtain the MGF $\mathcal{M}_\eta(s)$.

For convenience, let us denote a $(C+1)(L+1) \times 1$ channel matrix $\mathbf{A} = [\alpha(0,0) \cdots \alpha(0,L) \cdots \alpha(C,0) \cdots \alpha(C,L)]^T$. According to (4.4), $\mathbf{H}_p$ can be decomposed as $\mathbf{H}_p = \mathbf{W}_p \cdot \mathbf{A}$, where $\mathbf{W}_p = [\mathbf{w}_{p,0}^T \ \mathbf{w}_{p,1}^T \cdots \ \mathbf{w}_{p,M-1}^T]^T$ is an $M \times (C+1)(L+1)$ matrix, in which $\mathbf{w}_{p,n} = [\omega_{p,n}^{T_0+\tau_{0,0}} \ \omega_{p,n}^{T_0+\tau_{0,1}} \ \cdots \ \omega_{p,n}^{T_C+\tau_{C,L}}]^T$ and $\omega_{p,n} \triangleq \exp(-\mathbf{j}2\pi\Delta f(pM+n))$. After some manipulations, we can rewrite η in (4.8) as

$$\eta = \sum_{n=1}^M \mathrm{eig}_n(\boldsymbol{\Psi})|\beta_n|^2, \tag{4.10}$$

where β_n are iid complex Gaussian random variables with zero mean and unit variance, and $\mathrm{eig}_n(\boldsymbol{\Psi})$ are the eigenvalues of the matrix

$$\boldsymbol{\Psi} = \|\boldsymbol{\Delta}_p \mathbf{W}_p \boldsymbol{\Omega}^{\frac{1}{2}}\|^2, \tag{4.11}$$

in which $\boldsymbol{\Omega} = diag(\Omega_{0,0}, \ \Omega_{0,1}, \ldots, \ \Omega_{C,L})$ is a diagonal matrix formed from the average powers of multipath components. Thus, the MGF of η in (4.10) can be given by

$$\mathcal{M}_\eta(s) = \mathrm{E}\left[\prod_{n=1}^M (1 - s \ \mathrm{eig}_n(\boldsymbol{\Psi}))^{-1}\right]. \tag{4.12}$$

Observe that the eigenvalues $\mathrm{eig}_n(\boldsymbol{\Psi})$ depend on T_c and $\tau_{c,l}$ which are based on Poisson process. In general, it is difficult, if not possible, to determine $\mathcal{M}_\eta(s)$ in (4.12). However, for uncoded multiband system, i.e., when the number of jointly encoded subcarriers is $M = 1$, we can get a closed-form.

In case of no coding, the eigenvalue of matrix $\boldsymbol{\Psi}$ in (4.11) is $\text{eig}(\boldsymbol{\Psi}) = |d - \hat{d}|^2 \text{ eig}(\mathbf{W}_p \boldsymbol{\Omega} \mathbf{W}_p^{\mathcal{H}}) = |d - \hat{d}|^2$, in which $(\cdot)^{\mathcal{H}}$ denotes conjugate transpose operation, and the second equality follows from the fact that the matrix $\mathbf{W}_p \boldsymbol{\Omega} \mathbf{W}_p^{\mathcal{H}} = \sum_{c=0}^{C} \sum_{l=0}^{L} \Omega_{c,l} = 1$. By substituting $\text{eig}(\boldsymbol{\Psi}) = |d - \hat{d}|^2$ into (4.12), and then substituting the resulting MGF into (4.9), we arrive at the following result.

Theorem 4.1. *When there is no coding across subcarriers, the average PEP of a UWB system employing multiband OFDM is given by*

$$P_e = \frac{1}{\pi} \int_0^{\pi/2} \left(1 + \frac{\rho}{4 \sin^2 \theta} |d - \hat{d}|^2\right)^{-1} d\theta, \qquad (4.13)$$

for any channel model parameters.

The result in Theorem 4.1 is somewhat surprising since the performance of uncoded multiband UWB system does not depend on multipath arrival rates or decay factors. In addition, the performance of UWB system is the same as that of narrowband system in Rayleigh fading environment [81]. This implies that we cannot gain from the rich multipath-clustering property of UWB channels if the data is not encoded across subcarriers.

4.2.2 Approximate PEP Formulation

In this subsection, we establish a PEP approximation which allows us to obtain insightful understanding of the UWB systems when the information is jointly encoded across subcarriers.

According to ([82], p.29), the quadratic form in a zero-mean Gaussian random vector $\mathbf{x} = [x_1, \ldots, x_M]^T$ can be represented by a weighted summation of $|v_n|^2$, where v_n are mutually independent standard Gaussian random variables, and the

weights are the eigenvalues of the covariance matrix of $\mathbf{x}$. Observe from (4.8) that $\eta = (\boldsymbol{\Delta}_p \mathbf{H}_p)^{\mathcal{H}} \boldsymbol{\Delta}_p \mathbf{H}_p$ is in the quadratic form and $\mathrm{E}\left[\boldsymbol{\Delta}_p \mathbf{H}_p\right] = \mathbf{0}$. Therefore, using the representation of the quadratic form in ([82], p.29), we can approximate η as

$$\eta \approx \sum_{n=1}^{M} \mathrm{eig}_n(\boldsymbol{\Phi})|\mu_n|^2, \tag{4.14}$$

where μ_n are iid zero-mean Gaussian random variables with unit variance, and

$$\boldsymbol{\Phi} = \mathrm{E}\left[\boldsymbol{\Delta}_p \mathbf{H}_p (\boldsymbol{\Delta}_p \mathbf{H}_p)^{\mathcal{H}}\right] = \boldsymbol{\Delta}_p \mathbf{R}_M \boldsymbol{\Delta}_p^{\mathcal{H}}, \tag{4.15}$$

in which $\mathbf{R}_M = \mathrm{E}\left[\mathbf{H}_p \mathbf{H}_p^{\mathcal{H}}\right]$ is an $M \times M$ correlation matrix. Let the eigenvalues, $\mathrm{eig}_n(\boldsymbol{\Phi})$, be arranged in a non-increasing order as: $\mathrm{eig}_1(\boldsymbol{\Phi}) \geq \mathrm{eig}_2(\boldsymbol{\Phi}) \cdots \geq \mathrm{eig}_M(\boldsymbol{\Phi})$. By Ostrowski's theorem ([76], p.224), the eigenvalues of $\boldsymbol{\Phi}$ are given by

$$\mathrm{eig}_n(\boldsymbol{\Phi}) = \mathrm{eig}_n(\boldsymbol{\Delta}_p \mathbf{R}_M \boldsymbol{\Delta}_p^{\mathcal{H}}) = \nu_n \mathrm{eig}_n(\mathbf{R}_M), \tag{4.16}$$

where ν_n is a nonnegative real number that satisfies $\mathrm{eig}_M(\boldsymbol{\Delta}_p \boldsymbol{\Delta}_p^{\mathcal{H}}) \leq \nu_n \leq \mathrm{eig}_1(\boldsymbol{\Delta}_p \boldsymbol{\Delta}_p^{\mathcal{H}})$ for $n = 1, 2, \ldots, M$. From (4.14) and (4.16), we can approximate the MGF in (4.12) as

$$\mathcal{M}_\eta(s) \approx \prod_{n=1}^{M} \frac{1}{1 - s\nu_n \mathrm{eig}_n(\mathbf{R}_M)}. \tag{4.17}$$

Now, the remaining problem is to determine the matrix $\mathbf{R}_M$. We observe that the $(n, n')^{th}$ entry of the matrix $\mathbf{R}_M$ is $\mathrm{E}\left[H(n)H(n')^*\right]$ for $0 \leq n, n' \leq M - 1$. The elements on the main diagonal of $\mathbf{R}_M$ are given by

$$R(n, n) = \mathrm{E}\left[|H(n)|^2\right] = \sum_{c=0}^{C} \sum_{l=0}^{L} \mathrm{E}\left[|\alpha(c, l)|^2\right] = 1. \tag{4.18}$$

The off-diagonal elements of $\mathbf{R}_M$, $R(n, n')$ for $n \neq n'$, can be evaluated as follows:

$$
\begin{aligned}
R(n, n') &= \mathrm{E}\left[H(n)H(n')^*\right] \\
&= \sum_{c=0}^{C}\sum_{l=0}^{L} \mathrm{E}\left[\mathrm{E}\left[|\alpha(c,l)|^2\right]\exp(-\mathbf{j}2\pi(n-n')\Delta f(T_c + \tau_{c,l}))\right] \\
&\triangleq R(n - n').
\end{aligned}
\tag{4.19}
$$

Substitute (2.10) into (4.19), resulting in

$$
R(m) = \sum_{c=0}^{C}\sum_{l=0}^{L}\Omega_{0,0}G_{c,l}(m),
\tag{4.20}
$$

where

$$
G_{c,l}(m) = \mathrm{E}\left[\exp\left(-g\left(\frac{1}{\Gamma}, m\right)T_c - g\left(\frac{1}{\gamma}, m\right)\tau_{c,l}\right)\right],
\tag{4.21}
$$

and $g(a, m) \triangleq a + \mathbf{j}2\pi m\Delta f$.

To calculate $G_{c,l}(m)$ in (4.21), we denote x_i as an inter-arrival time between clusters i and $i - 1$. According to the Poisson distribution of the cluster delays, x_i can be modeled as iid exponential random variables with parameter Λ, and the delay of the cth cluster, T_c, can be expressed as $T_c = \sum_{i=0}^{c} x_i$. Similarly, let $v_{c,j}$ denote an inter-arrival time between rays j and $j-1$ in the cth cluster. We can also model $v_{c,j}$ as iid exponential random variables with parameter λ, and the delay of the lth path within cluster c can be given by $\tau_{c,l} = \sum_{j=0}^{l} v_{c,j}$. By re-writing $G_{c,l}(m)$ in terms of x_i and $v_{c,j}$, (4.21) can be simplified to

$$
\begin{aligned}
G_{c,l}(m) &= \mathrm{E}\left[\prod_{i=0}^{c}\exp\left(-g\left(\frac{1}{\Gamma}, m\right)x_i\right)\right]\mathrm{E}\left[\prod_{j=0}^{l}\exp\left(-g\left(\frac{1}{\gamma}, m\right)v_{c,j}\right)\right] \\
&= \left(\frac{\Lambda}{\Lambda + g(\frac{1}{\Gamma}, m)}\right)^c\left(\frac{\lambda}{\lambda + g(\frac{1}{\gamma}, m)}\right)^l.
\end{aligned}
\tag{4.22}
$$

Substitute (4.22) into (4.20), and use the fact that for UWB channels, the number of clusters C and the number of rays L are generally large. Then, we obtain

$$
R(m) = \Omega_{0,0}\frac{\Lambda + g(\frac{1}{\Gamma}, m)}{g(\frac{1}{\Gamma}, m)}\frac{\lambda + g(\frac{1}{\gamma}, m)}{g(\frac{1}{\gamma}, m)}.
\tag{4.23}
$$

Finally, by substituting (4.17) into (4.9), we can characterize the multiband UWB performance as follows.

Theorem 4.2. *When the information is jointly encoded across M $(1 \leq M \leq N)$ subcarriers, the average PEP of a multiband UWB system can be approximated as*

$$P_e \approx \frac{1}{\pi} \int_0^{\pi/2} \prod_{n=1}^{M} \left(1 + \frac{\rho \, \nu_n}{4 \sin^2 \theta} eig_n(\mathbf{R}_M)\right)^{-1} d\theta, \qquad (4.24)$$

where the $M \times M$ matrix $\mathbf{R}_M$ is given by

$$\mathbf{R}_M = \begin{pmatrix} 1 & R(1)^* & \cdots & R(M-1)^* \\ R(1) & 1 & \cdots & R(M-2)^* \\ \vdots & \vdots & \ddots & \vdots \\ R(M-1) & R(M-2) & \cdots & 1 \end{pmatrix}_{M \times M}, \qquad (4.25)$$

and $R(m)$ for $m = 1, 2, \ldots, M-1$ are defined in (6.11).

It is worth noting that the result in Theorem 4.2 can be straightforwardly extended to the case when interleaving or permutation over different subcarriers is applied. To be specific, if the data matrix is permuted such that the data symbol $d_p(n)$ is transmitted in subcarrier $\sigma_p(n)$ instead of subcarrier n, then the PEP performance of the permuted data matrix is of the same form as (4.24) with the off-diagonal elements of matrix $\mathbf{R}_M$ replaced by $R(n, n') = R(\sigma_p(n) - \sigma_p(n'))$.

In the sequel, we discuss the PEP approximations in Theorem 4.2 for two special cases to get some insightful understanding.

1. In case of no coding, i.e., $M = 1$, the correlation matrix in (4.25) becomes $\mathbf{R}_1 = 1$, and $\nu_1 = |d - \hat{d}|^2$. Thus, the PEP can be obtained from (4.24) as

$$P_e \approx \frac{1}{\pi} \int_0^{\pi/2} \left(1 + \frac{\rho}{4 \sin^2 \theta} |d - \hat{d}|^2\right)^{-1} d\theta, \qquad (4.26)$$

which is consistent with the exact PEP given in (4.13).

2. When the information is jointly encoded across 2 subcarriers, i.e., $M = 2$, the eigenvalues of matrix $\mathbf{R}_2$ are $1+|R(1)|$ and $1-|R(1)|$. Substituting these eigenvalues into (4.24), we obtain the approximate PEP

$$P_e \approx \frac{1}{\pi} \int_0^{\pi/2} \left(1 + \frac{\rho J + \rho^2 \nu_1 \nu_2 (1 - B^2)}{16 \sin^4 \theta} \right)^{-1} d\theta, \qquad (4.27)$$

where $J = 4 \sin^2 \theta \left[\nu_1 + \nu_2 + B(\nu_1 - \nu_2) \right]$ and

$$B = \Omega_{0,0} \frac{\left[(\Lambda + \frac{1}{\Gamma})^2 + b \right]^{\frac{1}{2}} \left[(\lambda + \frac{1}{\gamma})^2 + b \right]^{\frac{1}{2}}}{\left[(\frac{1}{\Gamma})^2 + b \right]^{\frac{1}{2}} \left[(\frac{1}{\gamma})^2 + b \right]^{\frac{1}{2}}}, \qquad (4.28)$$

and $b = (2\pi \Delta f)^2$. In UWB system, b is normally much less than $\frac{1}{\gamma^2}$ and $\frac{1}{\Gamma^2}$. Hence, (4.28) can be approximated by

$$B \approx \Omega_{0,0}(\Lambda\Gamma + 1)(\lambda\gamma + 1). \qquad (4.29)$$

Observe that for the uncoded multiband UWB system, the performance does not depend on the clustering characteristic. However, in case of jointly encoding across multiple subcarriers, the PEP in (4.24) reveals that the multiband UWB performance depends on the correlations in the frequency response among different subcarriers, $R(m)$, which in turn relate to the path arrival rates and decay factors. Specifically, if the number of jointly encoded subcarriers is $M = 2$, the result in (4.27) brings out that the UWB performance is related to the channel model parameters through the factor B defined in (4.28). This means the performance of multiband UWB system depends on both cluster and ray arrival rates as well as their decay factors. In a short-range (0-4 meters) line-of-sight environment, e.g. scenario for channel model 1 [68], the product of the cluster arrival rate and cluster decay factor can be much less than one ($\Lambda\Gamma \ll 1$). In such situation, (4.29) can be further simplified to $B \approx \Omega_{0,0}(\lambda\gamma + 1)$, which implies that the performance severely depends only on the ray arrival rate and ray decay factor. The intuition

behind this result is that when both cluster arrival rate and cluster decay factor are small, the effect of the first cluster will dominate. Hence, the performance can be approximated by taking into consideration only the first cluster. On the other hand, when both ray arrival rate and ray decay factor are small such that the product of these two parameters is much less than one ($\lambda\gamma \ll 1$), (4.29) reduces to $B \approx \Omega_{0,0}(\Lambda\Gamma + 1)$, which indicates that only the first path in each cluster seriously affects the performance.

For instance, suppose each data symbol d is transmitted repeatedly in two sub-carriers, and channel model parameters follow those specified in the IEEE 802.15.3a channel modeling report [68]. Let $\nu = |d - \hat{d}|^2$ and $\Delta f = 4.125$ MHz, then the approximate PEP can be obtained from (4.27) as follows:

- In case of CM 1, $\Lambda = 0.0233$, $\lambda = 2.5$, $\Gamma = 7.1$, $\gamma = 4.3$, $\Omega_{0,0} = 0.0727$:

$$B = 0.9852 \text{ and } P_e \approx \frac{1}{\pi} \int_0^{\frac{\pi}{2}} \left(1 + \frac{0.0294\rho^2\nu^2}{16\sin^4\theta} \right)^{-1} d\theta.$$

- In case of CM 4, $\Lambda = 0.0667$, $\lambda = 2.1$, $\Gamma = 24$, $\gamma = 12$, $\Omega_{0,0} = 0.0147$:

$$B = 0.8351 \text{ and } P_e \approx \frac{1}{\pi} \int_0^{\frac{\pi}{2}} \left(1 + \frac{0.3026\rho^2\nu^2}{16\sin^4\theta} \right)^{-1} d\theta.$$

We can see from the above examples that UWB performance in CM 4 is better than that in CM 1. This comes from the fact that the multipath components in CM 4 are more random than those in CM 1 (as illustrated in Fig. 4.1, which implies that compared with CM 1, CM 4 has less correlation in the frequency response among different subcarriers, and hence yields better performance.
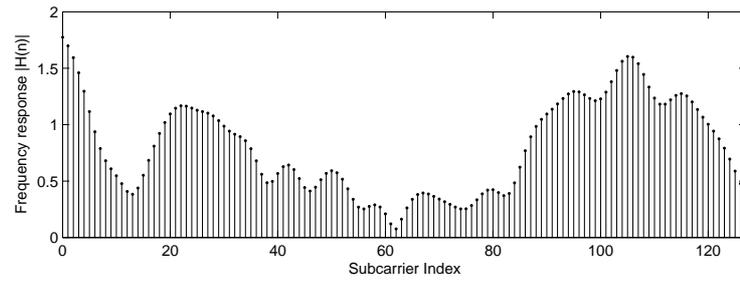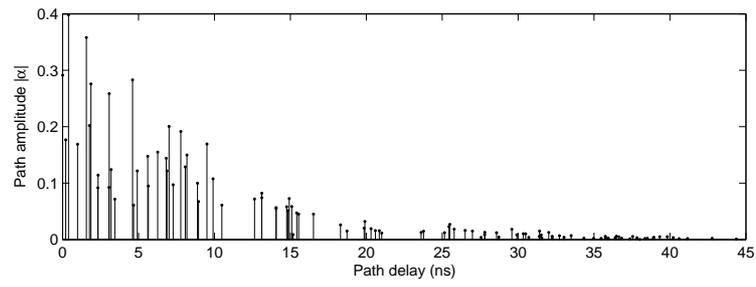
(a) Channel Model 1
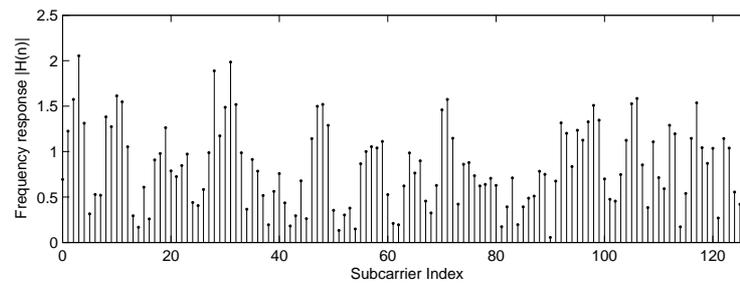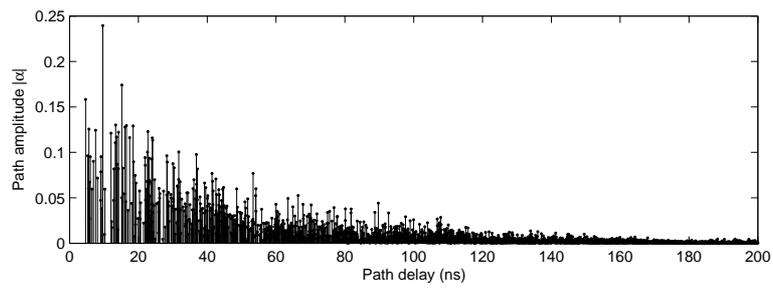
(b) Channel Model 4

Figure 4.1: One realization of UWB channel generated using the parameters for CM 1 and CM 4

4.2.3 Outage Probability

In this subsection, we consider the outage probability analysis for the multiband UWB system with the S-V fading model. The outage probability [81] is defined as the probability that the combined SNR, ζ, falls below a specified threshold, ζ_o, namely $P_{\text{out}} = P\left(\zeta \leq \zeta_o\right) = \int_0^{\zeta_o} p_\zeta(x)dx$, where $p_\zeta(x)$ denotes the PDF of ζ. Since the information is jointly en/decoded for each data matrix $\mathbf{D}_p$, the combined SNR can be defined as

$$\zeta = \frac{E_s \|X(\mathbf{D}_p)\mathbf{H}_p\|^2}{\mathrm{E}\left[\|\mathbf{Z}_p\|^2\right]} = \frac{\rho}{M} \sum_{n=0}^{M-1} |H_p(n)|^2, \tag{4.30}$$

in which $\rho = E_s/N_0$ as defined previously. Denote $\xi = \sum_{n=0}^{M-1} |H_p(n)|^2$, then the outage probability can be expressed as

$$P_{\text{out}} = P\left(\xi \leq \frac{M\zeta_o}{\rho}\right) = \int_0^{\frac{M\zeta_o}{\rho}} p_\xi(x)dx. \tag{4.31}$$

To determine the PDF $p_\xi(x)$, we first obtain the MGF of ξ from the MGF $\mathcal{M}_\eta(s)$ in (4.12) by replacing $\boldsymbol{\Delta}_p$ with an identity matrix. According to (4.11) and (4.12), $\mathcal{M}_\xi(s)$ for the case of no coding can be simply given by $\mathcal{M}_\xi(s) = \mathrm{E}\big[(1 - s\mathbf{W}_p\boldsymbol{\Omega}\mathbf{W}_p^{\mathcal{H}})^{-1}\big] = (1-s)^{-1}$, of which the corresponding PDF is $p_\xi(x) = \exp(-x)$ for $x \geq 0$ ([81], p.22). In case of jointly encoding across subcarriers, the MGF $\mathcal{M}_\xi(s)$ can be obtained from the approximation approach in Section 4.2.2 as

$$\mathcal{M}_\xi(s) \approx \prod_{n=1}^M \frac{1}{1 - s\mathrm{eig}_n(\mathbf{R}_M)} = \sum_{n=1}^M \frac{A_n}{1 - \mathrm{eig}_n(\mathbf{R}_M)}, \tag{4.32}$$

where the equality comes from the technique of partial fractions, $\mathbf{R}_M$ is defined in (4.25), and A_n is given by

$$A_n = \prod_{n'=1, n' \neq n}^M \frac{\mathrm{eig}_n(\mathbf{R}_M)}{\mathrm{eig}_n(\mathbf{R}_M) - \mathrm{eig}_{n'}(\mathbf{R}_M)}. \tag{4.33}$$

By applying the inverse Laplace transform to the MGF in (4.32), we obtain the PDF of ξ:

$$p_\xi(x) \approx \sum_{n=1}^{M} \frac{A_n}{\text{eig}_n(\mathbf{R}_M)} \exp\left(-\frac{x}{\text{eig}_n(\mathbf{R}_M)}\right), \quad x \geq 0. \tag{4.34}$$

Finally, substituting the above PDF $p_\xi(x)$ into (4.31) gives rise to the following results.

Theorem 4.3. *When there is no coding across subcarriers, the outage probability of a multiband UWB system is given by*

$$P_{out} = 1 - \exp\left(-\frac{\zeta_o}{\rho}\right) \tag{4.35}$$

for any channel model parameters. When the information is jointly encoded across M $(1 < M \leq N)$ subcarriers, the outage probability can be approximated as

$$P_{out} \approx \sum_{n=1}^{M} A_n \left(1 - \exp\left(-\frac{\zeta_o M}{\rho \, eig_n(\mathbf{R}_M)}\right)\right), \tag{4.36}$$

where $\mathbf{R}_M$ is specified in (4.25), and A_n is defined in (7.11).

From the above analysis, we can see that the outage probability follows the same behaviors as the average PEP. Specifically, the outage probability of an uncoded multiband UWB system does not depend on the clustering property of UWB channel, and it is the same as that for narrowband Rayleigh fading environment [81]. When the information is jointly encoded across multiple subcarriers, (4.36) discloses that the outage probability is related to the eigenvalues of the correlation matrix $\mathbf{R}_M$, which depends on the path arrival rates and decay factors.

To gain some insightful understanding on the outage probability formulation in (4.36), let us consider a specific example of jointly encoding across $M = 2$ subcarriers. In this case, the outage probability can be approximated as

$$P_{\text{out}} \approx 1 - 0.5\left(1 + B^{-1}\right)\exp\left(-\frac{2\zeta_o}{\rho(1+B)}\right) - 0.5\left(1 - B^{-1}\right)\exp\left(-\frac{2\zeta_o}{\rho(1-B)}\right), \tag{4.37}$$

where B is defined in (4.28). Since B takes any value between 0 and 1 ($0 < B < 1$), the higher the B the larger the outage probability P_{out} in (4.37). For instance,

- In case of CM 1, $B = 0.9852$;

$$P_{\text{out}} \approx 1 - 1.0075 \exp\left(-\frac{1.0075\zeta_o}{\rho}\right) + 0.0075 \exp\left(-\frac{134.91\zeta_o}{\rho}\right).$$

- In case of CM 4, $B = 0.8351$;

$$P_{\text{out}} \approx 1 - 1.0987 \exp\left(-\frac{1.0898\zeta_o}{\rho}\right) + 0.0987 \exp\left(-\frac{12.131\zeta_o}{\rho}\right).$$

From the above examples, we can see that when the SNR ρ is small, $\exp\left(-\frac{2\zeta_o}{\rho(1+B)}\right) \gg \exp\left(-\frac{2\zeta_o}{\rho(1-B)}\right)$, and hence the third term in (4.37) is negligible. The outage probability can then be approximated by

$$P_{\text{out}} \approx 1 - \exp\left(-\frac{\zeta_o}{\rho}\right) \tag{4.38}$$

for both CM 1 and CM 4. Such outage probability is the same as that for narrowband Rayleigh fading channel, which implies that in low SNR region we cannot gain from the multipath-clustering property of UWB channel. As the SNR increases, P_{out} for CM 4 drops faster than that for CM 1 due to the effect of the third term in P_{out} expressions. Explicitly, the term $0.0987 \exp\left(-\frac{12.131\zeta_o}{\rho}\right)$ for CM 4 increases with SNR ρ much faster than the term $0.0075 \exp\left(-\frac{134.91\zeta_o}{\rho}\right)$ for CM 1. Hence, the outage probability performance for CM 4 tends to be better than that for CM 1 at high SNR.

4.3   Analysis for UWB-MIMO Systems

The proposed analysis in the preceding section provides a simple but general approach for determining the performances of multiband UWB systems. In what

follows, we briefly describe a UWB-MIMO system model, and then apply the proposed approximation technique to characterize PEP performances of multiband UWB-MIMO system.

4.3.1 UWB-MIMO System Model

We consider a UWB-MIMO system with N_t transmit and N_r receive antennas. The channel impulse response from the ith transmit antenna to the jth receive antenna during the kth OFDM block is modeled as

$$h_{ij}^k(t) = \sum_{c=0}^{C} \sum_{l=0}^{L} \alpha_{ij}^k(c,l)\delta(t - T_c - \tau_{c,l}), \qquad (4.39)$$

where $\alpha_{ij}^k(c,l)$ is the multipath gain coefficient with $\mathrm{E}\left[|\alpha_{ij}^k(c,l)|^2\right] = \Omega_{c,l}$. We assume that the average powers $\Omega_{c,l}$ and the delays T_c and $\tau_{c,l}$ are the same for every transmit-receive link.

At the transmitter, the information is jointly encoded across N_t transmit antennas, M OFDM subcarriers, and K OFDM blocks. Each STF codeword can be expressed as a $KM \times N_t$ matrix

$$\mathbf{D}_p = \left[\ (\mathbf{D}_p^0)^T \ \ (\mathbf{D}_p^1)^T \ \ \cdots \ \ (\mathbf{D}_p^{K-1})^T \ \right]^T, \qquad (4.40)$$

where $\mathbf{D}_p^k = \left[\mathbf{d}_{p,1}^k \ \mathbf{d}_{p,2}^k \ \cdots \ \mathbf{d}_{p,N_t}^k\right]$ and $\mathbf{d}_{p,i}^k = \left[d_i^k(pM) \ d_i^k(pM+1) \ \cdots \ d_i^k(pM+M-1)\right]^T$ for $i = 1, 2, \ldots, N_t$ and $k = 0, 1, \ldots, K-1$. The symbol $d_i^k(n)$, $n = 0, 1, \ldots, N$, represents the complex symbol to be transmitted over subcarrier n by transmit antenna i during the kth OFDM symbol period. The matrix $\mathbf{D}_p$ is normalized to have average energy $\mathrm{E}\left[\|\mathbf{D}_p\|^2\right] = KMN_t$. At the kth OFDM block, each vector $\mathbf{d}_i^k \triangleq \left[(\mathbf{d}_{0,i}^k)^T \ (\mathbf{d}_{1,i}^k)^T \ \cdots \ (\mathbf{d}_{P-1,i}^k)^T \ \mathbf{0}_{(N-PM)\times 1}\right]^T$ is OFDM modulated, and transmitted by transmit antenna i.

The received signal at the nth subcarrier at receive antenna j during the kth OFDM symbol duration can be expressed as

$$y_j^k(n) = \sqrt{\frac{E_s}{N_t}} \sum_{i=1}^{N_t} d_i^k(n) H_{ij}^k(n) + z_j^k(n), \tag{4.41}$$

where $H_{ij}^k(n) = \sum_{c=0}^{C} \sum_{l=0}^{L} \alpha_{ij}^k(c,l) \exp[-\mathbf{j}2\pi n\Delta f(T_c + \tau_{c,l})]$ is the frequency response of the channel at subcarrier n between the ith transmit and the jth receive antenna during the kth OFDM block, $z_j^k(n)$ is the zero-mean Gaussian noise with variance N_0, and the factor $\sqrt{E_s/N_t}$ guarantees that the average energy per transmitted symbol is E_s, independent of the number of transmit antennas. We assume that the channel state information $H_{ij}^k(n)$ is known at the receiver, and the receiver exploits a maximum likelihood decoder, where the decoding process is jointly performed across N_r receive antennas.

Due to the band hopping, the K OFDM symbols in each STF codeword are sent over different subbands. With an ideal band hopping, we assume that the signals transmitted over K different frequency-bands undergo independent fading. We also assume that the MIMO channel is spatially uncorrelated, i.e., path gains $\alpha_{ij}^k(c,l)$ are independent for different paths and different pairs of transmit and receive antennas.

4.3.2 Pairwise Error Probability

Similarly, the PEP between two distinct STF codewords $\mathbf{D}_p$ and $\hat{\mathbf{D}}_p$ can be given by

$$P_e = \mathrm{E}\left[\mathrm{Q}\left(\sqrt{\frac{\rho}{2N_t} \sum_{j=1}^{N_r} \|\boldsymbol{\Delta}_p \, \mathbf{H}_{p,j}\|^2}\right)\right], \tag{4.42}$$

where $\boldsymbol{\Delta}_p = X(\mathbf{D}_p) - X(\hat{\mathbf{D}}_p)$ is a codeword difference matrix, in which $X(\mathbf{D}_p)$ converts each column of $\mathbf{D}_p$ into a diagonal matrix and results in an $KM \times KMN_t$

matrix: $X(\mathbf{D}_p) = X([\mathbf{d}_{p,1} \cdots \mathbf{d}_{p,N_t}]) = [diag(\mathbf{d}_{p,1}) \cdots diag(\mathbf{d}_{p,N_t})]$. In (4.42), $\mathbf{H}_{p,j}$ is a $KMN_t \times 1$ channel matrix formatted as $\mathbf{H}_{p,j} = \left[\mathbf{H}_{p,1j}^T \ \mathbf{H}_{p,2j}^T \cdots \mathbf{H}_{p,N_tj}^T \right]^T$, in which $\mathbf{H}_{p,ij} = \left[H_{ij}^0(pM) \ \cdots \ H_{ij}^0(pM+M-1) \ \cdots \ H_{ij}^{K-1}(pM) \ \cdots \ H_{ij}^{K-1}(pM+M-1) \right]^T$.

Following the same procedure as in single antenna transmission, we first obtain

$$\eta = \sum_{j=1}^{N_r} \left\| \mathbf{\Delta}_p \ \mathbf{H}_p \right\|^2 \approx \sum_{j=1}^{N_r} \sum_{n=1}^{M} \text{eig}_n(\mathbf{\Phi}_j) |\mu_{j,n}|^2, \tag{4.43}$$

where $\mathbf{\Phi}_j = \mathbf{\Delta}_p \mathbf{E} \left[\mathbf{H}_{p,j} \mathbf{H}_{p,j}^{\mathcal{H}} \right] \mathbf{\Delta}_p^{\mathcal{H}}$, and $\mu_{j,n}$ are iid zero-mean Gaussian random variables with unit variance. Based on the assumption of independent channels, the matrix $\mathbf{E} \left[\mathbf{H}_{p,j} \mathbf{H}_{p,j}^{\mathcal{H}} \right]$ can be simplified to $\mathbf{E} \left[\mathbf{H}_{p,j} \mathbf{H}_{p,j}^{\mathcal{H}} \right] = \mathbf{I}_{KN_t} \otimes \mathbf{R}_M$, where $\otimes$ denotes the Kronecker product [76], $\mathbf{I}_M$ represents an $M \times M$ identity matrix, and $\mathbf{R}_M$ is specified in (4.25). Therefore, we can rewrite the expression for $\mathbf{\Phi}_j$ in (4.43) as

$$\mathbf{\Phi}_j = (\mathbf{D}_p - \hat{\mathbf{D}}_p)(\mathbf{D}_p - \hat{\mathbf{D}}_p)^{\mathcal{H}} \circ (\mathbf{I}_K \otimes \mathbf{R}_M), \tag{4.44}$$

where $\circ$ denotes the Hadamard product [76]. To simplify the notation, we denote $\mathbf{S} \triangleq (\mathbf{D}_p - \hat{\mathbf{D}}_p)(\mathbf{D}_p - \hat{\mathbf{D}}_p)^{\mathcal{H}}$. Finally, substituting (4.44) into (4.43) and using the MGF of η, the average PEP between $\mathbf{D}_p$ and $\hat{\mathbf{D}}_p$ can be approximated as

$$P_e \approx \frac{1}{\pi} \int_0^{\pi/2} \prod_{n=1}^{KN_p} \left(1 + \frac{\rho}{4N_t \sin^2 \theta} \text{eig}_n \left(\mathbf{S} \circ (\mathbf{I}_K \otimes \mathbf{R}_M) \right) \right)^{-N_r} d\theta. \tag{4.45}$$

From (4.45), it is clear that the multiband UWB-MIMO performance depends on both STF codeword and channel model parameters through the eigenvalues of matrix $\mathbf{S} \circ (\mathbf{I}_K \otimes \mathbf{R}_M)$. If the information is repeated over K OFDM symbols, i.e., $\mathbf{D}_p^0 = \mathbf{D}_p^1 = \cdots = \mathbf{D}_p^{K-1}$, then the PEP in (4.45) becomes

$$P_e \approx \frac{1}{\pi} \int_0^{\pi/2} \prod_{n=1}^{M} \left(1 + \frac{\rho}{4N_t \sin^2 \theta} \text{eig}_n \left(\mathbf{S}_0 \circ \mathbf{R}_M \right) \right)^{-KN_r} d\theta, \tag{4.46}$$

where $\mathbf{S}_0 \triangleq (\mathbf{D}_p^0 - \hat{\mathbf{D}}_p^0)(\mathbf{D}_p^0 - \hat{\mathbf{D}}_p^0)^{\mathcal{H}}$. At high SNR, the approximate PEP in (4.46)

can be upper bounded as

$$P_e \lesssim \prod_{n=1}^{r} \left(\frac{\rho}{4N_t} \mathrm{eig}_n \left(\mathbf{S}_0 \circ \mathbf{R}_M \right) \right)^{-KN_r}, \tag{4.47}$$

which implies a coding gain of $\frac{1}{4N_t} \left(\prod_{n=1}^{r} \mathrm{eig}_n (\mathbf{S}_0 \circ \mathbf{R}_M) \right)^{1/r}$ and a diversity order of rKN_r, where r denotes the rank of matrix $\mathbf{S}_0 \circ \mathbf{R}_M$. Since UWB channel contains a large number of resolvable paths, $\mathbf{R}_M$ is generally of full rank. This leads to an interesting observation that the multiband UWB system achieves the same diversity advantage in different channel environment. Only the system coding gain that depends heavily on the cluster arriving fading paths. To get some insight, we provide a specific example in the succeeding subsection.

4.3.3 Example: Repetition STF Coding based on Alamouti's Structure

Consider a multiband UWB-MIMO system employing two transmit antennas and a repetition-coded STF code [34] based on Alamouti's structure [22]. Suppose the number of jointly encoded subcarriers M is an even integer, then the codeword $\mathbf{D}_p^k$ is given by

$$\mathbf{D}_p^k = \left(\mathbf{I}_2 \otimes \mathbf{1}_{\frac{M}{2} \times 1} \right) \begin{pmatrix} d_1 & d_2 \\ -d_2^* & d_1^* \end{pmatrix}, \tag{4.48}$$

where $\mathbf{1}_{m \times n}$ denotes an $m \times n$ all-one matrix, and d_i's are selected from BPSK or QPSK constellations. Note that $\mathbf{D}_p^k$ is the same for all k's. From the code structure in (4.48), we have

$$\mathbf{S}_0 \circ \mathbf{R}_M = \nu \left(\mathbf{I}_2 \otimes \mathbf{1}_{\frac{M}{2} \times \frac{M}{2}} \right) \circ \mathbf{R}_M = \nu \mathbf{I}_2 \otimes \mathbf{R}_{\frac{M}{2}}, \tag{4.49}$$

where $\nu \triangleq \sum_{i=1}^{2} |d_i - \hat{d}_i|^2$. Substituting (4.49) into (4.46) results in an approximate PEP

$$P_e \approx \frac{1}{\pi} \int_0^{\pi/2} \prod_{n=1}^{M/2} \left(1 + \frac{\rho\nu}{8\sin^2\theta} \mathrm{eig}_n\left(\mathbf{R}_{\frac{M}{2}}\right)\right)^{-2KN_r} d\theta. \tag{4.50}$$

The PEP in (4.50) can be easily obtained for any given values of M. For instance, the PEP expressions for the cases of jointly coding across two and four subcarriers are given as follows.

1. For $M = 2$, the approximate PEP is simply

$$P_e \approx \frac{1}{\pi} \int_0^{\pi/2} \left(1 + \frac{\rho\nu}{8\sin^2\theta}\right)^{-2KN_r} d\theta \leq \left(\frac{\rho\nu}{8}\right)^{-2KN_r},$$

which indicates the diversity gain of $2KN_r$ and the coding gain of 0.125ν, independent with the channel model parameters. The PEP in this case implies that we cannot gain from the multipath-clustering property of UWB channel.

2. For $M = 4$, the PEP can be approximated as

$$P_e \approx \frac{1}{\pi} \int_0^{\pi/2} \left(1 + \frac{\rho^2\nu^2(1 - B^2)}{64\sin^4\theta}\right)^{-2KN_r} d\theta$$
$$\lesssim \left(\frac{\rho\nu}{8}\sqrt{1 - \Omega_{0,0}^2(\Lambda\Gamma + 1)^2(\lambda\gamma + 1)^2}\right)^{-4KN_r}.$$

Clearly, the diversity gain is $4KN_r$ for each channel model, whereas the coding gain is about 0.0214ν for CM 1 and 0.0688ν for CM 4. Such coding advantage makes the performance of multiband UWB system under CM 4 superior to that under CM 1.

The results in this section discloses that regardless of the random-clustering behavior of UWB channels, the diversity gain can be improved by increasing the number of jointly encoded subcarriers, the number of jointly encoded OFDM symbols, or the number of antennas. Nevertheless, increasing the number of jointly

encoded subcarriers leads to the loss in coding gain. As shown in the above examples, a diversity order of four can be achieved by employing two transmit and two receive antennas. The same diversity order can also be obtained by employing one receive antenna but increasing the number of jointly encoded subcarriers from two to four. However, the coding gain reduces from 0.125ν to about 0.0214ν for CM 1 and 0.0688ν for CM 4.

4.4 Simulation Results

We performed simulations for a multiband UWB system with $N = 128$ subcarriers and the subband bandwidth of 528 MHz. Each OFDM symbol was of duration $T = 242.42$ ns. After adding the cyclic prefix of length 60.61 ns and the guard interval of length 9.47 ns, the symbol duration became 312.5 ns. The channel model parameters followed those for CM 1 and CM 4 [68]. In our simulations, the data matrix $\mathbf{D}$ in (4.2) were constructed via a repetition mapping. For single-antenna transmission, each data matrix $\mathbf{D}_p$ contained only one information symbol d_p, i.e., $\mathbf{D}_p = d_p \cdot \mathbf{1}_{M \times 1}$. The data matrix $\mathbf{D}_p$ for a system with two transmit antennas was constructed according to (4.48).

Figs. 4.2(a) and 4.2(b) are the comparisons between the theoretical PDF of the normalized SNR ξ given in (4.34) and computer simulations for the case of no coding and jointly encoding across two subcarriers. There is a good match between the theoretical and simulation results. Fig. 4.2(a) confirms the analysis in Section 4.2.3 that for uncoded system, the PDF of the SNR is the same for different channel environments. Fig. 4.2(b) shows that the PDF of the SNR of the coded system depends on the underlying channel model, as expected. Furthermore, Fig. 4.2(b) indicates that the system under CM 4 has more chance to take on larger SNR
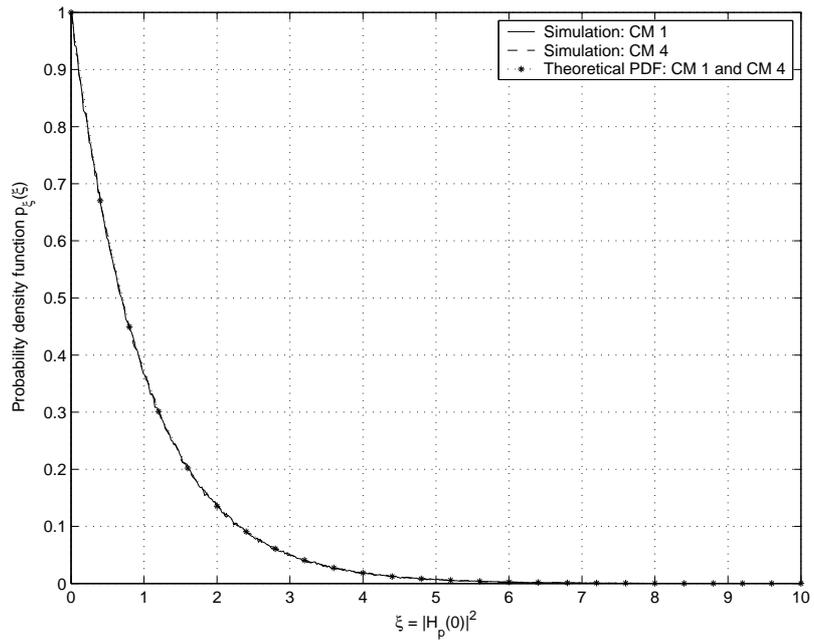
(a) No coding across subcarriers
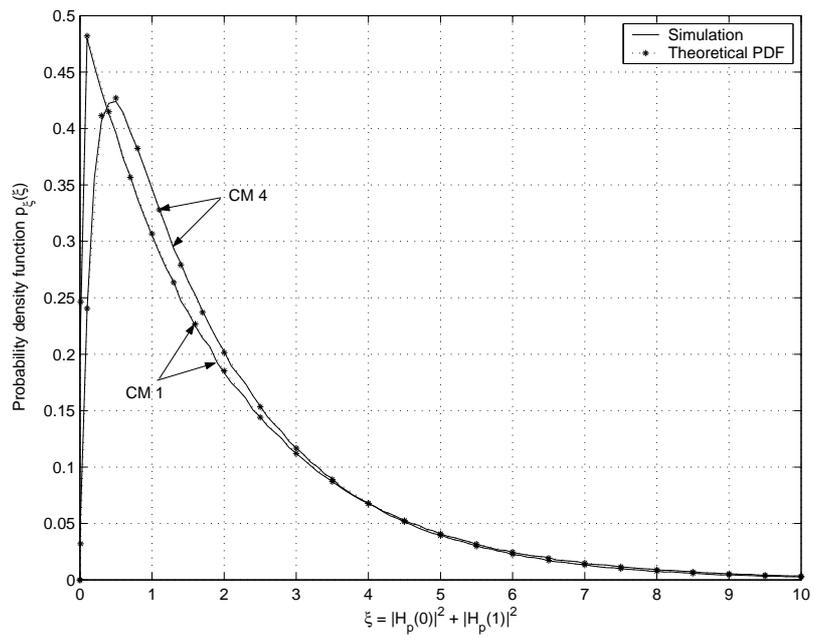
(b) Jointly encoding across two subcarriers

Figure 4.2: Probability density function.

94

values, which implies a better performance than that under CM 1.

Figs. 4.3 and 4.4 depict the average SER performances of single-antenna multi-band UWB system as functions of average SNR per bit (E_b/N_0) in dB. We used BPSK modulation for the performances in Fig. 4.3 and QPSK for those in Fig. 4.4. With BPSK symbols, the average SER is equivalent to the PEP performance. In case of QPSK, we used the union bound [81] to obtain the average SER from the PEP formulation. In Figs. 4.3(a) and 4.4(a), we show the simulated and theoretical performances of multiband UWB system without coding $(M = 1)$. We observe that the performances of UWB system in CM 1 and CM 4 are almost the same, and they are close to the exact PEP calculation in (4.13). The simulation results confirm the theoretical expectation that the performances of multiband UWB systems without coding across subcarriers are the same for every channel environment. Figures 4.3(b) and 4.4(b) show the performances of multiband UWB system with the information jointly encoded across two subcarriers $(M = 2)$. We can see that the theoretical approximations obtained from (4.24) are close to the simulated performances for both CM 1 and CM 4. In addition, the performance obtained under CM 4 is superior to that under CM 1, which is in agreement with the theoretical results in Section 4.2.2. Both Figures 4.3(b) and 4.4(b) validate that the PEP approximations can well reflect the multipath-rich and random-clustering characteristics on the performances of UWB systems.

Figs. 4.5(a) and 4.5(b) plot the outage probability P_{out} versus normalized average SNR ρ/ζ_o in dB. We can observe that the outage probability follows the same tendencies as the average SER. The uncoded system yields the same outage probability in both CM 1 and CM 4, whereas the coded system under CM 4 achieves a lower outage probability, hence better performance, than that with CM
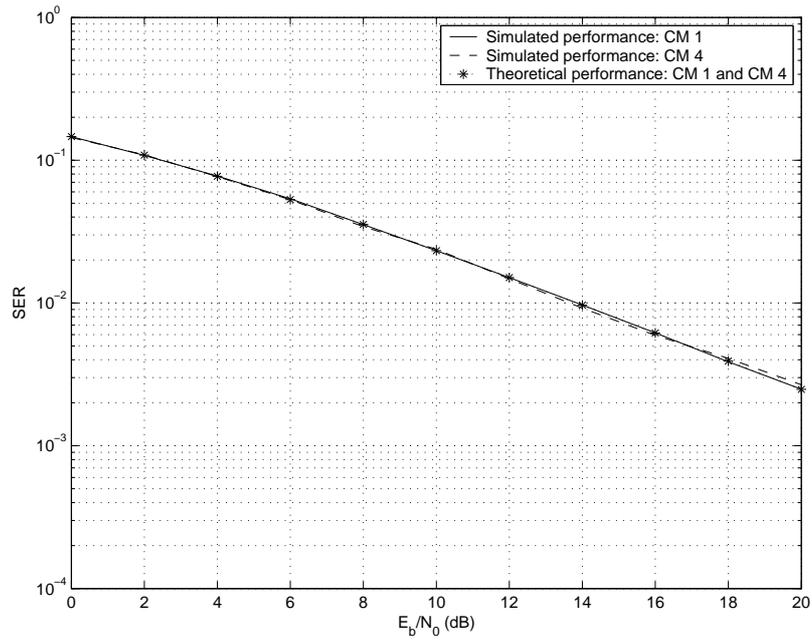
(a) No coding across subcarriers
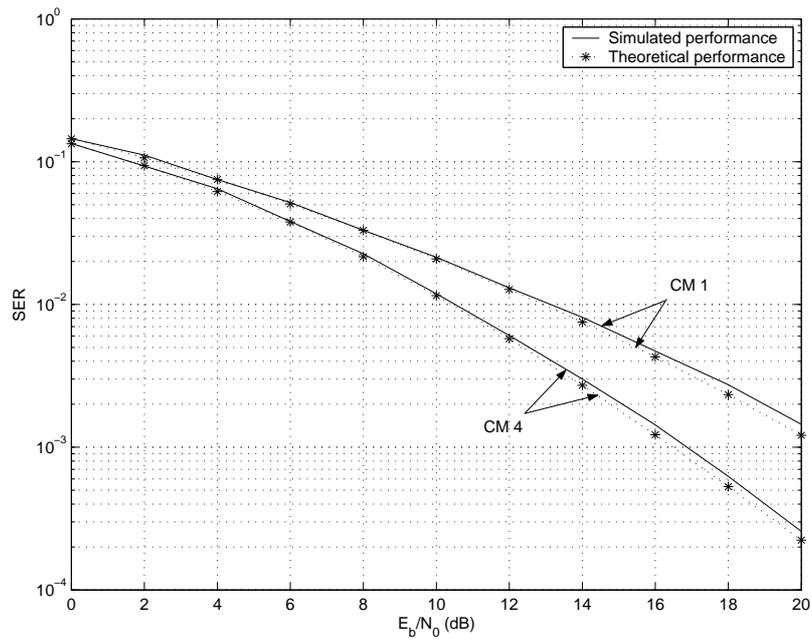
(b) Jointly encoding across two subcarriers

Figure 4.3: Performances of single-antenna multiband UWB system with BPSK symbols.
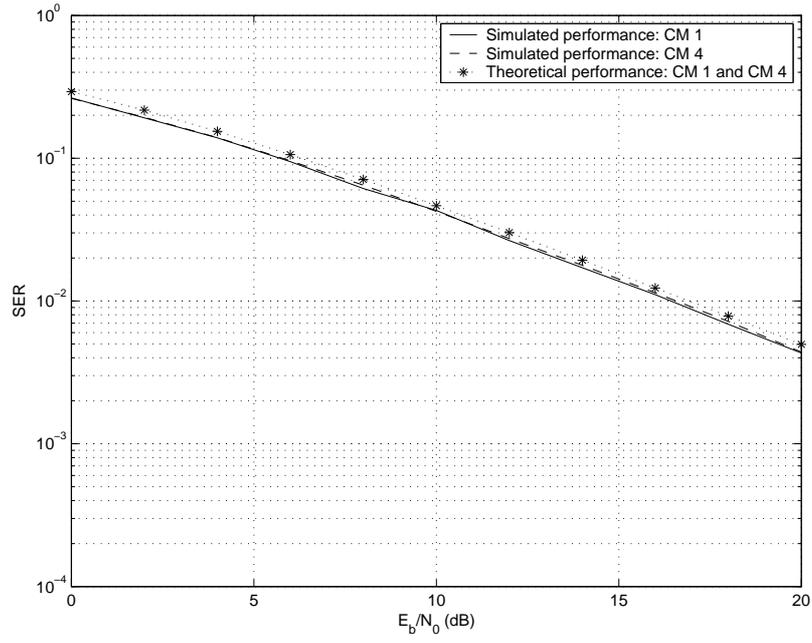
(a) No coding across subcarriers
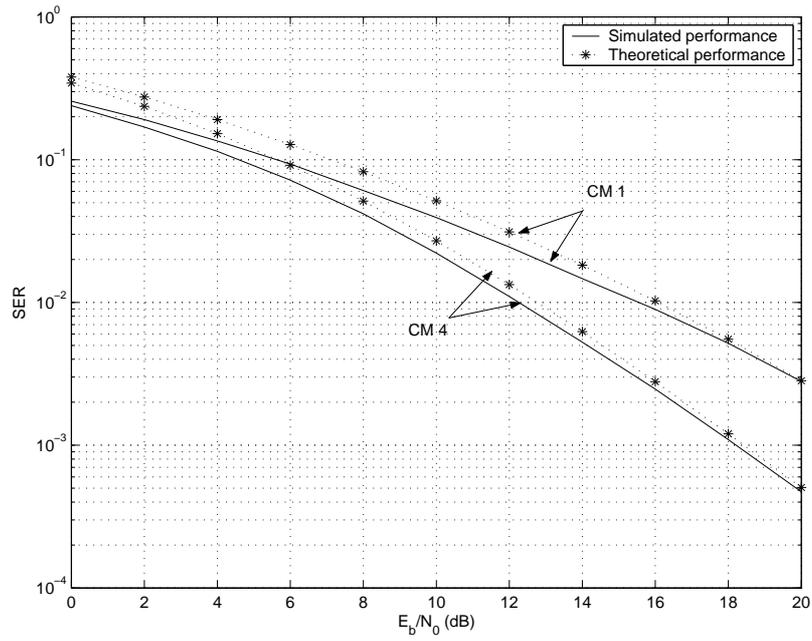
(b) Jointly encoding across two subcarriers

Figure 4.4: Performances of single-antenna multiband UWB system with QPSK symbols.
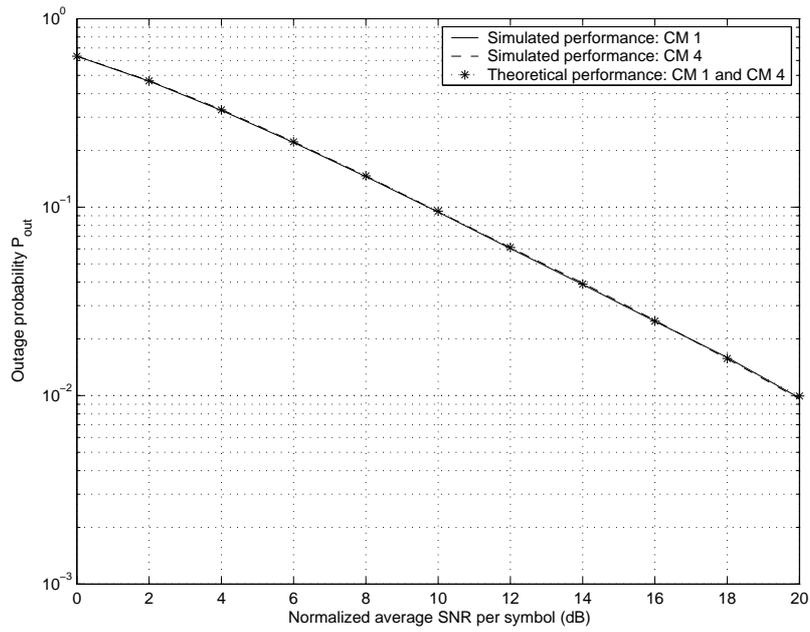
(a) No coding across subcarriers
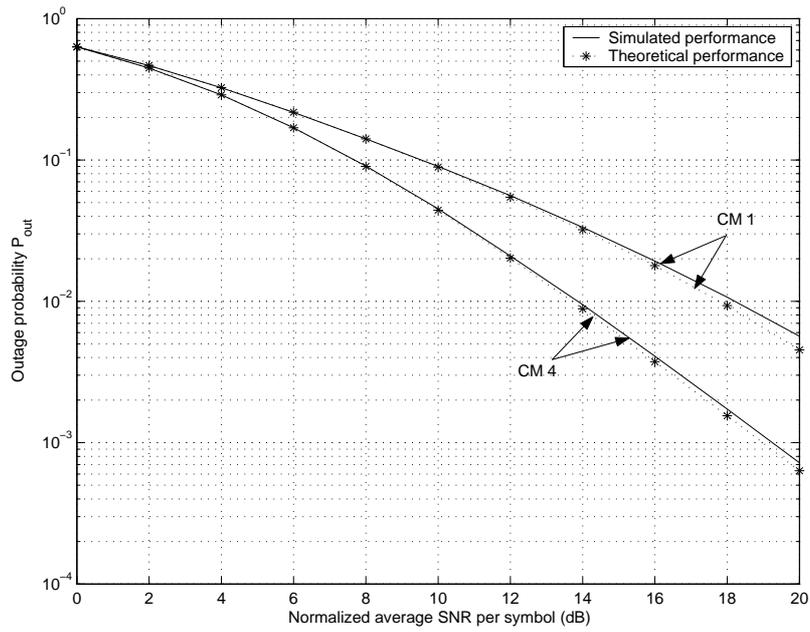
(b) Jointly encoding across two subcarriers

Figure 4.5: Outage probability of single-antenna multiband UWB system.

1.

Figs. 4.6(a) and 4.6(b) depict the SER performances for UWB-MIMO system with the information jointly encoded across $N_t = 2$ transmit antennas, $K = 1$ OFDM symbol, and $M = 2, 4$ subcarriers. Note that the theoretical SER was obtained from the union bound of the PEP formulation in (4.50). From both figures, we can see that the theoretical approximation in (4.50) correctly predicts the diversity and coding gains. From Fig. 4.6(b), it is clear that the multiband system under CM 4 outperforms that under CM 1 due to the larger coding gain. Fig. 4.6 also confirms our observation in Section 4.3 that increasing the number of jointly encoded subcarriers leads to the increase in the diversity gain, but the loss in the coding advantage.

4.5   Chapter Summary

In this chapter, we provide PEP and outage probability analysis that captures the unique multipath-rich and random-clustering characteristics of UWB channels. First, exact PEP and outage probability formulations are obtained for the case of no coding across subcarriers. Interestingly, both theoretical and simulation results reveal that the performances of uncoded multiband UWB systems do not depend on the clustering property. Then, we obtain PEP and outage probability approximations in case when the data is jointly encoded across multiple subcarriers. The theoretical approximations reveal that UWB performances depend heavily on the correlations in the channel frequency response among different subcarriers, which in turn relate to the cluster arrival rate, the ray arrival rate, and the cluster and ray decay factors. In case of jointly coding across two subcarriers, we can draw some interesting conclusions as follows. When the product of the cluster arrival
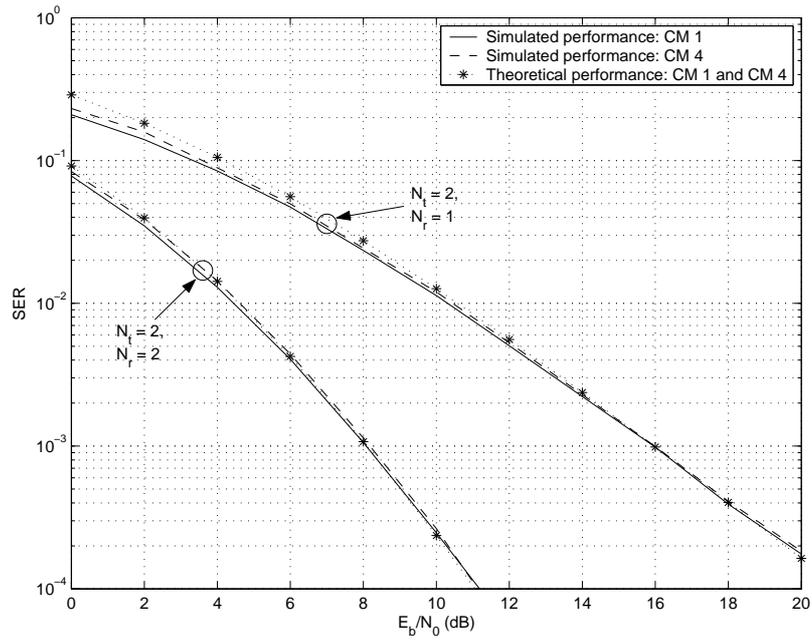
(a) Jointly encoding across two subcarriers
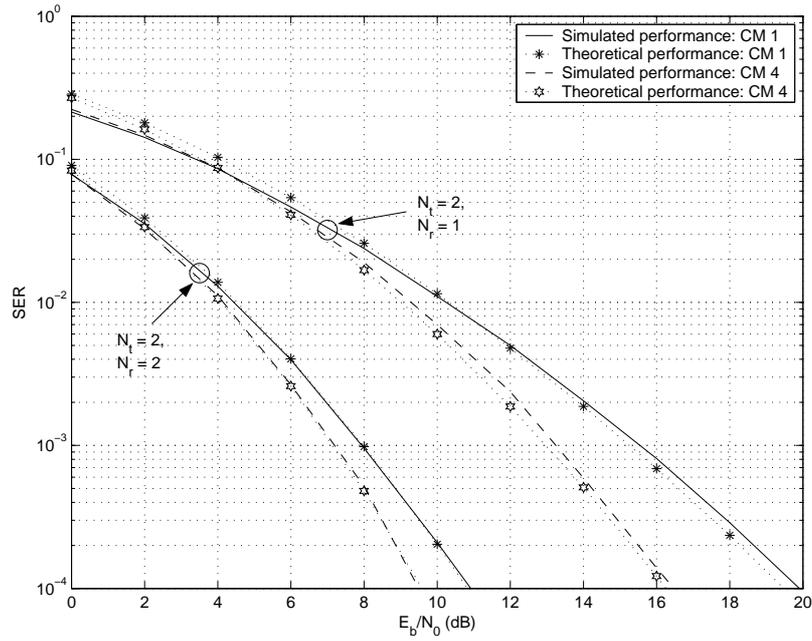
(b) Jointly encoding across four subcarriers

Figure 4.6: Performances of multiband UWB-MIMO system with QPSK symbols.

rate and cluster decay factor is small, e.g., in a short-range (0-4 meters) line-of-sight scenario, the effect of the first cluster will dominate and the UWB performance can be well approximated by taking into consideration only the first cluster. In contrast, when the product of the ray arrival rate and ray decay factor is much less than one, the performance seriously depends only on the first path in each cluster. Simulation results confirm that the theoretical analysis can successfully capture the effect of random-clustering phenomenon on the performances of multiband UWB system. Finally, we extend the analysis to that for UWB-MIMO systems. It turns out that the coding gain strongly relates to the channel model parameters. The diversity gain on the other hand, can be improved by increasing the number of jointly encoded subcarriers, the number of jointly encoded OFDM symbols, or the number of antennas, regardless of the random-clustering behavior of UWB channels.

Chapter 5

Power Controlled Channel Allocation for Multiuser Multiband UWB Systems

In order for a UWB device to coexist with other devices, the transmitted power level of UWB is strictly limited by the FCC spectral mask. Such limitation poses a significant design challenge to any UWB system. An efficient management of the limited power is thus a key feature to fully exploit the advantages of UWB. The low transmitted power of UWB emissions not only ensures long life-time for the energy-limited devices, but also reduces co-channel interference. In addition, UWB systems are expected to support an integration of multimedia traffic, such as voice, image, data, and video streams. This requires a cross layer algorithm that is able to allocate the available resources to a variety of users with different service rates in an effective way. An overview of resource allocation in UWB communications is provided in [41]. In [42], the authors considered a joint rate and power assignment problem that is central in multiuser UWB networks, and proposed a radio

resource sharing mechanism that performs a handshaking procedure to establish a communication link. In [46], the authors discussed a joint scheduling, routing, and power allocation problem with an objective to maximize the total utility of UWB system.

Most of the existing resource allocation schemes for UWB systems (see [41]- [46] and references therein) are based on single-band impulse radio technology. On the other hand, most research efforts on multiband UWB systems have been devoted to the physical layer issues [19], [48]- [49]. Some of the key issues in multiband UWB systems that remain largely unexplored are resource allocations such as power control and channel allocation. The current multiband proposal divides the subbands into groups, each comprising 2-3 subbands. A set of certain time-frequency codes is used to interleave the data within each band group [18]. This strategy lacks of the ability to allocate subbands optimally since the available subbands are not assigned to each user according to its channel condition. Moreover, in the multiband proposal [18], the transmitted power of each user is equally distributed among its assigned subbands without any power adaptation to the channel variations. So adaptive optimization of the subband assignment and power control can greatly improve the system performances of multiband UWB systems.

In this chapter, we propose a novel cross layer channel allocation scheme for multiband UWB wireless networks (e.g., a piconet, as in the IEEE 802.15.3 standard). By efficiently allocating the subbands, transmitted power, and data rates among all users, the proposed scheme enables the multiband UWB system to operate at a low transmit power level, while still achieving desired performance. First, we formulate a subband assignment and power allocation problem as an optimization problem whose goal is to minimize the overall transmit power provided that all

users achieve their requested data rates and desired packet error rate (PER), while the power spectral density complies with the FCC limit [4]. To take into account the fact that users in the multiband UWB system may have different data rates which in turn implies different channel coding rates, frequency spreading gains, and/or time spreading gains, our formulated problem considers not only the limitation on transmit power level, but also band hopping for users with different data rates. It turns out that the formulated problem is an integer programming problem whose complexity is NP hard. Then, to reduce the complexity of the formulated problem, we propose a fast suboptimal algorithm that can guarantee to obtain a near optimal solution, but requires low computational complexity. In order to ensure the system feasibility in variable channel conditions, we further develop a joint rate assignment and power controlled channel allocation algorithm that is able to allocate resources to the users according to three different system optimization goals, namely maximizing overall rate, achieving proportional fairness, and reducing maximal rate. Simulation results based on UWB channel model specified in the IEEE 802.15.3a standard [68] show that the proposed algorithm achieves up to 61% of transmitted power saving compared to standard multiband scheme [18]. Moreover, the proposed algorithm can also find feasible solutions adaptively when the initial system is not feasible for the rate requirements of the users.

An outline of this chapter is as follows. Section 5.1 describes the system model of multiband UWB. In Section 5.2, we first formulate the power controlled channel allocation problem. Then, a fast suboptimal scheme is developed. Finally, we propose a joint rate assignment and resource allocation algorithm to ensure the system feasibility. Simulation results are given in Section 5.3.
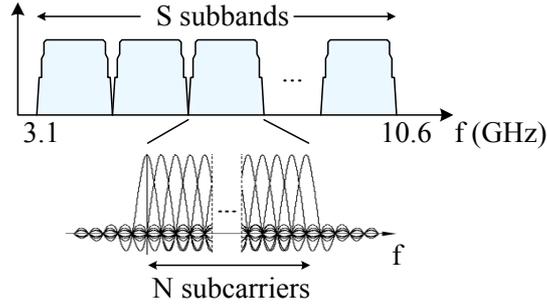
Figure 5.1: Illustration of Mulitband UWB Spectrum

5.1 System Model

We consider a UWB system using multiband OFDM in which the available UWB spectrum is divided into S subbands, as shown in Fig. 5.1. The UWB system employs OFDM with N subcarriers, which are modulated using QPSK. At each OFDM symbol period, the modulated symbol is transmitted over one of the S subbands. These symbols are time-interleaved across subbands. Different data rates are achieved by using different channel coding, frequency spreading, or time spreading rates. The frequency domain spreading is obtained by choosing conjugate symmetric inputs to the IFFT, while the time-domain spreading is achieved by repeating the same information in an OFDM symbol on two different subbands [18]. The receiver combines the information transmitted via different times or frequencies to increase the SNR of received data.

As listed in Table 5.1, the multiband UWB system provides data rates ranging from 53.3 Mbps to 480 Mbps. For the rates not higher than 80 Mbps, both time and frequency spreadings are performed, yielding the overall spreading gain of four. For the rates between 106.7 and 200 Mbps, only time-domain spreading is utilized which results in the overall spreading gain of two. The system with data

Table 5.1: Rate-Dependent Parameters

Data Rate (Mbps)	Modu-lation	Coding rate	Conjugate Symmetric Inputs to IFFT	Time Spreading Factor
53.3	QPSK	1/3	Yes	2
55	QPSK	11/32	Yes	2
80	QPSK	1/2	Yes	2
106.7	QPSK	1/3	No	2
110	QPSK	11/32	No	2
160	QPSK	1/2	No	2
200	QPSK	5/8	No	2
320	QPSK	1/2	No	1
400	QPSK	5/8	No	1
480	QPSK	3/4	No	1

rates higher than 200 Mbps exploits neither frequency nor time spreading, and the overall spreading gain is one. Forward error correction codes with coding rates of 1/3, 11/32, 1/2, 5/8 or 3/4 are employed to provide different channel protections with various data rates.

The channel model is based on the S-V model. It is worth noting that for most WPAN applications, the transmitter and receiver are stationary [83]. As a result, UWB channel is very slowly fading. The standard channel model assumes that the channel stays either completely static, or is time-invariant during the transmission of each packet [68], [83]. We assume that the channel state information is known at both the transmitter and the receiver.

We consider a multiuser multiband UWB scenario where K users simultaneously transmit their information. The kth user has the data rate R_k, which can be any value specified in Table 5.1. As shown in Table 5.1, if the rate is higher than 200 Mbps, there is no time spreading; otherwise, the time-domain spreading operation is performed with a spreading factor of two. In this case, any time-frequency code with a period of two can guarantee that each user will achieve the

additional diversity by transmitting the same information over two OFDM blocks. The time-frequency codes with period longer than two can also be used to improve the multiple access capability for asynchronous UWB wireless networks [19]. To simplify the problem formulation, we consider in this paper a multiband UWB system employing time-frequency codes of length two. The extension to UWB systems with longer time-frequency codes is straightforward.

In order to specify in which subbands each user can transmit its information, we define a $K \times S$ assignment matrix $\mathbf{A}$, whose $(k, s)^{th}$ element is denoted by a_{ks}, for $k = 1, 2, \ldots, K$ and $s = 1, 2, \ldots, S$. This a_{ks} represents the number of OFDM symbols that user k is allowed to transmit on the sth subband during two OFDM symbol periods. Assuming that each user utilizes one subband per transmission, a_{ks} can take any value from the set $\{0, 1, 2\}$. However, when the kth the data rate of the user is less than or equal to 200 Mbps, we need to ensure that the band hopping is performed to obtain the diversity from time spreading. In this case, a_{ks} is restricted to $a_{ks} \in \{0, 1\}$. Thus, the element of assignment matrix satisfies [84]

$$a_{ks} \in \phi(R_k) = \begin{cases} \{0, 1\}, & R_k \leq 200 \text{ Mbps}; \\ \{0, 1, 2\}, & R_k > 200 \text{ Mbps}. \end{cases} \tag{5.1}$$

During each OFDM symbol period, one user will occupy one subband. Since we consider the duration of two OFDM blocks, the assignment strategy needs to satisfy

$$\sum_{s=1}^{S} a_{ks} = 2, \quad k = 1, 2, \ldots, K. \tag{5.2}$$

In addition, to minimize the multiple access interference, each subband is assigned to a specific user at a time, and hence each subband can be used at most twice during two OFDM symbol periods. Therefore, the subband assignment also follows

$$\sum_{k=1}^{K} a_{ks} \leq 2, \quad s = 1, 2, \ldots, S. \tag{5.3}$$

Let $P_k^s(n)$ denote the transmitted power of the kth user at subcarrier n of the sth subband. Accordingly, the SNR of user k at the sth subband and the nth subcarrier is given by

$$\Gamma_k^s(n) = \frac{P_k^s(n)G_k^s(n)}{\sigma_k^2},\tag{5.4}$$

where $G_k^s(n)$ is the corresponding channel gain. We can express $G_k^s(n)$ as

$$G_k^s(n) = |H_k^s(n)|^2 \left(\frac{4\pi d_k}{\lambda_k^s}\right)^{-\nu},\tag{5.5}$$

in which $H_k^s(n)$ is the channel frequency response at subband s and subcarrier n, ν is the propagation loss factor, d_k represents the distance between the transmitter and receiver, $\lambda_k^s = 3 \times 10^8 / f_{c,k}^s$ is the wavelength of the transmitted signal, and $f_{c,k}^s$ is the center frequency of the waveform. In (5.4), σ_k^2 denotes the noise power at each subcarrier, which is defined as

$$\sigma_k^2 = 2 \times 10^{(-174+10\log_{10}(R_k)+N_F)/10},\tag{5.6}$$

where R_k is the data rate of the kth user, and N_F is the received noise figure referred to the antenna terminal [18]. As in the multiband standard, we assume that the noise power σ_k^2 is the same for every subcarrier within each subband. We assume an ideal band hopping such that the signal transmitted over different subband undergo independent fading, and there is no multiple access interference.

Due to the consideration for the simple transceiver of UWB, the current standard assumes that there is no bit loading and the power is equally distributed across subcarriers within each subband. Similarly, we assume that $P_k^s(n) = P_k^s(n')$ for any $0 \le n, n' \le N - 1$. Denote

$$P_k^s(n) = P_k^s, \quad n = 0, 1, \ldots, N - 1,\tag{5.7}$$

then the $K \times S$ power allocation matrix can be defined as $[\mathbf{P}]_{ks} = P_k^s$, in which $(k,s)^{th}$ component represents the transmitted power of the kth user in subband s.

5.2 Proposed Multiband Channel Allocation Algorithm

In the multiband frequency band plan [18], the subband center frequencies span a wide range from 3.43 GHz to 10.3 GHz. Consequently, different subbands tend to undergo different fading and propagation loss. Additionally, the channel condition for a specific subband may be good for more than one user. Therefore, to efficiently reduce the power consumption, we need to optimize the subband assignment matrix $\mathbf{A}$ and power allocation matrix $\mathbf{P}$ under some practical constraints.

In this section, first, we derive a generalized SNR expression for various UWB transmission modes. Second, we provide a necessary condition for the SNR so as to satisfy the PER requirement. Then, we propose a problem formulation to minimize the overall transmitted power provided that all users achieve their requested data rates and desired PER, while the transmitted power level is below the FCC limitation and rate parameters are according to the standard proposal given in Table 5.1. We develop a fast suboptimal scheme to solve the proposed problem. Finally, to ensure the system feasibility, we develop a joint rate adaptation, subband assignment, and power allocation algorithm.

5.2.1 Generalized SNR for Different Transmission Modes

Assuming that the channel state information is perfectly known at the receiver, the receiver employs a maximum ratio combiner (MRC) to combine the information transmitted via different times or frequencies. As a result, the average SNR at the output of MRC depends not only on the channel coding rate, but also the time and frequency spreading factors. The following proposition provides a generalized

expression of the average SNR for any data rates.

Proposition 5.1 *Assume maximum ratio combining and $P_k^s(n) = P_k^s$ for all subcarrier n, then the average SNR of the kth user is given by*

$$\bar{\Gamma}_k = \sum_{s=1}^{S} a_{ks} P_k^s F_k^s, \tag{5.8}$$

where

$$F_k^s \triangleq \frac{b_k}{N\sigma_k^2} \sum_{n=0}^{N-1} G_k^s(n), \tag{5.9}$$

and b_k is a constant that depends on the data rate of the kth user as follows:

$$b_k = \begin{cases} 2, & R_k \leq 80 \ Mbps; \\ 1, & 80 < R_k \leq 200 \ Mbps; \\ 1/2, & R_k > 200 \ Mbps. \end{cases} \tag{5.10}$$

Proof. Recall that when R_k is not higher than 80 Mbps, the information is spread across both time and frequency with the overall spreading gain of four. Consequently, the total SNR for the kth user at subcarrier n, $n = 0, 1, \ldots, N/2 - 1$, is

$$\Gamma_k(n) = \sum_{s=1}^{S} a_{ks} \left[\Gamma_k^s(n) + \Gamma_k^s(n + N/2) \right]. \tag{5.11}$$

Note that the SNR in (5.11) is based on the assumptions of no multiuser interference and no correlation among the data bits; it leads to an upper bound on the performance. Average (5.11) over $N/2$ subcarriers, resulting in the average SNR

$$\bar{\Gamma}_k = \frac{1}{N/2} \sum_{n=0}^{N/2-1} \Gamma_k(n) = \frac{1}{N/2} \sum_{n=0}^{N-1} \sum_{s=1}^{S} a_{ks} \Gamma_k^s(n). \tag{5.12}$$

By substituting (5.4) into (5.12) and assuming $P_k^s(n) = P_k^s$, we obtain

$$\bar{\Gamma}_k = \frac{2}{N} \sum_{n=0}^{N-1} \sum_{s=1}^{S} a_{ks} P_k^s \frac{G_k^s(n)}{\sigma_k^2} = \sum_{s=1}^{S} a_{ks} P_k^s \left(\frac{2}{N\sigma_k^2} \sum_{n=0}^{N-1} G_k^s(n) \right). \tag{5.13}$$

110

When R_k is between 106.7 and 200 Mbps, only time spreading is performed, and hence the total SNR at subcarrier n, $n = 0, 1, \ldots, N - 1$, becomes

$$\Gamma_k(n) = \sum_{s=1}^{S} a_{ks} \Gamma_k^s(n) = \sum_{s=1}^{S} a_{ks} \frac{P_k^s(n) G_k^s(n)}{\sigma_k^2}. \tag{5.14}$$

Thus, the average SNR can be obtained from (5.14) as

$$\bar{\Gamma}_k = \frac{1}{N} \sum_{n=0}^{N-1} \Gamma_k(n) = \sum_{s=1}^{S} a_{ks} P_k^s \left(\frac{1}{N\sigma_k^2} \sum_{n=0}^{N-1} G_k^s(n) \right). \tag{5.15}$$

For R_k higher than 200 Mbps, there is no spreading and the average SNR of the kth user is simply the average of $\Gamma_k^s(n)$ over N subcarriers and two subbands, i.e.,

$$\bar{\Gamma}_k = \frac{1}{2N} \sum_{n=0}^{N-1} \sum_{s=1}^{S} a_{ks} \Gamma_k^s(n) = \sum_{s=1}^{S} a_{ks} P_k^s \left(\frac{1}{2N\sigma_k^2} \sum_{n=0}^{N-1} G_k^s(n) \right). \tag{5.16}$$

Express (5.13), (5.15) and (5.16) in terms of F_k^s defined in (5.9) leading to the results in (5.8). $\qquad \square$

5.2.2 PER and Rate Constraint

A common performance requirement of UWB systems is to offer packet transmission with an error probability less than a desired threshold value. The PER metric is directly related to the BER performance, which in turn depends on the SNR at the output of the MRC. By keeping the SNR level higher than a specific value, the PER can be ensured to be lower than the PER threshold. In the sequel, we provide a necessary condition for the average SNR so as to satisfy the PER requirement.

Suppose the maximum PER is ε and the packet length is L bits, then the bit error probability after the channel decoder for the kth user, $\mathcal{P}_k$, needs to satisfy

$$1 - (1 - \mathcal{P}_k)^L \leq \varepsilon. \tag{5.17}$$

By the assumptions of the use of convolutional coding and Viterbi decoding with perfect interleaving, $\mathcal{P}_k$ is given by [7]

$$\mathcal{P}_k \leq \sum_{d=d_{free}}^{\infty} a_d \mathcal{P}_k(d), \tag{5.18}$$

where d_{free} is the free distance of the convolutional code, a_d denotes the total number of error events of weight d, and $\mathcal{P}_k(d)$ represents the probability of choosing the incorrect path with distance d from the correct path. Assume hard-decision decoding, then $\mathcal{P}_k(d)$ is related to the average BER, $\bar{B}_k$, as [7]

$$\mathcal{P}_k(d) = \sum_{l=(d+1)/2}^{d} C(d,l) \bar{B}_k^l (1-\bar{B}_k)^{d-l} \tag{5.19}$$

when d is odd, and

$$\mathcal{P}_k(d) = \sum_{l=d/2+1}^{d} C(d,l) \bar{B}_k^l (1-\bar{B}_k)^{d-l} + \frac{1}{2} C(d,\frac{d}{2}) \bar{B}_k^{\frac{d}{2}} (1-\bar{B}_k)^{\frac{d}{2}} \tag{5.20}$$

when d is even, where $C(d,l) \triangleq d!/[l!(d-l)!]$ is the combinatorial function. The average BER $\bar{B}_k$ can be obtained by averaging the conditional BER over the probability density function of the SNR at the output of MRC. With Γ_k denoting the instantaneous SNR at the MRC output, the conditional BER is given by [7]

$$B_k(\Gamma_k) = Q\left(\sqrt{\Gamma_k}\right), \tag{5.21}$$

where $Q(\cdot)$ is the Gaussian error function. From (5.17) and (5.18), we can see that for a given value of PER threshold ε, a corresponding BER threshold can be obtained. Since the error probability $\mathcal{P}_k$ in (5.18) is related to the coding rate through the parameters d_{free} and a_d, the BER requirement depends not only on the value of ε, but also on the data rate R_k. This implies that the SNR threshold is also a function of both ε and R_k. Let $\gamma(\varepsilon, R_k)$ be the minimum SNR of the kth user that is required to achieve the data rate R_k with PER less than ε. Then,

the necessary condition for the average SNR (defined in (5.8)) to satisfy the PER requirement is given by

$$\bar{\Gamma}_k = \sum_{s=1}^{S} a_{ks} P_k^s F_k^s \geq \gamma(\varepsilon, R_k). \tag{5.22}$$

5.2.3 Problem Formulation

The optimization goal is to minimize the overall transmitted power subject to the PER, rate, and FCC regulation constraints. Recall from (5.1) that the assignment matrix $\mathbf{A}$ has $a_{ks} \in \phi(R_k)$, $\forall k, s$. We can formulate the problem as follows:

$$\min_{\mathbf{A,P}} \quad P_{sum} = \sum_{k=1}^{K} \sum_{s=1}^{S} a_{ks} P_k^s \tag{5.23}$$

$$\text{s.t.} \begin{cases} \text{Rate and PER: } \sum_{s=1}^{S} a_{ks} P_k^s F_k^s \geq \gamma(\varepsilon, R_k), \ \forall k; \\ \text{Assignment (5.2): } \sum_{s=1}^{S} a_{ks} = 2, \ \forall k; \\ \text{Assignment (5.3): } \sum_{k=1}^{K} a_{ks} \leq 2, \ \forall s; \\ \text{Power: } P_k^s \leq P_{max}, \ \forall k, s, \end{cases}$$

where the first constraint in (5.23) is to ensure rate and PER requirements. The second and third constraints are described in Section 5.1. The last constraint is related to the limitation on transmitted power spectral density of -41.3 dBm/MHz, according to FCC Part 15 rules [4]. Here, P_{max} is the maximum power after taking into consideration the effects such as peak-to-average ratio.

If the elements in the assignment matrix $\mathbf{A}$ are binary, the problem defined in (5.23) can be viewed as a generalized form of generalized assignment problem [85] which is NP hard. Since the components of $\mathbf{A}$ can be 0, 1, or 2, the problem is an even harder integer programming problem. So the existing channel assignment approaches, e.g. in [86], are not applicable in (5.23). Although the optimal solution

can be found through full search, it is computationally expensive. To overcome the complexity issue, we propose in the subsequent subsection a fast suboptimal scheme, which is near optimal but has very low computational complexity.

5.2.4 Subband Assignment and Power Allocation Algorithm

The basic idea is a greedy approach to assign a_{ks} for a user step by step, so that the power consumption is minimized. The initialization is to set $\mathbf{A} = \mathbf{0}_{K \times S}$, define the user optimization list $K_{live} = \{1, 2, \dots, K\}$, and define the subband optimization list $S_{live} = \{1, 2, \dots, S\}$. First, each user makes a hypothesis that it can assign its transmission into different subbands regarding absence of other users. For each hypothesis, a dummy overall transmission power P_{dummy}^k is calculated. The user with the highest dummy overall transmitted power to achieve its rate will be assigned first, so that the best channel is assigned to the user that can reduce the overall power most. Then, this user is removed from the optimization list K_{live}. Since each subband can only accommodate one user per symbol period and we consider two OFDM symbol periods, when a subband is assigned twice, this subband is removed from the optimization list S_{live}. Then, we go to the first step for the rest of the users to assign their transmissions into the rest of the subbands. This iteration is continued until all users are assigned with their subbands, i.e., $K_{live} = \emptyset$. Finally, the algorithm checks if the maximum power is larger than the power limitation. If yes, an outage is reported; otherwise, the final values of $\mathbf{A}$ and $\mathbf{P}$ are obtained. The proposed algorithm can be described as follows:

Initialization: $a_{ks} = 0$, $\forall k, s$, $K_{live} = \{1, \dots, K\}$, $S_{live} = \{1, \dots, S\}$
Iteration: Repeat until $K_{live} = \emptyset$ or $S_{live} = \emptyset$

1. For $k \in K_{live}$
   $P_{dummy}^k = \min \sum_{s=1}^{S} a_{ks} P_k^s$ s.t. $a_{ks} \in S_{live}$

End

2. Select k' with the maximal $P_{dummy}^k, \forall k$, assign the corresponding $a_{k's}$ to $\mathbf{A}$, and update $\mathbf{P}$.

3. $K_{live} = K_{live} \backslash k'$

4. If $\sum_{k=1}^{K} a_{ks'} = 2$, $S_{live} = S_{live} \backslash s', \forall s'$.

End: If $(\max(\mathbf{P}) > P_{max})$ or $(S_{live} = \emptyset$ and $K_{live} \neq \emptyset)$, an outage is reported. Otherwise, return $\mathbf{A}$ and $\mathbf{P}$.

The complexity of the proposed algorithm is only $O(K^2 S)$. Although the algorithm is suboptimal, simulation results illustrated in the succeeding section shows that the proposed fast suboptimal algorithm has very close performances to the optimal solutions obtained by full search. Another complexity issue is that for the proposed scheme, power control is needed for each subband [1]. This will increase the system complexity slightly, but from the simulation results, we can see that the performance improvement is significant. Moreover, the proposed algorithm can be implemented by the master node to manage the power and subband usages of all users in a UWB picocell system, as adopted in the IEEE 802.15.3a standard [8]. The signaling information needed to be broadcasted at the master node includes the band hopping sequence of each user and the corresponding transmitted power. The algorithm is updated when a new user joins the network or when the channel link quality of each user changes considerably. Such update does not frequently occurs thanks to the small size of the picocell and the stationary nature of most transceivers in WPAN applications.

---

[1] But no power control or bit loading for subcarriers within each subband

5.2.5 Joint Rate Assignment and Resource Allocation Algorithm

Since the transmitted power in each subband is limited by maximal power P_{max}, solutions to (5.23) may not exist in some situations, such as when the requested rates of the users are high but the channel conditions are poor. Under such conditions, some desired rates of the users cannot be satisfied, and we call that the system is infeasible. When the system is not feasible, the requested rates need to be reduced. Here, we develop a joint rate assignment and power controlled channel allocation algorithm that is able to obtain the feasible solutions adaptively when the initial system is not feasible for the rate requirements of the users. Basically, the proposed algorithm comprises two main stages, namely resource allocation and rate adaptation stages. Fig. 5.2 shows the flow chart diagram of the proposed algorithm.

At the initialization step, the data rate of the kth user, R_k, $k = 1, 2, \ldots, K$ is set to its requested rate. After the initial setting, the first stage is to perform the subband and power allocation using the algorithm described in the previous subsection. If there is a solution for this assignment, then it is done. Otherwise, an outage will be reported, indicating the requested rates of the users are too high for the current channel conditions. In this case, we proceed to the second stage where the rate adaptation is performed.

In the rate adaptation stage, the algorithm chooses only one user, reduces its rate to the next lower rate as listed in Table 5.1. In order to specify which user to be selected we consider three different goals, namely maximizing overall rate,
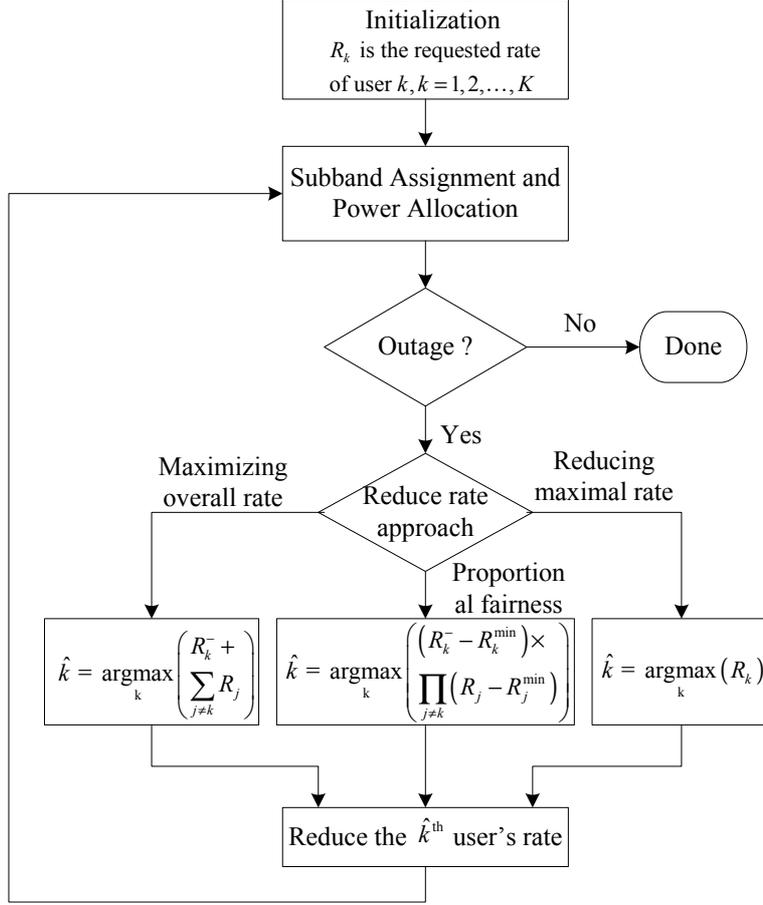
Figure 5.2: Flow chart of the proposed algorithm.

achieving proportional fairness [87] [2], and reducing maximal rate. In particular, given the data rate of the kth user, R_k, we denote its one-step reduced rate by R_k^-. For instance, from Table 5.1, the reduced rate R_k^- corresponding to a rate $R_k = 320$ Mbps is $R_k^- = 200$ Mbps. Note that when the rate R_k reaches the minimum allowable rate of 53.3 Mbps, we let $R_k^- = R_k$, i.e., the rate R_k is not

---

[2]Note that proportional fairness is achievable when the utility is a log function. In this paper, we have discrete and non-convex case, so the same product form is used as the system performance goal instead of the log function. From the simulations, this goal achieves tradeoff of performances and fairness between the maximal rate goal and reducing maximal rate goal.

further reduced. Then, the user $\hat{k}$ whose rate will be reduced can be determined according to the performance goals as:

$$
\hat{k} = \begin{cases} \arg\max_k R_k^- + \sum_{j=1,j\neq k}^K R_j, & \text{Maximizing overall rate;} \\ \arg\max_k \left(R_k^- - R_k^{min}\right) \times \prod_{j=1,j\neq k}^K \left(R_j - R_j^{min}\right), & \text{Proportional fairness;} \\ \arg\max_k(R_k), & \text{Reducing maximal rate,} \end{cases}
$$
(5.24)

where R_k^{min} denotes a minimal rate requirement for user k. With maximizing overall rate approach, the overall system rate is maximized in every reduction step. In case of the proportional fairness approach, the product of rates minus minimal rate requirements [87] is maximized. For reducing maximal rate approach, the highest rate in the system will be reduced. Note that if there is still no solution to the assignment after the rates of all users are reduced to the minimum allowable rate, then an outage is reported. This indicates that the system under the current channel conditions cannot support the transmission of all K users at the same time. The proposed joint resource allocation and rate adaptation algorithm is summarized as follows.

Initialization: Iteration index $n' = 0$, $R_k(0) = $ requested rate of user k, $k = 1, 2, \ldots K$

Iteration:

1. Given $R_k(n')$, solve subband assignment and power allocation problem in (5.23).

2. If (5.23) has a solution, the algorithm ends. Otherwise,

   - If $R_k(n') = R_k^-(n'), \forall k$, then an outage is reported and the algorithm ends.
   - Solve (5.24) to obtain $\hat{k}$.
   - Update the rates: $R_k(n'+1) = \begin{cases} R_k^-(n'), & k = \hat{k}; \\ R_k(n'), & \text{otherwise.} \end{cases}$
   - Set $n' = n' + 1$.

5.3 Simulation Results

To illustrate the performance of the proposed schemes, we perform simulations for multiband UWB systems with $N = 128$ subcarriers, $S = 14$ subbands, and the subband bandwidth of 528 MHz. Following the IEEE 802.15.3a standard proposal [18], we utilize the subbands with center frequencies $2904 + 528 \times n_b$ MHz, $n_b = 1, 2, \ldots, 14$. The OFDM symbol is of duration $T_{FFT} = 242.42$ ns. After adding the cyclic prefix of length $T_{CP} = 60.61$ ns and the guard interval of length $T_{GI} = 9.47$ ns, the symbol duration becomes $T_{SYM} = 312.5$ ns. The maximum transmitted power is -41.3 dBm/MHz, and the PER is maintained such that PER $< 8\%$ for a 1024 byte packet. The average noise power follows (5.6) with $N_F = 6.6$ dB, and the propagation loss factor is $\nu = 2$.

We consider a multiuser scenario in which each user is located at a distance of less than 4 meters from the central base station. The performance is evaluated in multipath channel environments specified in the IEEE 802.15.3a channel modeling sub-committee report [68]. We employ channel model 1 and 2, which are based on channel measurements over the range of 0-4 meters. The simulated channels were constant during the transmission of each packet, and independent from one packet to another. In each simulation, we averaged over a minimum of 50000 channel realizations.

5.3.1 Subband Assignment and Power Allocation

In this subsection, we present the average transmitted power and the outage probability curves for multiband UWB systems. Here, the outage probability is the probability that the requested rate cannot be supported under the constraints

in (5.23). We compare the performances of the proposed scheme with those of the current multiband scheme in the standards proposal [18].

For Figs. 5.3(a) and 5.3(b), the number of users is fixed to $K = 3$, while each user is randomly located at the distance of 1 to 4 meters from the base station. In Fig. 5.3(a), we illustrate the average transmitted power as a function of the data rates for standard multiband scheme, the proposed fast suboptimal scheme, and the optimal scheme obtained by full search. It is apparent that the proposed algorithm greatly reduces the average transmitted power compared to that in standard proposal. In addition, the proposed algorithm can achieve almost the same performance to the optimal scheme. The results show that both fast suboptimal and optimal approach can reduce about 60% of average transmitted power at low rates (53.3-200 Mbps) and up to 35% at high rates (320-480 Mbps). Notice that the curves are not smooth because of the discrete nature of the problem. Fig. 5.3(b) shows the outage probability versus the transmission rates. We can see that the proposed scheme achieves lower outage probability than that of the standard multiband scheme for any rates. For instance, at 110 Mbps, the outage probability of the proposed scheme is 5.5×10^{-3}, whereas that of the standard multiband scheme is 2.3×10^{-2}.

We also consider a multiuser system with different number of users, each located at a fixed position of about 4 meters from the base station. Specifically, the distance between the kth user and the base station is specified as $d_k = 4 - 0.1(k - 1)$ for $k = 1, 2, \ldots, K$. In Figs. 5.4(a) and 5.4(b), we show the average transmitted power and outage probability as functions of number of users for the data rates of 55, 80, and 110 Mbps. In both figures, we use the standard multiband scheme and the proposed scheme. We can observe from Fig. 5.4(a) that the transmitted
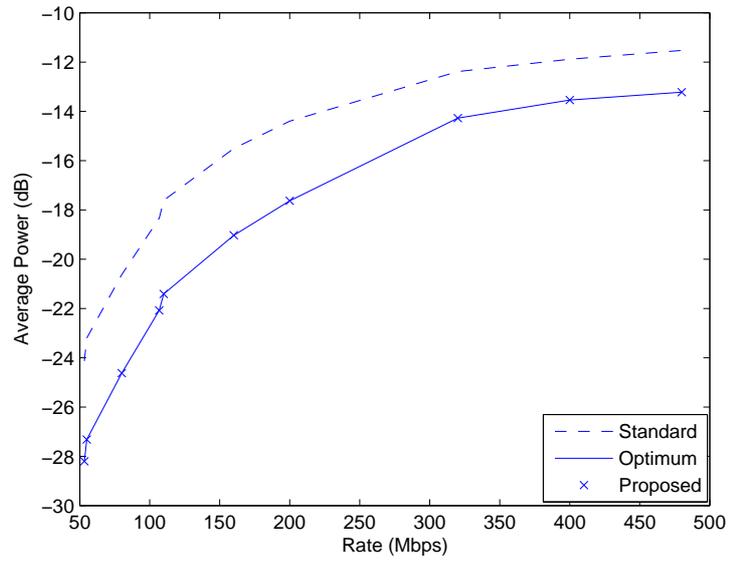
(a) Average Power vs. Rates
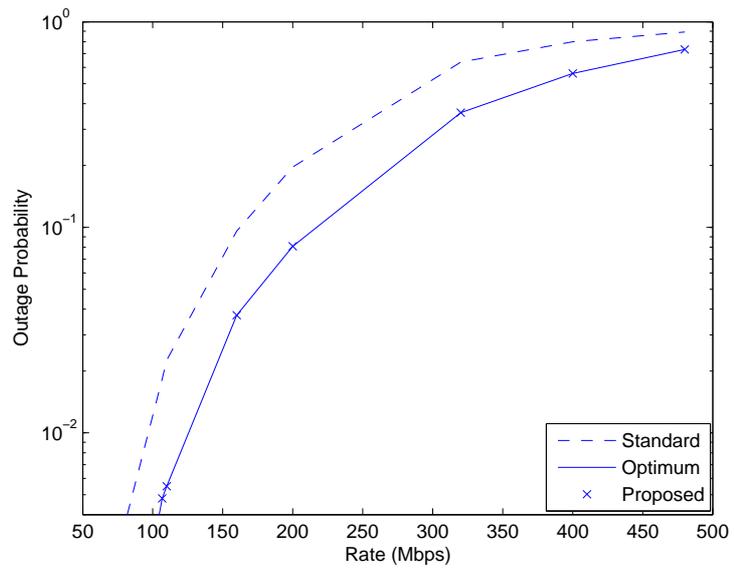
(b) Outage Probability vs. Rates

Figure 5.3: Performances of three-user system with random location.
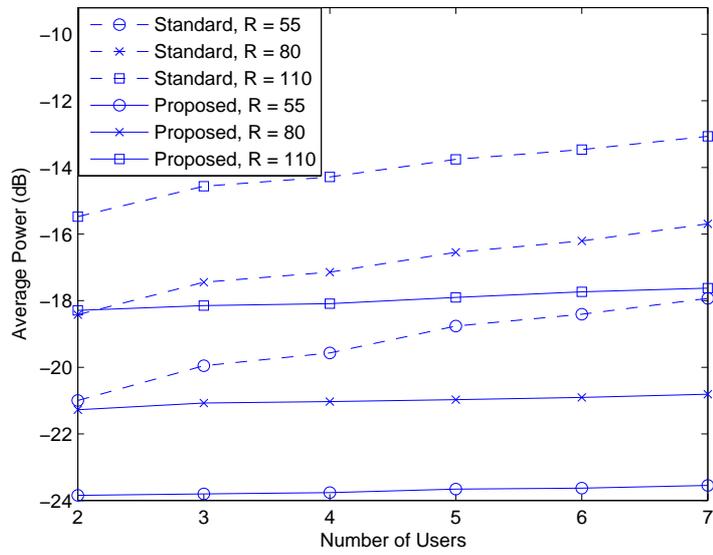
(a) Average Power vs. Number of Users
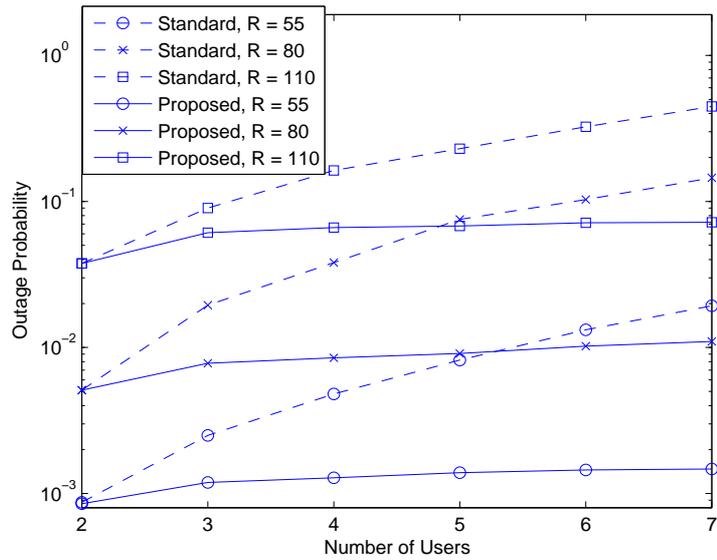
(b) Outage Probability vs. Number of Users

Figure 5.4: Performances of multiple-user system.

power increases with the number of users. This results from the limited available subbands with good channel conditions. When the number of users is large, some users have to occupy the subbands with worse channel conditions. Comparing the proposed algorithm with standard multiband approach, we can see that the proposed scheme achieves lower transmitted power for all the rate requirements.

Fig. 5.4(b) shows that the outage probability increases with the number of users. This is due to the fact that as the number of users increases, the system is more crowded and may not be feasible to support all these users at all times. Observe that at any rate, the performance of the standard multiband scheme degrades as the number of users increases. On the other hand, when the proposed scheme is employed, the effect of the number of users to the outage probability is insignificant when the rates are not higher than 110 Mbps. As we can see, the proposed algorithm achieves smaller outage probabilities than those of the standard scheme under all conditions.

5.3.2 Joint Rate Assignment and Resource Allocation

This subsection illustrates the performances of the proposed joint rate assignment and resource allocation algorithm for multiband system. We consider a multiuser system with different number of users. Each user is randomly located at the distance of 1 to 4 meters from the base station. The requested rates of users are also randomly selected from the set $\{200, 320, 400, 480\}$ Mbps, and the minimum rate requirement is $R_k^{min} = 50$ Mbps $\forall k$ for proportional fairness goal. The joint rate assignment and resource allocation algorithm proposed in Section 5.2.5 is performed for each set of requested rates and channel conditions.
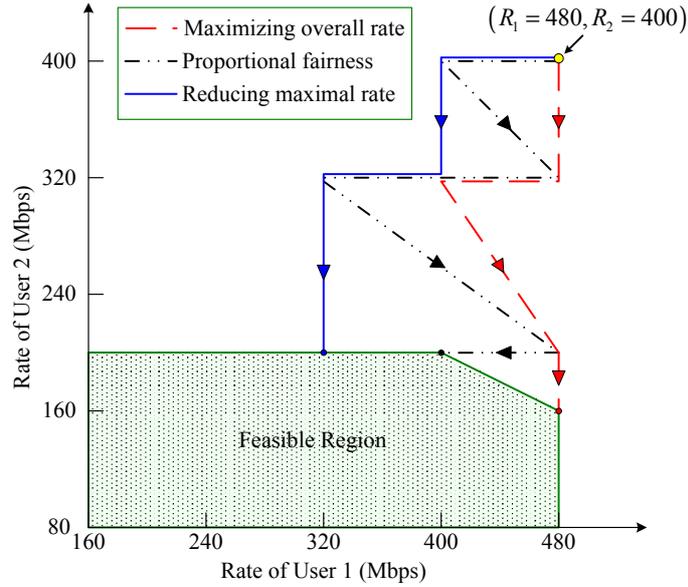
Figure 5.5: One realization of rate adaptation for two-user system.

Fig. 5.5 illustrates one realization of rate adaptation for a two-user system with three different goals. The shaded area represents the feasible range for R_1 and R_2 in the current channel conditions. In this example, the requested rates are $R_1 = 480$ and $R_2 = 400$ Mbps, and both users are located at about 4 meters from the base station. We can observe from Fig. 5.5 that the reducing maximal rate approach has lowest overall rate in every adaptation step. This is because the highest rate in the system can always be reduced. On the other hand, the maximizing overall rate approach tends to reduce the lower rate since most low rates have smaller decreasing step size than high rates. Although the maximizing overall rate approach always yields superior system performance, it is unfair to those applications with low data rates. The proportional fairness goal provides the performance that is between the maximizing overall rate approach and reducing maximal rate approach.
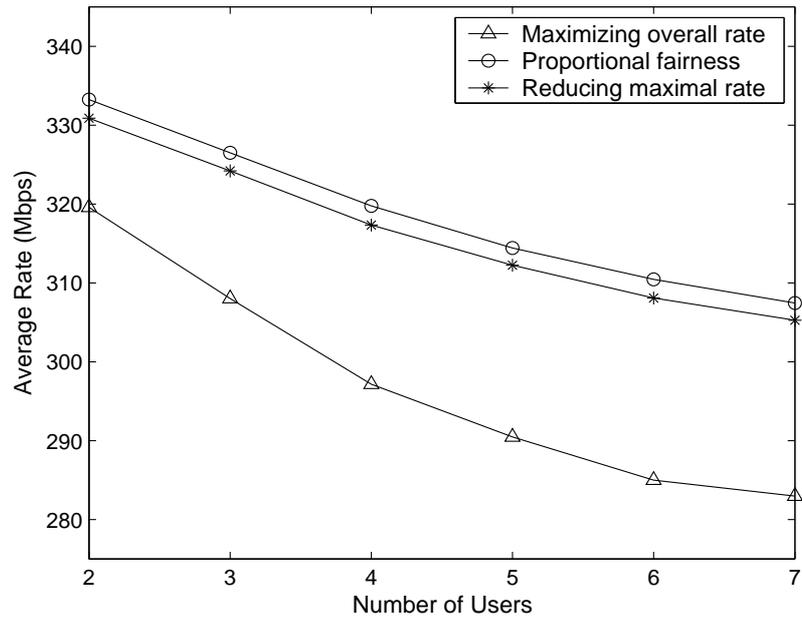
(a) Average Rate vs. Number of Users
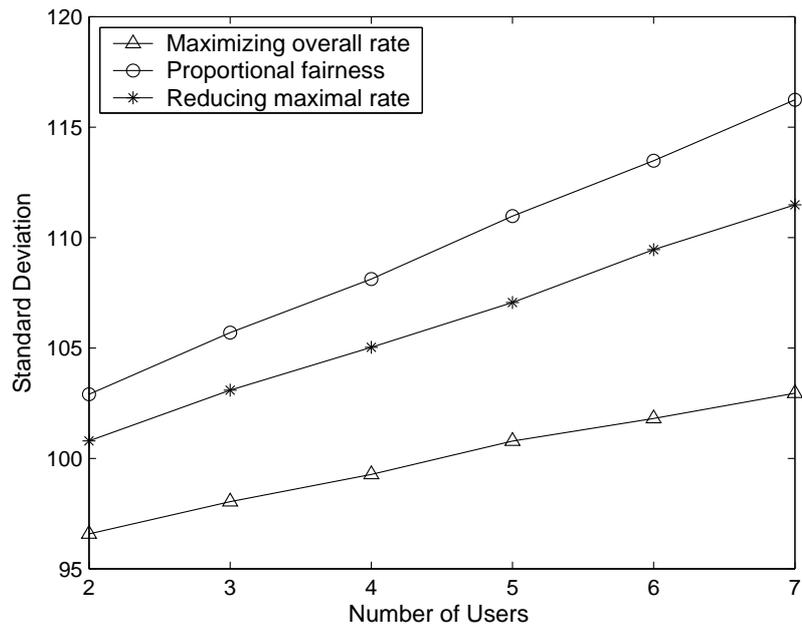
(b) Standard Deviation vs. Number of Users

Figure 5.6: Average rate and standard deviation of multiple-user system.

125

Figs. 5.6(a) and 5.6(b) show the average system performance versus the number of users. In Fig. 5.6(a), we present the performances in term of the average data rates of the users. We can see that the average rates of all three approaches decrease when the number of users increases. This is due to the limited subbands with good channel conditions. As the number of user increases, some users need to occupy subbands with poor channel conditions, and hence their feasible rates tend to be lower than the requested rates. Comparing the performances of three approaches, we can see that the proportional fairness yields slightly lower average rate than that of the maximizing overall rate approach, and both proportional fairness and maximizing overall rate approaches achieve much higher rates than that of the reducing maximal rate approach.

In Fig. 5.6(b), we show the standard deviations of the data rates of the users for three approaches. Here the standard deviation represents the fairness of allocation among users. We can observe that the standard deviation for every scheme increases with the number of users since the larger the number of users, the higher the variation of the rates. At any fixed number of user, the reducing maximal rate approach results in smallest standard deviation, and its standard deviation slightly increases with the number of users. This is because the feasible rates obtained from the reducing maximal rate approach are close to each other. In contrast, the maximizing overall rate scheme can yield the feasible rates of around 100 to 480 Mbps at the same time. Thus, its standard deviation increases much faster with the number of users. The standard deviation of proportional fairness approach is between the other two schemes. So the proportional fairness approach is a tradeoff between the maximal rate approach and reducing maximal rate approach for both performances and fairness.

5.4 Chapter Summary

Low power consumption is one of the key elements to make multiband UWB technology to be the solution for future indoor wireless communications. We propose in this chapter an efficient cross layer algorithm for allocating subband and power among users in a multiband UWB system. The proposed scheme aims to reduce power consumption without compromising performance. We propose a general framework to minimize the overall transmitted power under the practical implementation constraints. The formulated problem is NP hard; however, with the proposed fast suboptimal algorithm, we can reduce the computational complexity to only $O(K^2S)$, where K is the number of users and S is the number of subbands.

Simulation results show that the proposed algorithm achieves comparable performances to those of complex optimal full search algorithm, and can save up to 61% of power consumption compared to the multiband OFDM scheme currently proposed in the IEEE 802.15.3a standard. Moreover, the proposed algorithm can obtain the feasible solutions adaptively when the initial system is not feasible for the rate requirements of the users. Among three different system optimization goals used in the proposed rate adaptation algorithm, the proportional fairness approach turns out to be a tradeoff between the maximal rate approach and reducing maximal rate approach for both performances and fairness.

Chapter 6

Performance Enhancement with Cooperative Protocols

Due to the limitation on the transmitted power level, any UWB system faces significant design challenges to achieve the desired performance and coverage range. To this date, limited works have been proposed to improve the coverage of UWB systems. One approach is through the use of analog repeaters as used in conventional cellular systems. For example, pulse position modulation UWB repeater was proposed in [88]. Although the analog repeaters are simple, they suffer from noise amplification, which has confined their applications to specific scenarios. Another approach that has been considered is the employment of MIMO technology in UWB systems. Nevertheless, it might not be easy to have multiple antennas installed in the UWB devices. One possible way to overcome this problem and to benefit from the performance enhancement introduced by MIMO systems is through an employment of cooperative communications in UWB.

The research works in [59]- [62] have proved the significant potential of cooper-

ative diversity in wireless networks. Current UWB technology, on the other hand, relies on a non-cooperative transmission, in which the diversity can be obtained only from MIMO coding or information repetition at the transmitter [19], [56]- [58]. Furthermore, many UWB devices are expected to be in home and office environments; most of these devices are not in active mode simultaneously, but they can be utilized as relays to help the active devices. Additionally, due to the TDMA mechanism of the MAC and the network structure of the IEEE 802.15.3a WPAN standard [8], the cooperative protocols can be adopted in UWB WPANs. These facts motivate us to introduce the concept of cooperative diversity in UWB systems as an alternative approach to improve the UWB performance and coverage without the requirement of additional antennas or network infrastructures.

In this chapter, we propose to enhance the performance of UWB systems with cooperative protocols. The proposed framework is based on DF cooperative protocol; however, other cooperative protocols such as AF protocol can be applied in a similar way. The SER performance analysis and optimum power allocation are provided for cooperative UWB multiband OFDM systems. In order to capture the unique multipath-clustering property of UWB channels [68], the SER performance is characterized in terms of the cluster and the ray arrival rates. Based on the established SER formulations, we determine optimum power allocations for cooperative UWB multiband OFDM systems with two different objectives, namely minimizing overall transmitted power and maximizing system coverage. When the subbands are not fully occupied, we propose to further improve the performance of cooperative UWB systems by allowing the source to repeat its information on one subband, while the relay helps forward the source information on another subband. The improved cooperative UWB scheme is compatible to the current multiband

OFDM standard proposal [18], which allows multiuser transmission using different subbands. Both analytical and simulation results show that the proposed cooperative UWB scheme achieves up to 43% power saving and up to 85% coverage extension compared with non-cooperative UWB at the same data rate. By allowing the source and the relay to transmit simultaneously, the performance of cooperative UWB can be further improved up to 52% power saving and up to 100% coverage extension compared with non-cooperative scheme.

An outline of this chapter is as follows. Section 6.1 describes the system models of non-cooperative and cooperative UWB systems employing multiband OFDM. In Section 6.2, we analyze the SER performance of the cooperative UWB multiband OFDM system with DF protocol. In Section 6.3, we study the optimum power allocation with the objectives to minimize overall transmitted power and to maximize the coverage. An improved cooperative UWB scheme is proposed in Section 6.4. Simulation results are given in Section 6.5.

6.1 System Model

We consider a UWB multiband OFDM system [18] as proposed in the IEEE 802.15.3a standard [8]. The channel model is based on the S-V model for indoor channels [73].

6.1.1 Non-Cooperative UWB multiband OFDM System

In a non-cooperative UWB multiband OFDM system, each source transmits information directly to its destination. We consider the case when the time-domain spreading with a spreading factor of two is performed. In this scenario, the same

| Pre-amble | PLCP Header | $\mathbf{x}_1$ | $\mathbf{x}_1$ | $\mathbf{x}_2$ | $\mathbf{x}_2$ | ... | $\mathbf{x}_{S/2}$ | $\mathbf{x}_{S/2}$ | FCS | Tail bits | Pad bits |

Frame payload

(a) Non-Cooperative (time spreading gain of two)

| Pre-amble | PLCP Header | $\mathbf{x}_1$ | $\mathbf{x}_2$ | $\mathbf{x}_3$ | $\mathbf{x}_4$ | ... | $\mathbf{x}_{S-1}$ | $\mathbf{x}_S$ | FCS | Tail bits | Pad bits |

(b) Cooperative (no time spreading)

—— Phase 1
– – Phase 2
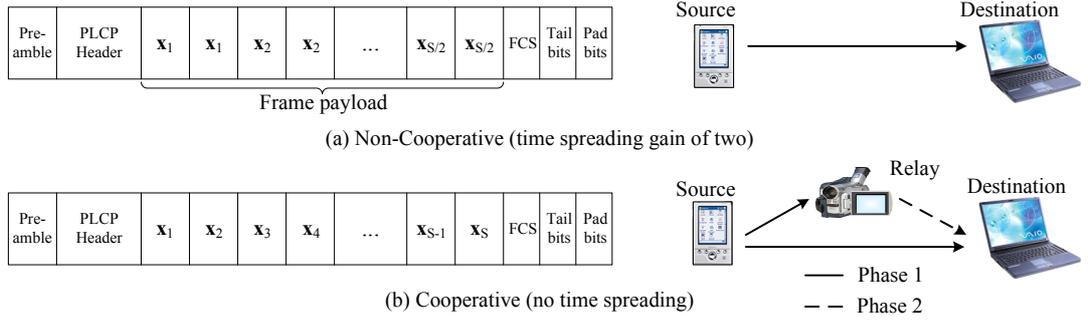
Figure 6.1: Illustrations of non-cooperative and cooperative UWB multiband OFDM systems with the same data rate.

information is transmitted repeatedly over two consecutive OFDM symbols, which can be sent on different subbands to gain the diversity from time spreading. Fig. 6.1(a) depicts the frame structure for the multiband OFDM system with time spreading gain of two. In Fig. 6.1, $\mathbf{x}_i$ ($1 \leq i \leq S$) denotes a vector of data symbols to be transmitted in each OFDM symbol, and S represents the number of OFDM symbols contained in the frame payload. With the choice of cyclic prefix length greater than the duration of the channel impulse response, OFDM allows for each UWB subband to be divided into a set of orthogonal narrowband subcarriers. At the destination, the received signal at the nth subcarrier during the kth OFDM symbol duration can be modeled as

$$y_{s,d}^k(n) = \sqrt{P_k}H_{s,d}^k(n)x(n) + z_{s,d}^k(n), \tag{6.1}$$

where $x(n)$ denotes an information symbol to be transmitted at subcarrier n, $H_{s,d}^k(n)$ represents the frequency response of the channel from the source to the destination, and $z_{s,d}^k(n)$ is additive noise. The superscript index k, $k = 1$ and 2, is used to distinguish the signals in two consecutive OFDM symbols. In (6.1), P_k is the transmitted power at the source. As in the current multiband standard

131

proposal [18], we assume that the power P_k is equal for all subcarriers. Since time spreading is performed, $x(n)$ is the same in both OFDM symbols. The noise term $z_{s,d}^k(n)$ is modeled as a complex Gaussian random variable with zero mean and variance N_0. From (2.7), the channel frequency response is given by

$$H_{s,d}^k(n) = \sigma_{s,d}^2 \sum_{c=0}^{C} \sum_{l=0}^{L} \alpha_{s,d}^k(c,l) e^{-\mathbf{j}2\pi n\Delta f[T_{s,d}(c)+\tau_{s,d}(c,l)]}, \tag{6.2}$$

where the subscript $\{s,d\}$ indicates the channel link from the source to the destination. With an ideal band hopping, we assume that the signal transmitted over different frequency bands undergo independent fading, i.e., $H_{s,d}^k(n)$ are independent for different k.

Note that when frequency-domain spreading is performed, the same information can be transmitted in more than one subcarrier. For subsequent performance evaluation, we denote Φ_n as a set of subcarriers that carry the information $x(n)$. For instance, to minimize the correlation among the channel frequency response at different subcarriers, Φ_n can be given by [29]: $\Phi_n = \{n\}$ $(0 \le n \le N-1)$ if $g_F = 1$ and $\Phi_n = \{n, \ n+N/2\}$ $(0 \le n \le N/2-1)$ if $g_F = 2$, where N is the total number of subcarriers, and g_F represents the frequency spreading gain. Such frequency-domain spreading increases the frequency diversity, and hence improves the performance of UWB systems with low data rates.

6.1.2 Cooperative UWB Multiband OFDM Systems

We consider cooperative communications over UWB multiband OFDM system with two users. This two-user cooperation will serve as a basic building block for future study on multiuser UWB systems. In a cooperative UWB system, each user can be a source node that sends its information to the destination, or it can be

a relay node that helps transmit the other user's information. The cooperation strategy comprises two transmission phases. In Phase 1, the source sends the information to its destination, and the information is also received by other users at the same time. In Phase 2, the source is silent, while the relay helps forward the source information. Suppose the DF cooperative protocol is used, then the relay decodes the received information and forwards the decoded symbols to the destination. We consider the case when the time-domain spreading is not performed at the source. In this scenario, the data frame which is transmitted from the source in Phase 1 and from the relay in Phase 2 can be depicted as in Fig. 6.1(b). Suppose non-cooperative UWB and cooperative UWB schemes have the same frequency spreading gain. Then, we can see from Figs. 6.1(a) and 6.1(b) that the non-cooperative UWB scheme with time spreading and the cooperative UWB scheme without time spreading achieve the same data rate.

In Phase 1, the received signal at the destination is the same as (6.1) with $k = 1$, and the received signal at the relay can be written as

$$y_{s,r}(n) = \sqrt{P_1}H_{s,r}(n)x(n) + z_{s,r}(n), \tag{6.3}$$

in which $H_{s,r}(n)$ is the channel frequency response from the source to the relay, and $z_{s,r}(n)$ is additive noise. In Phase 2, the relay forwards the decoded symbol with power P_2 to the destination only if the symbol is decoded correctly; otherwise, the relay does not send or remain idle. For mathematical tractability, we assume that the relay can judge whether the decoded information is correct[1]. The received

---

[1]Practically, this can be done at the relay by applying a simple SNR threshold on the received data. Although, it can lead to some error propagation, but for practical ranges of operating SNR, the event of error propagation can be assumed negligible.

signal at the destination in Phase 2 can be specified as [65]

$$y_{r,d}(n) = \sqrt{\tilde{P}_2} H_{r,d}(n) \, x(n) + z_{r,d}(n), \tag{6.4}$$

where $H_{r,d}(n)$ is the channel frequency response from the relay to the destination, and $z_{r,d}(n)$ is additive noise. The transmitted power $\tilde{P}_2 = P_2$ if the relay correctly decodes the transmitted symbol $x(n)$ from the source; otherwise $\tilde{P}_2 = 0$, i.e., the relay does not send or remains idle. The multipath channels of source-relay link and relay-destination link are also modeled according to the S-V model with the total energy of the multipath components given by $\sigma_{s,r}^2$ and $\sigma_{r,d}^2$, respectively. The noise $z_{s,r}(n)$ and $z_{r,d}(n)$ are complex Gaussian distributed with zero mean and variance N_0. We assume that the channel state information is known at the receiver, but not at the transmitter. The channel coefficients are assumed to be independent for different transmit-receive links. As in the non-cooperative transmission, the information can be repeatedly transmitted in different subcarriers to obtain the frequency diversity when the desired data rate is low. The destination employs a MRC [81] to combine the information transmitted via different times (Phase 1 and Phase 2) or frequencies.

6.2 SER Analysis for Cooperative UWB Multiband OFDM

In this section, we analyze the average SER performance of cooperative UWB multiband OFDM systems with DF protocol. Following the multiband standard proposal [18], we focus on the analysis for UWB systems with M-PSK signals. The analysis for the systems with M-QAM signals is similar.

6.2.1 DF Cooperative UWB Multiband OFDM

In this subsection, we provide closed-form SER formulations for DF cooperative UWB systems. With the knowledge of channel state information, the destination detects the transmitted symbols by coherently combining the received signals from the source and the relay. Assume that each transmitted symbol has unit energy, then the instantaneous SNR of the MRC output can be written as [81]

$$\eta = \frac{P_1}{N_0} \sum_{n \in \Phi_n} |H_{s,d}(n)|^2 + \frac{\tilde{P}_2}{N_0} \sum_{n \in \Phi_n} |H_{r,d}(n)|^2, \tag{6.5}$$

where Φ_n is the set of subcarriers that carry the information $x(n)$ as defined in the previous section. Suppose the M-PSK modulation is used, then conditional SER can be expressed as [81]

$$P_e|_{\{H\}} = \Psi(\eta) \triangleq \frac{1}{\pi} \int_0^{\pi - \pi/M} \exp\left(-\frac{b\eta}{\sin^2 \theta}\right) d\theta, \tag{6.6}$$

where $b = \sin^2(\pi/M)$. Recall that the relay forwards the transmitted symbol $x(n)$ with power P_2 to the destination only if the symbol is decoded correctly. That is $\tilde{P}_2 = P_2$ if the relay decodes the transmitted symbol correctly; otherwise $\tilde{P}_2 = 0$. Assume that the relay has perfect knowledge of the channel gain coefficients $H_{s,r}(n)$, and the MRC is used to combine the information transmitted via different frequencies. Then, the instantaneous SNR at the MRC output is given by $\eta_{s,r} = \frac{P_1}{N_0} \sum_{n \in \Phi_n} |H_{s,r}(n)|^2$, and the conditional probability of incorrect decoding at the relay is $\Psi(\eta_{s,r})$. Taking into account the two possible cases of $\tilde{P}_2$, the conditional SER in (6.6) can be re-expressed as

$$P_e|_{\{H\}} = \Psi(\eta)|_{\tilde{P}_2=0} \Psi(\eta_{s,r}) + \Psi(\eta)|_{\tilde{P}_2=P_2} \left[1 - \Psi(\eta_{s,r})\right]. \tag{6.7}$$

Substitute (6.5) into (6.7) and average over the channel realizations, resulting in the average SER

$$
\begin{aligned}
\mathrm{P}_e = & \frac{1}{\pi^2} \int_0^{\pi-\pi/M} \mathcal{M}_{\eta_{s,d}} \Big(\frac{b}{\sin^2\theta}\Big) d\theta \int_0^{\pi-\pi/M} \mathcal{M}_{\eta_{s,r}} \Big(\frac{b}{\sin^2\theta}\Big) d\theta \\
& + \frac{1}{\pi} \int_0^{\pi-\pi/M} \mathcal{M}_{\eta_{s,d}} \Big(\frac{b}{\sin^2\theta}\Big) \mathcal{M}_{\eta_{r,d}} \Big(\frac{b}{\sin^2\theta}\Big) d\theta \left[1 - \frac{1}{\pi} \int_0^{\pi-\pi/M} \mathcal{M}_{\eta_{s,r}} \Big(\frac{b}{\sin^2\theta}\Big) d\theta \right],
\end{aligned}
$$

$$(6.8)$$

where $\mathcal{M}_\eta(s) = \mathrm{E}\big[\exp(-s\eta)\big]$ is the MGF of η [81], $\eta_{s,d} = \frac{P_1}{N_0} \sum_{n\in\Phi_n} |H_{s,d}(n)|^2$, and $\eta_{r,d} = \frac{P_2}{N_0} \sum_{n\in\Phi_n} |H_{r,d}(n)|^2$. Note that the channel frequency responses, and hence the MGFs of $\eta_{s,d}$, $\eta_{s,r}$ and $\eta_{r,d}$, are in terms of the multipath gain coefficients whose amplitudes are Rayleigh distributed, as well as the multipath delays T_c and $\tau_{c,l}$ which are based on Poisson process. If the information is not jointly encoded across subcarriers, i.e., the frequency spreading gain is $g_F = 1$, $\mathcal{M}_{\eta_{x,y}}(s)$ can be determined as

$$
\mathcal{M}_{\eta_{x,y}}(s) = \left(1 + \frac{sP_x\sigma_{x,y}^2}{N_0}\right)^{-1},
$$

$$(6.9)$$

where $P_x = P_1$ if x represents the source and $P_x = P_2$ if x represents the relay. If the data is jointly encoded across multiple subcarriers, it is difficult, if not impossible, to obtain closed-form formulations of the MGFs in (6.8). In this case, we exploit an approximation approach in the previous chapter which allows us to approximate the MGF of $\eta_{x,y}$ as

$$
\mathcal{M}_{\eta_{x,y}}(s) \approx \prod_{n\in\Phi_n} \left(1 + \frac{sP_x\sigma_{x,y}^2\beta_n(\mathbf{R}_{x,y})}{N_0}\right)^{-1},
$$

$$(6.10)$$

where $\beta_n(\mathbf{R}_{x,y})$ denotes the eigenvalues of a matrix $\mathbf{R}_{x,y}$, and $\mathbf{R}_{x,y}$ is a correlation matrix whose each diagonal component is one and the $(i,j)^{th}$ $(i \neq j)$ component is given by

$$\mathbf{R}_{x,y}(i,j) = \Omega_{x,y}(0,0) \frac{\Lambda_{x,y} + \Gamma_{x,y}^{-1} + \mathbf{j}2\pi(n_i - n_j)\Delta f}{\Gamma_{x,y}^{-1} + \mathbf{j}2\pi(n_i - n_j)\Delta f} \; \frac{\lambda_{x,y} + \gamma_{x,y}^{-1} + \mathbf{j}2\pi(n_i - n_j)\Delta f}{\gamma_{x,y}^{-1} + \mathbf{j}2\pi(n_i - n_j)\Delta f},$$

(6.11)

in which n_i denotes the ith element in the set Φ_n. By substituting the MGFs in (6.9) and (6.10) into (6.8), we can express the SER of DF cooperative UWB system as

$$\begin{aligned}
\mathrm{P}_e \approx{} & F\left(\prod_{n\in\Phi_n}\left(1 + \frac{bP_1\sigma_{s,d}^2\beta_n(\mathbf{R}_{s,d})}{N_0\sin^2\theta}\right)\right) F\left(\prod_{n\in\Phi_n}\left(1 + \frac{bP_1\sigma_{s,r}^2\beta_n(\mathbf{R}_{s,r})}{N_0\sin^2\theta}\right)\right) \\
& + F\left(\prod_{n\in\Phi_n}\left(1 + \frac{bP_1\sigma_{s,d}^2\beta_n(\mathbf{R}_{s,d})}{N_0\sin^2\theta}\right)\left(1 + \frac{bP_2\sigma_{r,d}^2\beta_n(\mathbf{R}_{r,d})}{N_0\sin^2\theta}\right)\right) \\
& \times \left[1 - F\left(\prod_{n\in\Phi_n}\left(1 + \frac{bP_1\sigma_{s,r}^2\beta_n(\mathbf{R}_{s,r})}{N_0\sin^2\theta}\right)\right)\right],
\end{aligned}$$

(6.12)

where

$$F(x(\theta)) = \frac{1}{\pi}\int_0^{\pi-\pi/M} \frac{1}{x(\theta)}d\theta.$$

(6.13)

Note that the average SER in (6.12) is exact if $\Phi_n = \{n\}$, i.e., the frequency spreading gain is $g_F = 1$.

In (6.12), we provide a SER formulation for general DF cooperative UWB systems. Such SER formulation involves integrations, so it is hard to get some insightful understanding of the UWB system performance. To get more insight, we provide in what follows the SER approximations that involve no integrations. We focus on the SER performance for two special cases that have been considered in the multiband standard proposal [18].

1. If frequency spreading gain is $g_F = 1$, the average SER can be expressed as

$$P_e = F\left(1 + \frac{bP_1\sigma_{s,d}^2}{N_0\sin^2\theta}\right)F\left(1 + \frac{bP_1\sigma_{s,r}^2}{N_0\sin^2\theta}\right)$$
$$+ F\left(\left(1 + \frac{bP_1\sigma_{s,d}^2}{N_0\sin^2\theta}\right)\left(1 + \frac{bP_2\sigma_{r,d}^2}{N_0\sin^2\theta}\right)\right)\left[1 - F\left(1 + \frac{bP_1\sigma_{s,r}^2}{N_0\sin^2\theta}\right)\right],$$

(6.14)

which is the same as that of cooperative narrowband system in Rayleigh fading environment. It has been shown in [65] that when all channel links are available, i.e., $\sigma_{s,d}^2 \neq 0$, $\sigma_{s,r}^2 \neq 0$, and $\sigma_{r,d}^2 \neq 0$, the SER (6.14) can be upper-bounded by

$$P_e \leq \frac{A_1^2}{b^2\rho_1^2\sigma_{s,d}^2\sigma_{s,r}^2} + \frac{A_2}{b^2\rho_1\rho_2\sigma_{s,d}^2\sigma_{r,d}^2},$$

(6.15)

where $\rho_i = P_i/N_0$ and

$$A_i = \frac{1}{\pi}\int_0^{\pi - \pi/M}\sin^{2i}\theta d\theta.$$

(6.16)

Specifically, we have $A_1 = \frac{M-1}{2M} + \frac{1}{4\pi}\sin\frac{2\pi}{M}$ and $A_2 = \frac{3(M-1)}{8M} + \frac{1}{4\pi}\sin\frac{2\pi}{M} - \frac{1}{32\pi}\sin\frac{4\pi}{M}$ [65]. The upper bound in (6.15) is loose at low SNR, but it is tight at high SNR [65]. However, UWB systems may operate at low SNR due to the limitation on the transmitted power level. In what follows, we provide a SER approximation that is close to the exact SER for every SNR, and does not involve integrations. Observe that all the integrands in the right hand side of (6.14) can be written as $F\left((p(\sin^2\theta) + c)/\sin^{2i}\theta\right)$, where i is a positive integer, c is a constant that does not depend on θ, and $p(x)$ denotes a polynomial function of x. By bounding $p(\sin^2\theta)$ with $p(1)$ and removing

the negative term in (6.14), the SER can be approximated by

$$P_e \approx \frac{A_1^2}{1 + b\rho_1(\sigma_{s,d}^2 + \sigma_{s,r}^2) + b^2\rho_1^2\sigma_{s,d}^2\sigma_{s,r}^2}$$
$$+ \frac{A_2}{1 + b(\rho_1\sigma_{s,d}^2 + \rho_2\sigma_{r,d}^2) + b^2\rho_1\rho_2\sigma_{s,d}^2\sigma_{r,d}^2}. \tag{6.17}$$

2. If frequency spreading gain is $g_F = 2$, the eigenvalues of the correlation matrix $\mathbf{R}_{x,y}$ are $1 + B_{x,y}$ and $1 - B_{x,y}$, where

$$B_{x,y} = \Omega_{x,y}(0,0)\frac{\left[(\Lambda_{x,y} + \Gamma_{x,y}^{-1})^2 + q\right]^{\frac{1}{2}}\left[(\lambda_{x,y} + \gamma_{x,y}^{-1})^2 + q\right]^{\frac{1}{2}}}{\left[(\Gamma_{x,y}^{-1})^2 + q\right]^{\frac{1}{2}}\left[(\gamma_{x,y}^{-1})^2 + q\right]^{\frac{1}{2}}}, \tag{6.18}$$

in which $q = (2\pi\mu\Delta f)^2$ and μ denotes the subcarrier separation. Substituting the eigenvalues of correlation matrices $\mathbf{R}_{s,d}$, $\mathbf{R}_{s,r}$ and $\mathbf{R}_{r,d}$ into (6.12), we can simplify the approximate SER to

$$P_e \approx F(V_{s,d})F(V_{s,r}) + F(V_{s,d}V_{r,d})[1 - F(V_{s,r})], \tag{6.19}$$

where

$$V_{x,y} = 1 + \frac{bP_x\sigma_{x,y}^2}{N_0\sin^2\theta}\left(1 + \frac{bP_x\sigma_{s,d}^2(1 - B_{x,y}^2)}{N_0\sin^2\theta}\right).$$

Following the same approximation approach as in [65], we obtain an approximate SER at high SNR as

$$P_e \approx \frac{A_2^2}{b^4\rho_1^4\sigma_{s,d}^4\sigma_{s,r}^4(1 - B_{s,d}^2)(1 - B_{s,r}^2)} + \frac{A_4}{b^4\rho_1^2\rho_2^2\sigma_{s,d}^4\sigma_{r,d}^4(1 - B_{s,d}^2)(1 - B_{r,d}^2)}. \tag{6.20}$$

Similar to the case of no frequency spreading, a tighter approximate SER can be obtained by replacing $p(\sin^2\theta)$ with $p(1)$. The resulting SER can be

expressed as

$$P_e \approx \frac{1}{1 + b\rho_1\sigma_{s,d}^2 + b^2\rho_1^2\sigma_{s,d}^4(1 - B_{s,d}^2)} \left(\frac{A_2^2}{1 + b\rho_1\sigma_{s,r}^2 + b^2\rho_1^2\sigma_{s,r}^4(1 - B_{s,r}^2)} \right.$$
$$\left. + \frac{A_4}{1 + b\rho_2\sigma_{r,d}^2 + b^2\rho_2^2\sigma_{r,d}^4(1 - B_{r,d}^2)} \right).$$

$$(6.21)$$

In Fig. 6.2, we compare the above SER approximations with SER simulation curves in case of cooperative UWB system with frequency spreading gain of one and two. The simulated multiband OFDM system has $N = 128$ subcarriers, the subband bandwidth is 528 MHz, and the channel model parameters follow those for CM 1 [68]. In case of frequency spreading gain $g_F = 2$, the subcarrier separation is chosen as $\mu = N/2 = 64$. For fair comparison, we plot average SER curves as functions of P/N_0. In case of frequency spreading gain $g_F = 1$, the theoretical calculation (6.14) matches with the simulation curve. With frequency spreading gain $g_F = 2$, the SER approximation (6.19) is also close to the simulation curve, except for some difference at low SNR which is due to the approximation of the Poisson behavior of the multipath components. The SER approximations (6.15) and (6.20) are loose at low SNR but they are tight at high SNR, as expected. Moreover, the SER approximations (6.17) and (6.21) are close to the simulation curves for the entire SNR range.

It is worth noting that the SER analysis provided in this section includes two-hop relay communication scenario as a special case. Specifically, the performance of the two-hop relay system can be obtained from (6.12) by replacing $\sigma_{s,d}^2$ with 0.
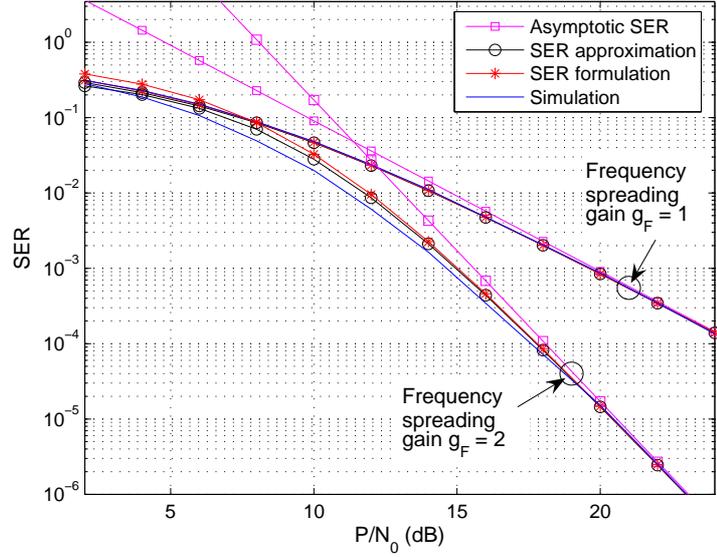
Figure 6.2: Comparison of the SER formulations and the simulation result for the DF cooperative UWB system. We assume that $\sigma_{s,d}^2 = \sigma_{s,r}^2 = \sigma_{r,d}^2 = 1$, and $P_1 = P_2 = P/2$.

The resulting SER of the two-hop relay cooperative UWB system is

$$
\mathrm{P}_e \approx F\left(\prod_{n\in\Phi_n}\left(1+\frac{bP_1\sigma_{s,r}^2\beta_n(\mathbf{R}_{s,r})}{N_0\sin^2\theta}\right)\right) + F\left(\prod_{n\in\Phi_n}\left(1+\frac{bP_2\sigma_{r,d}^2\beta_n(\mathbf{R}_{r,d})}{N_0\sin^2\theta}\right)\right.
$$
$$
\left. \times\left[1-F\left(\prod_{n\in\Phi_n}\left(1+\frac{bP_1\sigma_{s,r}^2\beta_n(\mathbf{R}_{s,r})}{N_0\sin^2\theta}\right)\right)\right]\right).
$$

$$(6.22)$$

Following the same procedure as above, (6.22) can be tightly upper bounded at high SNR as

$$
\mathrm{P}_e \leq \frac{A_1 N_0}{b}\left(\frac{1}{P_1\sigma_{s,r}^2}+\frac{1}{P_2\sigma_{r,d}^2}\right) \qquad \text{if } g_F = 1; \qquad (6.23)
$$

$$
\mathrm{P}_e \approx \frac{A_2^2 N_0^2}{b^2}\left(\frac{1}{P_1^2\sigma_{s,r}^4(1-B_{s,r}^2)}+\frac{1}{P_2^2\sigma_{r,d}^4(1-B_{r,d}^2)}\right) \text{ if } g_F = 2. \qquad (6.24)
$$

6.2.2 Comparison of Cooperative and Non-Cooperative UWB Multiband OFDM

We provide in this subsection performance comparison between the cooperative and non-cooperative UWB multiband OFDM systems with the same transmission data rate.

Consider a non-cooperative UWB system with time spreading gain of two, as described in Section 6.1.1. With an assumption of the ideal band hopping, the average SER can be given by

$$
\mathrm{P}_e \approx F \left(\prod_{n \in \Phi_n} \left(1 + \frac{bP_1 \sigma_{s,d}^2 \beta_n(\mathbf{R}_{s,d})}{N_0 \sin^2 \theta} \right) \prod_{n \in \Phi_n} \left(1 + \frac{bP_2 \sigma_{s,d}^2 \beta_n(\mathbf{R}_{s,d})}{N_0 \sin^2 \theta} \right) \right). \tag{6.25}
$$

In non-cooperative UWB system, it is general to put power equally on the source in two time slots [19]. By letting $P_1 = P_2 = P/2$ and removing all 1's in (6.25), the SER of non-cooperative UWB systems can be expressed as

$$
P_e \approx \left(\frac{b\sigma_{s,d}^2}{2\sqrt{A_2}} \frac{P}{N_0} \right)^{-2} \qquad \text{if } g_F = 1; \tag{6.26}
$$

$$
P_e \approx \left(\frac{b\sigma_{s,d}^2 \sqrt{1 - B_{s,d}^2}}{2A_4^{\frac{1}{4}}} \frac{P}{N_0} \right)^{-4} \qquad \text{if } g_F = 2. \tag{6.27}
$$

The above results indicate that the diversity order of non-cooperative UWB system with time spreading is twice frequency spreading gain $(2g_F)$, as expected. Moreover, the coding gain is $G_{NC} = b\sigma_{s,d}^2/(2\sqrt{A_2})$ if the frequency spreading gain $g_F = 1$ and $G_{NC} = b\sigma_{s,d}^2 \sqrt{1 - B_{s,d}^2}/(2A_4^{\frac{1}{4}})$ if $g_F = 2$.

In cooperation systems, we do not really have the notion of coding since the information is not jointly encoded at the source. However, jointly combining the transmitted signals from the direct link and the relay link also results in the system performance of a form $P_e = (G_{DF}P/N_0)^{-\Delta}$, where Δ is the diversity order and

G_{DF} represents the overall cooperation gain of the cooperative UWB systems. Let us denote $r = P_1/P$ as the power ratio of the transmitted power P_1 at the source over the total power P. According to (6.15) and (6.20), the approximate SER of DF cooperative UWB system can be expressed as

$$P_e \approx \left(\frac{b\sigma_{s,d}\sigma_{s,r}\sigma_{r,d}r}{\sqrt{A_1^2\sigma_{r,d}^2 + A_2\sigma_{s,r}^2 r/(1-r)}} \frac{P}{N_0} \right)^{-2} \qquad \text{if } g_F = 1; \quad (6.28)$$

$$P_e \approx \left(\frac{b\sigma_{s,d}\sigma_{s,r}\sigma_{r,d}r[(1-B_{s,d}^2)(1-B_{s,r}^2)(1-B_{r,d}^2)]^{\frac{1}{4}}}{[A_2^2\sigma_{r,d}^2(1-B_{r,d}^2) + A_4\sigma_{s,r}^2(1-B_{s,r}^2)r^2/(1-r)^2]^{\frac{1}{4}}} \frac{P}{N_0} \right)^{-4} \qquad \text{if } g_F = 2. \quad (6.29)$$

We can see that the cooperative UWB systems also achieve the diversity gain of twice frequency spreading gain. However, the cooperation gain depends not only on the channel quality of the source-destination link, but also on the channel qualities of the source-relay link as well as the relay-destination link. Since both non-cooperative and cooperative UWB systems achieve the same diversity order, it is interesting to compare the coding gain and the cooperation gain. We define the ratio between these two gains as $\xi = G_{DF}/G_{NC}$. From the SER expressions in (6.26)-(6.29), we have

$$\xi = \frac{2\sigma_{s,r}\sigma_{r,d}r}{\sigma_{s,d}} \left(\frac{A_1^2}{A_2}\sigma_{r,d}^2 + \frac{r}{1-r}\sigma_{s,r}^2 \right)^{-\frac{1}{2}} \qquad \text{if } g_F = 1; \quad (6.30)$$

$$\xi = \frac{2\sigma_{s,r}\sigma_{r,d}r}{\sigma_{s,d}} \left(\frac{A_2^2}{A_4}\frac{(1-B_{s,d}^2)}{(1-B_{s,r}^2)}\sigma_{r,d}^2 + \frac{r^2}{(1-r)^2}\frac{(1-B_{s,d}^2)}{(1-B_{r,d}^2)}\sigma_{s,r}^2 \right)^{-\frac{1}{4}} \qquad \text{if } g_F = 2. \quad (6.31)$$

Note that if all the channel links are of the same qualities, e.g., $\sigma_{s,d}^2 = \sigma_{s,r}^2 = \sigma_{r,d}^2 = 1$, then $\xi < 1$ for any value of the power ratio $0 < r < 1$, which implies that the non-cooperative transmission is preferable. The reason behind this is that the signals from the source and that from the relay are sent through the links with equal qualities. However, the source is the most reliable node since it has

the original copy of the signals, while the relay may not be able to acquire the original signal due to the noisy channel between the source and the relay. As a result, the non-cooperative systems whose all signals come from the source yield better performance than the cooperative system in which some of the signals come from the relay. On the other hand, when the link between the source and the relay or that between the relay and the destination have better quality than the source-destination link, e.g., when the relay is located between the source and the destination, then the DF cooperation gain, G_{DF}, could be greater than the coding gain, G_{NC}, depending on the power ratio r and the channel qualities. In the subsequent section, we determine the power ratio and the relay location that lead to the optimum performance of cooperative UWB systems.

6.3 Optimum Power Allocation for Cooperative UWB Multiband OFDM

In this section, we provide the optimum power allocation for cooperative UWB multiband OFDM system with two different objectives, namely minimizing overall transmitted power and maximizing the coverage. First, we formulate a problem to minimize the overall transmitted power under the constraints on performance requirement and power spectral density limitation. The optimum power allocation is determined based on the tight SER approximations in the previous section. Then, we determine an optimum power allocation such that the coverage of UWB system is maximized.

6.3.1 Power Minimization using Cooperative Communications

We determine in this subsection optimum power allocation based on the SER formulations derived in Section 6.2. Our objective is to minimize the overall transmitted power under the constraint on the SER performance and the transmitted power level. For notation convenience, let us define $\mathbf{P} = [P_1 \ P_2]^T$ as a power allocation vector. Now we can formulate the optimization problem as

$$\min_{\mathbf{P}} \quad P = \sum_i P_i \tag{6.32}$$

$$\text{s.t.} \begin{cases} \text{Performance: } \mathrm{P}_e \leq \varepsilon; \\ \text{Power: } P_i \leq P_{max}, \ \forall i, \end{cases}$$

where ε denotes the required SER and P_{max} is the maximum transmitted power for each subcarrier. The first constraint in (6.32) is to ensure the performance requirement. The average SER P_e follows the SER formulation in (6.8). The second constraint is related to the limitation on the transmitted power level.

For simplicity and for better understanding the system performance, let us consider at first the formulated problem in (6.32) without the maximum power constraint. Applying the Lagrange multiplier method, the optimum power allocation can be obtained by solving $1 + \zeta \partial \mathrm{P}_e / \partial P_1 = 0$, $1 + \zeta \partial \mathrm{P}_e / \partial P_2 = 0$, and $\mathrm{P}_e - \varepsilon = 0$, where ζ represents the Lagrange multiplier. In Section 6.2, we provide theoretical SER approximations that are close to the simulated SER. Based on such SER approximations, we can determine the optimum power allocation as follows. According to the tight SER approximations (6.17) and (6.21), the optimum power allocation for cooperative UWB system can be obtained by solving

the following equations:

$$\frac{A_i^2}{f_{s,r}}\left(\frac{1}{f_{s,r}}\frac{\partial f_{s,r}}{\partial P_1}+\frac{1}{f_{s,d}}\frac{\partial f_{s,d}}{\partial P_1}\right)-\frac{A_{2i}}{f_{r,d}}\left(\frac{1}{f_{s,d}}\frac{\partial f_{s,d}}{\partial P_1}-\frac{1}{f_{r,d}}\frac{\partial f_{r,d}}{\partial P_2}\right) = 0$$

$$\frac{1}{f_{s,d}}\left(\frac{A_i^2}{f_{s,r}}+\frac{A_{2i}}{f_{r,d}}\right)-\varepsilon = 0, \quad (6.33)$$

where i denotes the frequency spreading gain and A_i is specified in (6.16). If the frequency spreading gain is $g_F = 1$, $f_{s,d} = 1+b\rho_1\sigma_{s,d}^2$, $f_{s,r} = 1+b\rho_1\sigma_{s,r}^2$, and $f_{r,d} = 1+b\rho_2\sigma_{r,d}^2$. If the frequency spreading gain is $g_F = 2$, $f_{s,d} = 1+b\rho_1\sigma_{s,d}^2+b^2\rho_1^2\sigma_{s,d}^4(1-B_{s,d}^2)$, $f_{s,r} = 1+b\rho_1\sigma_{s,r}^2+b^2\rho_1^2\sigma_{s,r}^4(1-B_{s,r}^2)$, and $f_{r,d} = 1+b\rho_2\sigma_{r,d}^2+b^2\rho_2^2\sigma_{r,d}^4(1-B_{r,d}^2)$. At high enough SNR, the asymptotic optimum power allocation can be obtained from the tight SER upper bound (6.15) in case of $g_F = 1$ and from the SER approximation (6.20) in case of $g_F = 2$. According to the SER upper bound in (6.15), the asymptotic optimum power allocation for cooperative UWB system with $g_F = 1$ can be determined as

$$P_1 = rP \text{ and } P_2 = (1-r)P, \quad (6.34)$$

where

$$P = \frac{N_0}{br\sigma_{s,d}\sigma_{s,r}\sigma_{r,d}}\left(\frac{A_2r\sigma_{s,r}^2+A_1^2(1-r)\sigma_{r,d}^2}{\varepsilon(1-r)}\right)^{1/2}; \quad (6.35)$$

$$r = \frac{\sigma_{s,r}+\sqrt{\sigma_{s,r}^2+(8A_1^2/A_2)\sigma_{r,d}^2}}{3\sigma_{s,r}+\sqrt{\sigma_{s,r}^2+(8A_1^2/A_2)\sigma_{r,d}^2}}. \quad (6.36)$$

Based on the SER approximation (6.20), the asymptotic optimum power allocation for the system with frequency spreading gain $g_F = 2$ can be written in the same form as (6.34) with

$$P = \frac{N_0}{br\sigma_{s,d}\sigma_{s,r}\sigma_{r,d}}\left(\frac{A_4r^2\sigma_{s,r}^4(1-B_{s,r}^2)+A_2^2(1-r)^2\sigma_{r,d}^4(1-B_{r,d}^2)}{\varepsilon(1-r)^2(1-B_{s,d}^2)(1-B_{s,r}^2)(1-B_{r,d}^2)}\right)^{1/4}, \quad (6.37)$$

and r being the solution to an equation: $(2c_{s,r} + c_{r,d})r^3 - (c_{s,r} + 3c_{r,d})r^2 + 3c_{r,d}r - c_{r,d} = 0$, where $c_{s,r} = A_4\sigma_{s,r}^4(1 - B_{s,r}^2)$ and $c_{r,d} = 2A_2^2\sigma_{r,d}^4(1 - B_{r,d}^2)$ are constants that depend on the average channel quality of the source-relay link and the relay-destination link, respectively. By solving the polynomial equation, we arrive after some manipulation at

$$r = \frac{4^{\frac{1}{3}}c^2 + 2(c_{s,r} + 3c_{r,d})c + 4^{\frac{2}{3}}(c_{s,r}^2 - 12c_{s,r}c_{r,d})}{6(2c_{s,r} + c_{r,d})c}, \tag{6.38}$$

in which $c = \left(72c_{s,r}c_{r,d} + 2c_{s,r}^2 - 27c_{r,d}^2 + 3(2c_{s,r} + c_{r,d})\sqrt{3(4c_{s,r}c_{r,d} + 27c_{r,d}^2)}\right)^{\frac{1}{3}}$.

The results in (6.36) and (6.38) reveal that the asymptotic power allocation of cooperative UWB systems with any frequency spreading gain does not rely on the channel link between the source and the destination. It depends only on the channel link between the source and the relay and the channel link between the relay and the destination. If the link quality between the source and the relay is the same as that between the relay and the destination, then the power ratio is simplified to

$$r = \frac{1 + \sqrt{1 + (8A_1^2/A_2)}}{3 + \sqrt{1 + (8A_1^2/A_2)}} \qquad \text{if } g_F = 1; \tag{6.39}$$

$$r = \frac{c^2 + (A_4 + 6A_2^2)c - 24A_2^2A_4 + A_4^2}{6(A_4 + A_2^2)c} \quad \text{if } g_F = 2, \tag{6.40}$$

where $c = \left[A_4\left(18A_2^2(4A_4 - 3A_2^2) + A_4^2 + 6A_2(A_4 + A_2^2)\sqrt{3(2A_4 + 27A_2^2)}\right)\right]^{\frac{1}{3}}$, and A_i depend on specific modulation signals. If QPSK modulation is used, then $r = 0.6207$ in case of frequency spreading gain $g_F = 1$ and $r = 0.5925$ in case of $g_F = 2$. Observe from (6.39) and (6.40) that when the source-relay link and relay-destination link are of the same quality, the asymptotic power ratio does not depend on the clustering property of UWB channels, regardless of the frequency spreading gain. In general, this is not the case, especially when frequency spreading

Table 6.1: Comparisons between optimum power allocation obtained via exhaustive search and analytical results.

Multipath Energy			Gain	Search	From (6.33)	From (6.35),(6.37)
$\sigma_{s,r}^2$	$\sigma_{s,r}^2$	$\sigma_{r,d}^2$	g_F	r	r	r
1	10	1	1	0.5321	0.5356	0.5247
1	10	1	2	0.5072	0.5095	0.5023
1	1	10	1	0.7873	0.7772	0.7968
1	1	10	2	0.8082	0.7882	0.8316

is performed. As we can see from (6.37) and (6.38), the optimum power allocation for UWB system with frequency spreading gain of two generally depends on both the channel gains and the multipath clustering property of UWB channels.

Table 6.1 provides comparisons between the optimum power allocation obtained via exhaustive search to minimize the SER formulation in (6.12), the one obtained by solving (6.33), and the one provided by the closed form expressions in (6.35) and (6.37). The required SER performance is set at 5×10^{-2}. We consider the DF cooperation system under 2 different scenarios: $\sigma_{s,d}^2 = \sigma_{r,d}^2 = 1$ and $\sigma_{s,r}^2 = 10$ as well as $\sigma_{s,d}^2 = \sigma_{s,r}^2 = 1$ and $\sigma_{r,d}^2 = 10$. Channel model parameters of each channel link are based on CM 1. We can see that the optimum power allocations obtained by solving (6.33) and by closed form expressions in (6.35), (6.37) agree with that obtained via exhaustive search for all considered scenarios. Furthermore, Table 6.1 illustrates that the optimum power allocation does not strongly depend on the spreading gain, but it relies mostly on the channel link quality. If the link quality between the source and the relay is much better than that between the relay and the destination, then the power should be equally allocated at the source and the relay. If the source-relay link has much less quality than the relay-destination link, then more power is allocated at the source. This is in consistent with the results in [65] in which it was shown that in order for a cooperation system to achieve a

Table 6.2: Power ratio of cooperative and non-cooperative UWB multiband OFDM systems

Multipath Energy			P_{DF}/P_{NC}	
$\sigma_{s,d}^2$	$\sigma_{s,r}^2$	$\sigma_{r,d}^2$	$g_F = 1$	$g_F = 2$
1	1	1	1.7189	1.0709
1	10	1	0.5287	0.5689
1	1	10	0.2132	0.5545

performance diversity of two, the source-relay link and the relay-destination link should be balanced.

In the sequel, we compare the total transmitted power used in non-cooperative and cooperative systems to achieve the same SER performance. According to the SER expressions in Section 6.2.2, the ratio between the power of cooperative and non-cooperative UWB systems with the same spreading gain can be expressed as

$$\frac{P_{DF}}{P_{NC}} = \frac{N_0 P_e^{-1/\Delta} G_{DF}^{-1}}{N_0 P_e^{-1/\Delta} G_{NC}^{-1}} = \frac{G_{NC}}{G_{DF}} = \frac{1}{\xi}. \tag{6.41}$$

Substituting (6.30) and (6.36) into (6.41), the ratio P_{DF}/P_{NC} for the UWB systems with frequency spreading gain $g_F = 1$ is given by

$$\frac{P_{DF}}{P_{NC}} = \frac{\sigma_{s,d}(3 + K_1)}{2(1 + K_1)} \left(\frac{A_1^2}{A_2 \sigma_{s,r}^2} + \frac{1 + K_1}{2\sigma_{r,d}^2} \right)^{1/2}, \tag{6.42}$$

where $K_1 = \sqrt{1 + 8A_1^2 \sigma_{r,d}^2/(A_2 \sigma_{s,r}^2)}$. For the systems with frequency spreading gain $g_F = 2$, the ratio P_{DF}/P_{NC} can be calculated from (6.31) and (6.38) as

$$\frac{P_{DF}}{P_{NC}} = \frac{6\sigma_{s,d}c(2c_{s,r} + c_{r,d})}{2\sigma_{s,r}\sigma_{r,d}(K_2 + 2c(c_{s,r} + 3c_{r,d}))}$$
$$\times \left(\frac{A_2^2(1 - B_{s,d}^2)\sigma_{r,d}^2}{A_4(1 - B_{s,r}^2)} + \frac{(K_2 + 2c(c_{s,r} + 3c_{r,d}))^2(1 - B_{s,d}^2)\sigma_{s,r}^2}{(K_2 - 10c_{s,r}c)^2(1 - B_{r,d}^2)} \right)^{1/4}, \tag{6.43}$$

where $K_2 = 4^{\frac{1}{3}}c^2 + 4^{\frac{2}{3}}(c_{s,r}^2 - 12c_{s,r}c_{r,d})$. Tables 6.2 demonstrates the ratios P_{DF}/P_{NC} for UWB systems with different channel qualities. The channel model parameters

are the same for every link. In this scenario, (6.42) and (6.43) disclose that the ratio P_{DF}/P_{NC} does not depend on the clustering property of UWB channels. If all the channel links are of the same quality, then the non-cooperative transmission requires less transmitted power than the cooperative transmission. However, if the channel quality of either source-relay link or relay-destination link is very good, then cooperative transmission significantly reduces the transmitted power. As shown in Table 6.2, cooperative scheme with high quality link between source and relay yields about 50% power saving compared to non-cooperative scheme. In case of high quality link between relay and destination, the cooperative scheme can save up to 78% of transmitted power compared to the non-cooperative scheme.

We have determined the optimum power allocation for the cooperative UWB multiband OFDM system without taking into consideration the limitation on the transmitted power level. With the maximum power limitation, it is difficult to obtain a closed form solution to the problem in (6.32). In this case, we provide a solution as follows. Let P_1 and P_2 be the transmitted powers that are obtain by solving (6.32) without the maximum power constraint, and let $\hat{P}_1$ and $\hat{P}_2$ denote our solution.

- If $\min\{P_1, P_2\} > P_{max}$, then there is no feasible solution to (6.32).

- Else if $\max\{P_1, P_2\} \leq P_{max}$, then $\hat{P}_1 = P_1$ and $\hat{P}_2 = P_2$;

- Otherwise,

  i) Let $j = \arg\max_i\{P_1, P_2\}$ and $j' = \arg\min_i\{P_1, P_2\}$.

  ii) Set $P_j = P_{max}$ and find $P_{j'}$ such that the desired SER performance is satisfied, i.e., $P_{j'}$ is obtained by solving $P_e - \varepsilon = 0$ where P_e is according to (6.23) or (6.24) with P_j replaced by P_{max}.

iii) If the obtained $P_{j'} \leq P_{max}$, then $\hat{P}_j = P_{max}$ and $\hat{P}_{j'} = P_{j'}$;

Otherwise, there is no feasible solution to (6.32).

The case of no feasible solution to (6.32) indicates that the UWB system under the current channel conditions cannot satisfy the performance requirement even by exploiting the cooperative diversity. In this scenario, an additional subband can be utilized to further increase the diversity gain and improve the system performance as discussed in Section 6.4.

6.3.2 Coverage Enhancement using Cooperative Communications

The coverage of UWB system can be specified by the maximum distance between the source and the destination that the system is able to offer transmission with an error probability less than the desired threshold value. In this subsection, we determine the optimum power allocation and the relay location so as to maximize the coverage of cooperative UWB multiband OFDM system.

We take into account the effect of the geometry on the channel link qualities by assuming that the total multipath energy between any two nodes is proportional to the distance between them. Particularly, the total multipath energy $\sigma^2_{x,y}$ is modeled by [7]

$$\sigma^2_{x,y} = \kappa \, D^{-\nu}_{x,y}, \tag{6.44}$$

where κ is a constant whose value depends on the propagation environment, ν is the propagation loss factor, and $D_{x,y}$ represents the distance between node x and node y. Given a fixed total transmitted power P, we aim to find the optimum power allocation $r = P_1/P$ such that the distance between the source and the
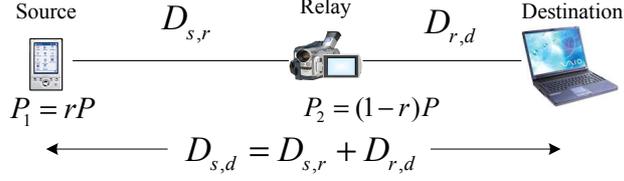
Figure 6.3: Coverage enhancement using cooperative UWB multiband OFDM

destination $D_{s,d}$ is maximized. Based on the SER performance obtained in the previous section, we can see that the performance of cooperative UWB system is related not only to the power allocation but also the location of the nodes. In order to maximize the distance $D_{s,d}$, it is obvious that the optimum relay location must be on the line joining the source and the destination, as shown in Fig. 6.3. This comes from the fact that if the relay is located in any location in a two dimensional plane, its distances to both the source and the destination are always longer than their corresponding projections on the line joining the source and the destination. In this case, the distance between the source and the destination can be written as a summation of the distance of the source-relay link and that of the relay-destination link, i.e., $D_{s,d} = D_{s,r} + D_{r,d}$. The questions are how far from the source that the relay should be located, and how much power we should put at the source and at the relay so as to maximize the distance $D_{s,d}$. To answer these questions, we jointly determine the distance $D_{s,r}$, the distance $D_{r,d}$, and the power ratio r such that the coverage range $D_{s,d}$ is maximize. We formulate an optimization as follows:

$$\max_{r, D_{s,r}, D_{r,d}} \quad D_{s,r} + D_{r,d} \tag{6.45}$$

$$\text{s.t.} \begin{cases} \text{Performance: } P_e \leq \varepsilon; \\ \text{Power: } rP \leq P_{max}, \ (1-r)P \leq P_{max}, \ 0 < r < 1. \end{cases}$$

152

To get some insights, we provide in what follows the solution to (6.45) without constraint on the transmitted power level. With consideration of the maximum power constraint, a similar solution to the discussion at the end of Section 6.3.1 can be employed. As we will show later in Section 6.5, the solution to (6.45) with power constraint follows the same trend as that without power constraint. By applying the Lagrange multiplier method, the solutions to (6.45) can be obtained by solving the first order optimality conditions: $1 + \zeta \partial P_e / \partial D_{s,r} = 0$, $1 + \zeta \partial P_e / \partial D_{r,d} = 0$, $\partial P_e / \partial r = 0$, and $P_e - \varepsilon = 0$, where ζ is the Lagrange multiplier. Although the SER upper bound (6.15) and the asymptotic SER approximation (6.20) are simple, they are based on the assumption that all channel links are always available. Due to such assumption, the SERs (6.15) and (6.20) are not applicable for the problem in (6.45), in which two nodes can be located far away from each other. In what follows, we are going to determine the optimum power allocation and the optimum distances based on the SER formulation (6.12) and the SER approximations (6.17) and (6.21).

We consider at first the UWB system with frequency spreading gain $g_F = 1$. According to the tight SER approximation (6.17) and the first order optimality conditions, the optimum power allocation and distance must satisfy the necessary condition:

$$\frac{A_1^2 r D_{s,r}^{-\nu-1}}{(1 + b\rho k r D_{s,r}^{-\nu})^2} - \frac{A_2(1 - r)D_{r,d}^{-\nu-1}}{(1 + b\rho k(1 - r)D_{r,d}^{-\nu})^2} = 0. \tag{6.46}$$

From (6.46), we can find the power ratio r as a function of the distances $D_{s,r}$ and $D_{r,d}$. Then, solving $\partial P_e / \partial r = 0$ and $P_e - \varepsilon = 0$ simultaneously, we obtain the optimum power ratio and distances $D_{s,r}$ and $D_{r,d}$. Similarly, the maximum coverage of UWB system with frequency spreading gain $g_F = 2$ can be obtained as follows.

By evaluating the first order optimality conditions based on the approximate SER in (6.21), we obtain the necessary condition:

$$\frac{A_2^2 r D_{s,r}^{-\nu-1}[1 + 2b\rho kr(1 - B_{s,r}^2)D_{s,r}^{-\nu}]}{[1 + b\rho kr D_{s,r}^{-\nu} + b^2\rho^2 k^2 r^2(1 - B_{s,r}^2)D_{s,r}^{-2\nu}]^2}$$
$$- \frac{A_4(1 - r)D_{r,d}^{-\nu-1}[1 + 2b\rho k(1 - r)(1 - B_{r,d}^2)D_{r,d}^{-\nu}]}{[1 + b\rho k(1 - r)D_{r,d}^{-\nu} + b^2\rho^2 k^2(1 - r)^2(1 - B_{r,d}^2)D_{r,d}^{-2\nu}]^2} = 0. \qquad (6.47)$$

Then, the optimum power ratio r and optimum distances $D_{s,r}$ and $D_{r,d}$ can be determined by solving (6.47) together with $\partial P_e/\partial r = 0$ and $P_e - \varepsilon = 0$.

We also perform an exhaustive search to solve the optimization problem in (6.45) based on the SER formulation in (6.12). In Tables 6.3 and 6.4, we compare the optimum power allocation and the optimum distances obtained via exhaustive search and that obtained by solving the first order optimality conditions. We consider the UWB multiband OFDM system with frequency spreading gains $g_F = 1$ in Table 6.3 and $g_F = 1$ in Table 6.4. Clearly, the analytical results closely match with the results from the exhaustive search for all frequency spreading gains. Moreover, we can see that the optimum power allocation and the optimum relay location depends on the total power P/N_0. When P/N_0 is small, the maximum coverage can be achieved by putting the relay as far from the source as possible, and allocate almost all of the total transmitted power P at the source. However, when P/N_0 is high ($P/N_0 > 30$ dB), this is not the case. In such scenario, putting the relay close to the middle and allocate about half of the power at the relay results in longer coverage than putting the relay farthest away from the source. We can intuitively explain these results as follows. At small SNR, the transmitted power is not large enough for the cooperation system to achieve the performance of diversity order two. Therefore, the forwarding role of the relay is less important and we should use almost all of the transmitted power at the source. On the other

Table 6.3: Power allocation, relay location, and maximum coverage of cooperative UWB multiband OFDM systems with frequency spreading gain: $g_F = 1$.

P/N_0 (dB)	Exhaustive Search			Analytical Solution		
	r	$D_{s,r}$	$D_{s,d}$	r	$D_{s,r}$	$D_{s,d}$
25	0.86	13.00	14.06	0.88	13.74	14.87
30	0.86	23.12	25.01	0.83	23.37	25.70
35	0.55	15.53	33.82	0.58	15.12	33.98

Table 6.4: Power allocation, relay location, and maximum coverage of cooperative UWB multiband OFDM systems with frequency spreading gain: $g_F = 2$

P/N_0 (dB)	Exhaustive Search			Analytical Solution		
	r	$D_{s,r}$	$D_{s,d}$	r	$D_{s,r}$	$D_{s,d}$
25	0.89	17.11	19.14	0.88	17.31	19.79
30	0.85	30.24	35.81	0.84	30.17	35.46
35	0.52	13.21	43.87	0.54	13.27	43.92

hand, at high enough SNR, the diversity order of two can be achieved. In this case, the relay should be located in the middle to balance the channel quality of source-relay link and relay-destination link.

6.4   Improved Cooperative UWB Multiband OFDM

The current multiband standard proposal [18] allows several UWB devices to transmit at the same time using different subbands. However, in a short-range scenario, the number of UWB devices that simultaneously transmit their information tend to be smaller than the number of available subbands. Therefore, we can make use of the unoccupied subbands so as to improve the performance of cooperative UWB systems. The improved cooperative UWB strategy are as follows.

Let the time-domain spreading with spreading factor of two is performed at the source. The improved cooperative UWB scheme comprises two phases, each corresponding to one OFDM symbol period. In Phase 1, the source broadcasts

Figure 6.4: Illustration of an improved cooperative UWB multiband OFDM scheme.

its information to both destination and relay using one subband. In Phase 2, the source repeats the information using another subband so as to gain the diversity from time spreading. At the same time, the relay forwards the source information using an unoccupied subband. The destination combines the received signals from the source directly in Phase 1 and Phase 2, and the signal from the relay in Phase 2. Fig. 6.4 illustrates an example of the improved cooperative UWB system. In Fig. 6.4, the source and the relay are denoted respectively by S and R. It is worth noting that the improved cooperative UWB scheme is compatible with the current multiband standard proposal [18] which allows multiuser transmission using different subbands. In addition, the proposed scheme yields the same data rate as the non-cooperative scheme with the same spreading gain.

Similar to Section 6.1.1, we denote P_1 and P_2 as the transmitted power at the source in Phase 1 and Phase 2, respectively. The received signals from the direct link in Phase 1 and Phase 2 can be modeled as in (6.1). Let us denote P_3 as the transmitted power at the relay. Accordingly, the received signal from the relay link can be written as (6.4) by replacing $\tilde{P}_2$ with $\tilde{P}_3$. By the use of MRC detector, the received signals $y_{s,d}^1$, $y_{s,d}^2$, and $y_{r,d}$ are optimally combined. The SNR of the MRC output can be expressed as

$$\eta = \frac{P_1}{N_0} \sum_{n \in \Phi_n} |H_{s,d}^1(n)|^2 + \frac{P_2}{N_0} \sum_{n \in \Phi_n} |H_{s,d}^2(n)|^2 + \frac{\tilde{P}_3}{N_0} \sum_{n \in \Phi_n} |H_{r,d}(n)|^2. \qquad (6.48)$$

Assuming an ideal band hopping, the average SER of the improved cooperative UWB system is

$$P_e = \frac{1}{\pi^2} \int_0^{\pi-\pi/M} \mathcal{M}_{\eta_{s,d}}^2 \left(\frac{b}{\sin^2\theta}\right) d\theta \int_0^{\pi-\pi/M} \mathcal{M}_{\eta_{s,r}} \left(\frac{b}{\sin^2\theta}\right) d\theta$$
$$+ \frac{1}{\pi} \int_0^{\pi-\pi/M} \mathcal{M}_{\eta_{s,d}}^2 \left(\frac{b}{\sin^2\theta}\right) \mathcal{M}_{\eta_{r,d}} \left(\frac{b}{\sin^2\theta}\right) d\theta \left[1 - \frac{1}{\pi} \int_0^{\pi-\pi/M} \mathcal{M}_{\eta_{s,r}} \left(\frac{b}{\sin^2\theta}\right) d\theta\right].$$

$$(6.49)$$

Following the same procedures as in Section 6.2, we can approximate the SER in (6.49) as

$$P_e \approx \frac{1}{(1 + b\rho_1\sigma_{s,d}^2)(1 + b\rho_2\sigma_{s,d}^2)} \left(\frac{A_1 A_2}{1 + b\rho_1\sigma_{s,r}^2} + \frac{A_3}{1 + b\rho_3\sigma_{r,d}^2}\right) \tag{6.50}$$

in case of frequency spreading gain $g_F = 1$, and

$$P_e \approx \frac{1}{g_{s,d}(\rho_1)g_{s,d}(\rho_2)} \left(\frac{A_2 A_4}{g_{s,r}(\rho_1)} + \frac{A_6}{g_{r,d}(\rho_3)}\right) \tag{6.51}$$

for the system with $g_F = 2$. In (6.51), we denote $g_{x,y}(\rho_i) = 1 + b\rho_i\sigma_{x,y}^2 + b^2\rho_i^2\sigma_{x,y}^4(1 - B_{x,y}^2)$ and $\rho_i = P_i/N_0$. If all channel links are available, the SER for the cooperative UWB system with frequency spreading gain $g_F = 1$ can be upper bounded at high SNR by

$$P_e \leq \frac{A_1 A_2}{b^3 \rho_1^2 \rho_2 \sigma_{s,d}^4 \sigma_{s,r}^2} + \frac{A_3}{b^3 \rho_1 \rho_2 \rho_3 \sigma_{s,d}^4 \sigma_{r,d}^2}. \tag{6.52}$$

With frequency spreading gain $g_F = 2$, the asymptotic SER performance can be approximated as

$$P_e \approx \frac{1}{b^4 \rho_1^2 \rho_2^2 \sigma_{s,d}^8 (1 - B_{s,d}^2)} \left(\frac{A_2 A_4}{b^2 \rho_1^2 \sigma_{s,r}^4 (1 - B_{s,r}^2)} + \frac{A_6}{b^2 \rho_3^2 \sigma_{r,d}^4 (1 - B_{r,d}^2)}\right). \tag{6.53}$$

Suppose the total transmitted power is $P_1 + P_2 + P_3 = P$, and let $r_i = P_i/P$ for $i = 1, 2, 3$, denote the power ratio of the transmitted power P_i over the total power
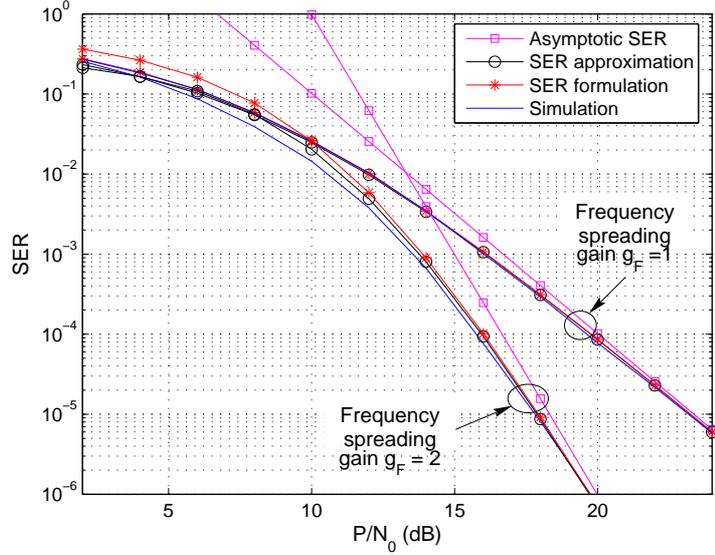
157

Figure 6.5: Comparison of the SER formulations and the simulation result for the improved cooperative UWB multiband OFDM system. We assume that $\sigma_{s,d}^2 = \sigma_{s,r}^2 = \sigma_{r,d}^2 = 1$, and $P_1 = P_2 = P_3 = P/3$.

P. The SER formulations in (6.52) and (6.53) can be written as

$$P_e \leq \left(\frac{b[\sigma_{s,d}^4 \sigma_{s,r}^2 \sigma_{r,d}^2 r_1^2 r_2]^{\frac{1}{3}}}{[A_1 A_2 \sigma_{r,d}^2 + A_3 \sigma_{s,r}^2 r_1/r_3]^{\frac{1}{3}}} \frac{P}{N_0} \right)^{-3} \qquad \text{if } g_F = 1; \quad (6.54)$$

$$P_e \approx \left(\frac{b[r_1^4 r_2^2 \sigma_{s,d}^8 \sigma_{s,r}^4 \sigma_{r,d}^4 (1 - B_{s,d}^2)^2 (1 - B_{s,r}^2)(1 - B_{r,d}^2)]^{\frac{1}{6}}}{[A_2 A_4 \sigma_{r,d}^4 (1 - B_{r,d}^2) + A_6 \sigma_{s,r}^4 (1 - B_{s,r}^2) r_1^2/r_3^2]^{\frac{1}{6}}} \frac{P}{N_0} \right)^{-6} \quad \text{if } g_F = 2. \quad (6.55)$$

From (6.54) and (6.55), we can conclude that the improved cooperative UWB system provides an overall performance of diversity order $3g_F$. This confirms our expectation that the diversity order increases with the number of subbands used for transmission. Fig. 6.5 depicts the SER performance of improved cooperative UWB system as a function of P/N_0. We consider the UWB system with frequency spreading gains $g_F = 1$ and 2. The channel model parameters of each link are based on CM 1. We can see that the theoretical formulations (6.49), (6.50), and (6.51)

158

closely match with the simulation curve. Moreover, the simple SER approximations (6.52) and (6.53) are tight at high SNR. Based on the SER formulations, we can determine the optimum power allocation for the improved cooperative UWB system as follows.

In the sequel, we focus on minimizing the total transmitted power under the constraint on the error rate performance. Define $\mathbf{P} = [P_1\ P_2\ P_3]^T$ as a power allocation vector. Then, the optimum power allocation can be determined by solving the problem in (6.32). As in Section 6.3.1, we consider at first the problem (6.32) without the maximum power constraint to get some insight. By applying the Lagrange multiplier method and considering the first order optimality conditions, we can show that the optimum power allocation vector $\mathbf{P}$ must satisfy the necessary conditions:

$$\frac{\partial P_e}{\partial P_1} = \frac{\partial P_e}{\partial P_2} = \frac{\partial P_e}{\partial P_3}. \tag{6.56}$$

Solving (6.56) and $\mathrm{P}_e = \varepsilon$ simultaneously, we get the optimum power allocation $\mathbf{P}$. Based on the tight SER approximation in (6.52), the asymptotic optimum power allocation for the improved cooperative UWB system with frequency spreading gain $g_F = 1$ can be determined as

$$P_1 = \frac{2rP}{3},\ \ P_2 = \frac{P}{3},\ \text{and}\ P_3 = \frac{2(1-r)P}{3}, \tag{6.57}$$

where r is given in (6.36), and

$$P = \frac{N_0}{3b} \left(\frac{A_1 A_2 \sigma_{r,d}^2 + A_3 \sigma_{s,r}^2 r/(1-r)}{4\varepsilon r^2 \sigma_{s,d}^4 \sigma_{s,r}^2 \sigma_{r,d}^2} \right)^{1/3}. \tag{6.58}$$

The result in (6.57) reveals that the asymptotic optimum power allocation at the source in Phase 2 does not depend on the channel link quality. That is one-third of the total transmitted power P should be allocated at the source in Phase 2.

159

Table 6.5: Comparisons between optimum power allocation obtained via exhaustive search and analytical results.

Path Variance			Gain	Exhaustive Search			Solution in (6.57)		
$\sigma_{s,r}^2$	$\sigma_{s,r}^2$	$\sigma_{r,d}^2$	g_F	r_1	r_2	r_3	r_1	r_2	r_3
1	10	1	1	0.5367	0.3158	0.1476	0.5154	0.3333	0.1512
1	10	1	2	0.6175	0.2400	0.1425	0.5515	0.3333	0.1151
1	1	10	1	0.3530	0.3335	0.3135	0.3456	0.3333	0.3211
1	1	10	2	0.3374	0.3331	0.3294	0.3348	0.3333	0.3319

Then, the rest of the power is allocated at the relay and the source in Phase 1 according to the channel quality of the source-relay link and the relay-destination link. Observe from (6.36) that r takes values between $1/2$ and 1. This implies that more than one-third of P should be allocated at the source in Phase 1, and less than one-third of P should be allocated at the relay. In case of frequency spreading gain $g_F = 2$, the asymptotic optimum power allocation is the same as (6.57) with r given in (6.38) and the total power P given by

$$P = \frac{N_0}{3b} \left(\frac{A_2 A_4 \sigma_{r,d}^4 (1 - B_{r,d}^2) + A_6 \sigma_{s,r}^2 (1 - B_{s,r}^2) r/(1 - r)}{16\varepsilon r^4 \sigma_{s,d}^8 \sigma_{s,r}^4 \sigma_{r,d}^4 (1 - B_{s,d}^2)(1 - B_{s,r}^2)(1 - B_{r,d}^2)} \right)^{1/6}. \tag{6.59}$$

In Table 6.5, we compare the asymptotic optimum power allocation in (6.57) with the optimum power allocation obtained by exhaustive search based on the SER in (6.49). All channel links are based on CM 1, and the target error rate performance is 5×10^{-2}. It is clear that the analytical solution in (6.57) agrees with the results from the exhaustive search. For UWB system with the maximum power constraint, the power allocation can be determined by a similar procedure to that at the end of Section 6.3.1. Furthermore, the optimum power allocation that maximize the coverage can be obtained in a similar way to that in Section 6.3.2. We omit them here due to space limitations.
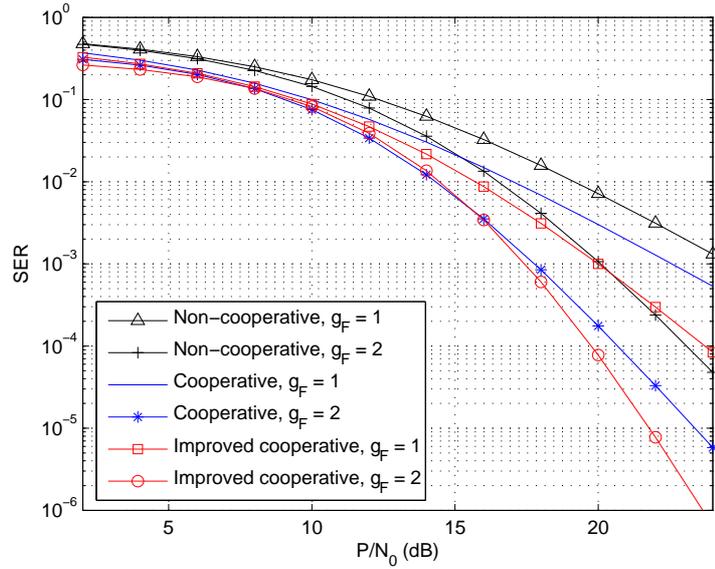
Figure 6.6: SER performance of UWB systems versus P/N_0.

6.5 Simulation Results

We perform computer simulations to compare the performance of the proposed cooperative UWB schemes and to validate the theoretical results derived in this paper. In all simulations, we consider UWB multiband OFDM system with 128 subcarriers and the subband bandwidth of 528 MHz. Each OFDM subcarrier is modulated using QPSK. We assume that the effect of inter-symbol interference is mitigated by the use of cyclic prefix. The propagation loss factor is $\nu = 2$ and the total multipath energy is modeled by $\sigma_{x,y}^2 = D_{x,y}^{-2}$. The channel model parameters follows those specified in the IEEE 802.15.3a standard [68]. In all simulations, the source is located at position (0, 0).

In Fig. 6.6, we compare the average SER performances of UWB systems with different cooperation strategies. The locations of the relay and the destination are fixed at (1m, 0) and (2m, 0), respectively. All channel links are modeled by

161

CM 1. The total transmitted power is equally allocated. For fair comparison, we present the SER curves as functions of P/N_0. From Fig. 6.6, we can see that both non-cooperative and cooperative UWB systems achieve an overall performance of diversity order $2g_F$. In case of frequency spreading gain $g_F = 1$, the cooperative UWB system outperform the non-cooperative system with a SER performance of about 2 dB. This agrees with the analysis in (6.30) which shows that the performance gain of the DF cooperative UWB compared with the non-cooperative UWB is $\xi = [(1 + A_1^2/A_2)\sigma_{s,d}^2]^{1/2} = 1.59$. In case of frequency spreading gain $g_F = 2$, the performance of cooperative system is about 2.5 dB better than that of non-cooperative system. This also corresponds to the analysis in (6.31) in which the performance gain ξ can be calculated as $\xi = [(1 + A_2^2/A_4)\sigma_{s,d}^2]^{1/4} = 1.81$. Additionally, Fig. 6.6 illustrates that the cooperative and improved cooperative UWB systems yield almost the same performance at low P/N_0. At high P/N_0, the improved cooperative UWB system provides the performance of diversity order $3g_F$ and yields about 2 dB performance improvement compared to the cooperative UWB system.

Figs. 6.7 and 6.8 compare the total transmitted power of non-cooperation and cooperation systems. We plot P/N_0 versus location of the destination. In cooperation system, the relay is located in the middle between the source and the destination, i.e., $D_{s,d} = D_{s,r}/2$. All channel links are modeled by CM 4. The transmitted power is allocated such that overall transmitted power is minimized and the SER satisfies a performance requirement of 5×10^{-2}. In Fig. 6.7, we consider UWB systems without limitation on the transmitted power level. By increasing the frequency spreading gain from 1 to 2, the overall transmitted power can be reduced by 60%. With the same frequency spreading gain, the cooperative
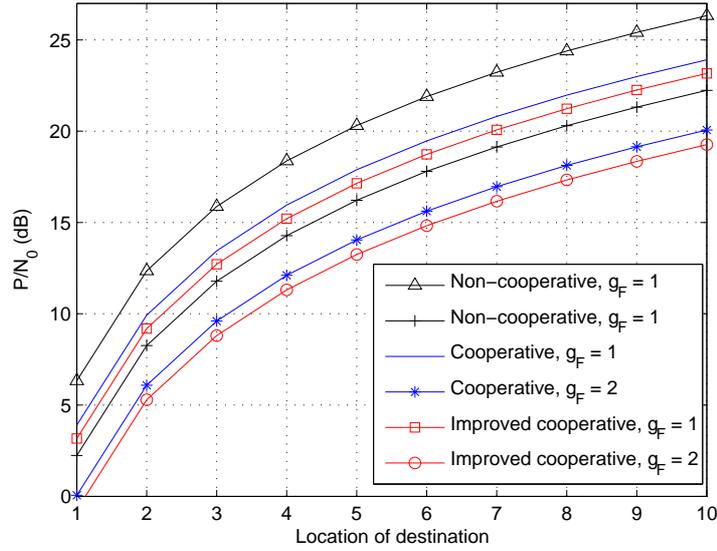
Figure 6.7: P/N_0 versus destination location for UWB systems without power limitation.

scheme achieves 43% power saving compared to the non-cooperative scheme. This is in consistent with the analytical results in (6.42) and (6.43), in which the power ratio of cooperative and non-cooperative scheme can be calculated as $P_{DF}/P_{NC} = 0.59$ in case of $g_F = 1$ and $P_{DF}/P_{NC} = 0.54$ in case of $g_F = 2$. Fig. 6.7 also shows that using the improved cooperative UWB scheme can achieve up to 52% power saving compared to the non-cooperative scheme. In Fig. 6.8, we take into consideration the constraint on transmitted power level and allocate the power based on the suboptimal solution provided in Section 6.3.1. The power limitation is set at $P_i/N_0 \leq 19$ dB. The tendencies observed in Fig. 6.8 are similar to those observed in Fig. 6.7. The improve cooperative scheme saves about 50% overall transmitted power in case of $g_F = 1$ and saves about 20% in case of $g_F = 2$.

Next, we study the coverage of UWB system under different cooperation strate-
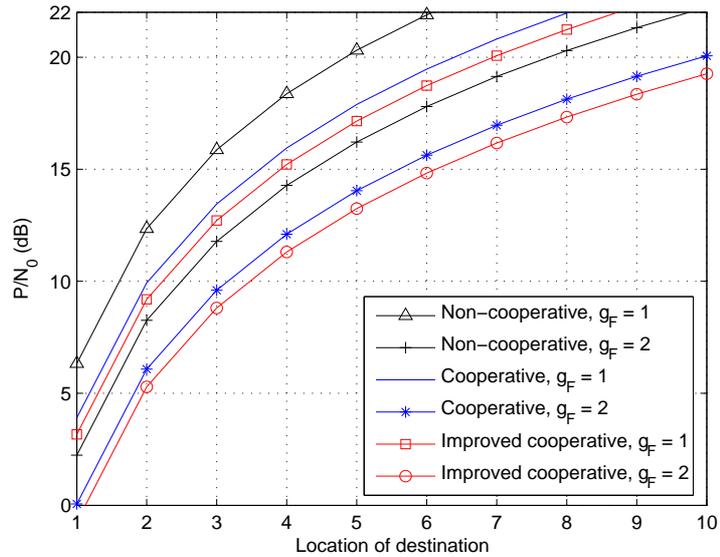
Figure 6.8: P/N_0 versus destination location for UWB systems with power limitation.

gies. All channel links are based on CM 4. The SER performance requirement is fixed at 5×10^{-2}. In Fig. 6.9, we plot the maximum distance between source and destination versus the distance between source and relay in case of $P/N_0 = 22$ dB. We observe that by increasing the frequency spreading gain from 1 to 2, the non-cooperative scheme increases the coverage by 60% whereas the cooperative scheme increases the coverage by 40%. Moreover, the coverage of cooperative scheme increases as the relay is located farther away from the source. This agrees with our study in Section 6.3.2 which shows that at small P/N_0, the longer the distance between the source and relay, the longer the distance between the source and destination. For example, if the relay is located at 1m away from the source, the cooperative scheme increases the coverage by about 5%. On the other hand, if the distance between source and relay increases to 8m, the cooperative scheme can increase the coverage by about 58% compared with the non-cooperative scheme.
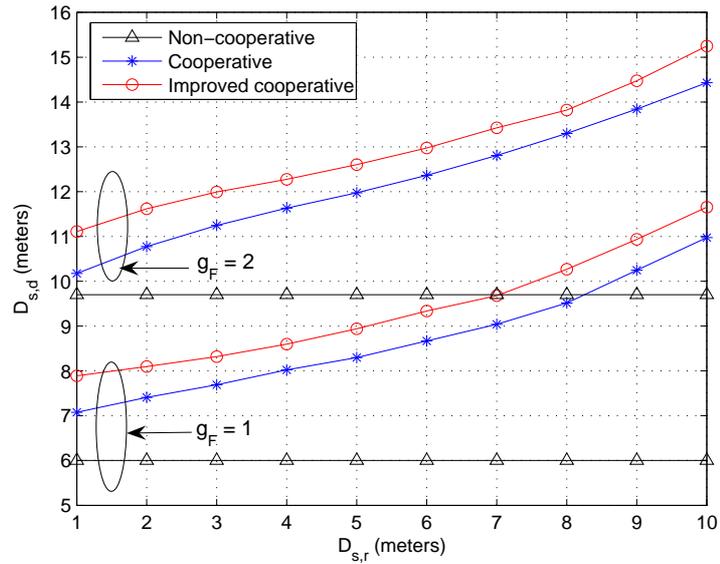
Figure 6.9: Distance between source and destination versus distance between source and relay.

With the improved cooperative scheme, the coverage can be further increased by 70%.

In Fig. 6.10, we depicts the coverage of UWB system as a function of P/N_0. For cooperative scheme, the relay location and the power allocation are designed such that the distance $D_{s,d}$ is maximized. We can clearly see from the figure that the coverage increases as P/N_0 increases. With the same P/N_0 and the same transmission data rate, the coverage of UWB system can be increased up to 85% using the cooperative scheme, and it can be increased up to 100% using the improved cooperative scheme. In Fig. 6.11, we take into account the maximum power constraint. The transmitted power level is limited by $P_i/N_0 \leq 19$ dB. From Fig. 6.11, we can see that the coverage of UWB system with the maximum power constraint follows the same tendencies as in case of no power limitation.
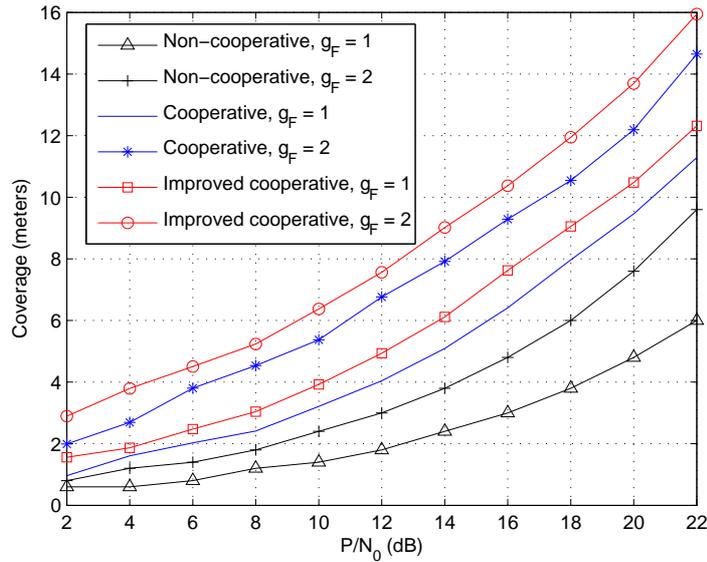
Figure 6.10: Maximum transmission range versus P/N_0 for UWB systems without power limitation.

6.6 Chapter Summary

In this chapter, we propose to enhance the performance of UWB systems by employing cooperative communications. We analyze the SER performance and provide optimum power allocation of cooperative UWB multiband OFDM systems with decode-and-forward cooperative protocol. It turns out that both non-cooperative and cooperative schemes achieve the same diversity order of twice the frequency spreading gain, which is independent to the clustering behavior of UWB channels. However, by taking advantage of the relay location and properly allocating the transmitted power, cooperative UWB scheme can achieve superior performances to the non-cooperative UWB scheme at the same data rate. We also propose to further improve the performance of the cooperative UWB scheme by allowing the source and the relay nodes to simultaneously retransmit the infor-
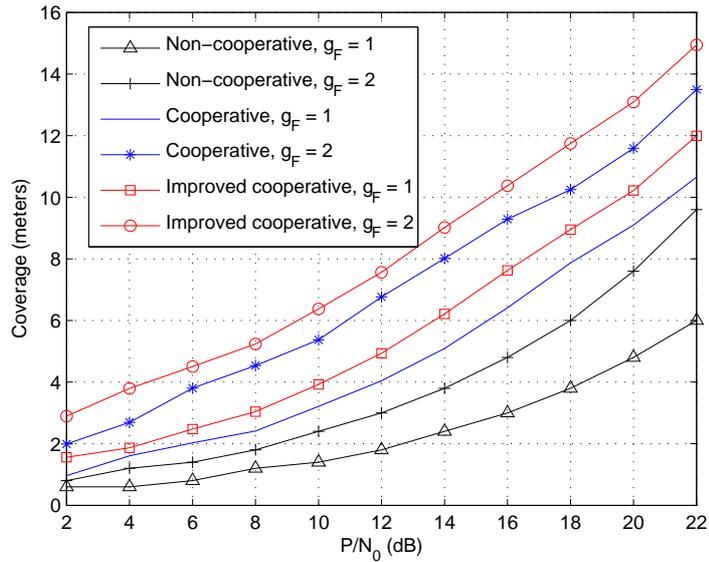
Figure 6.11: Maximum transmission range versus P/N_0 for UWB systems with power limitation.

mation. With an objective to minimize the overall transmitted power, we show by both theoretical and simulation results that the cooperative UWB multiband OFDM system can save up to 43% of the transmitted power. With an objective to maximize the coverage, both the optimum relay location and optimum power allocation depend on the SNR. At low SNR, the maximum coverage is achieved when the relay is located farthest away from the source, and the source uses almost all of the transmitted power. On the other hand, at high SNR, the coverage is maximized when the relay is located in the middle between the source and the destination, and approximately equal power is allocated at the source and the relay. Simulation results show that the cooperative UWB can increase the coverage range up to 85% compared with the non-cooperative UWB scheme. By allowing both source and relay to retransmit data simultaneously, the improved cooperative UWB system achieves up to 52% power saving and up to 100% coverage extension.

167

Chapter 7

Bandwidth-Efficient OFDM Cooperative Protocol

In broadband communications, OFDM is an effective means to capture multipath energy, mitigate the intersymbol interferences, and offer high spectral efficiency. OFDM is used in many communications systems, e.g., WLANs as specified by the IEEE 802.11a/g standard and UWB WPANs as in the IEEE 802.15.3a WPAN standard. To improve the performance of OFDM systems, the fundamental concept of cooperative diversity can be applied. Nevertheless, special modulations/cooperation strategies are needed to efficiently exploit the available multiple carriers. In [89], an oversampling technique is used in combination with the intrinsic properties of OFDM symbols to provide efficient resource utilization. An application of space-time cooperation in OFDM systems was investigated in [90]. In [91], pairing of users and level of cooperation are jointly determined to minimize overall transmitted power of OFDM system. Most of the existing works are based on fixed relaying protocols, in which the relays always repeat the source infor-

mation. Moreover, these works rely on an assumption of fixed channel variances which implies a fixed network topology and fixed source-relay pairs.

In this chapter, we propose an OFDM cooperative protocol that improves spectral efficiency over those based on fixed relaying protocols while achieving the same performance of full diversity. By exploiting limited feedback from the destination node, the proposed protocol allows each relay to help forward information of multiple sources in one OFDM symbol. To specify how relay-source pairs should be assigned, we propose a practical relay-assignment scheme in which the relays are fixed at optimum locations. We investigate the implementation of the proposed cooperative protocol in OFDM networks considering the random users' spatial distribution. Outage probability is provided as a performance measure of the proposed protocol. A lower bound on the outage probability of any relay-assignment schemes is established, and the performance of the proposed relay-assignment schemes is analyzed. Furthermore, we investigate the application of the proposed protocol to enhance the performance of UWB communications. In UWB wireless indoor scenarios, both theoretical and simulation results show that the proposed cooperative protocol can achieve 75% power saving and 200% coverage extension compared to the non-cooperative UWB system proposed in the IEEE 802.15.3a standard.

An outline of this chapter is as follows. Section 7.1 describes the system models of cooperative OFDM wireless networks. Section 7.2 presents the proposed cooperative OFDM protocol and relay assignment scheme. In Section 7.3, we analyze the outage performance of the proposed protocol. Simulation results are given in Section 7.4.

7.1 System Model

We consider an OFDM wireless network such as a WLAN or a WPAN with a circular cell of radius ρ. The cell contains one central node and multiple users, each communicating with the central node. The central node can be a base station or an access point in case of the WLAN, and it can be a piconet coordinator in case of the WPAN. Suppose the central node is located at the center of the cell, and K users are uniformly located within the cell. Then, the user's distance D from the central node has the probability density function (PDF)

$$p_D(D) = \frac{2D}{\rho^2}, \quad 0 \leq D \leq \rho, \tag{7.1}$$

and the user's angle is uniformly distributed over $[0, 2\pi)$. We assume that each node is equipped with single antenna, and its transmission is constrained to half-duplex mode, i.e., any node cannot transmit and receive simultaneously [60]. We consider an uplink scenario where all users transmit their information to the central node. Similar to that specified in the IEEE 802.11a/g standard and the IEEE 802.15.3a standard proposal [19], the data packet of each user consists of preamble, header, and frame payload which carries several OFDM data symbols. The header includes the pilot symbols which allow channel estimation to be performed at the central node. Channel access within the cell is based on orthogonal multiple access mechanism as used in many current OFDM wireless networks.

We consider the S-V fading model as specified in (2.7). The channel fading for each transmit-receive link is assumed to stay constant during the transmission of each packet. This assumption is reasonable for slow fading scenarios including UWB environments [68]. With the choice of cyclic prefix length greater than the duration of the channel impulse response, OFDM allows the frequency-band to be

divided into a set of orthogonal narrowband subcarriers. Accordingly, the received signal at subcarrier n of destination d (central node) from source user s can be modeled as

$$y_{s,d}(n) = \sqrt{P_{NC}kD_{s,d}^{-\nu}}H_{s,d}(n)x_s(n) + z_{s,d}(n), \qquad (7.2)$$

where P_{NC} is the transmitted power at the source in non-cooperative mode, $x_s(n)$ denotes an information symbol to be transmitted from the source s at subcarrier n, $H_{s,d}(n)$ represents the frequency response at the nth subcarrier of the channel from the source to the destination, and $z_{s,d}(n)$ is an additive noise. The power P_{NC} is assumed equal for all subcarriers, i.e., no bit loading is performed, as in the current multiband OFDM standard proposal [19]. In (7.2), k is a constant whose value depends on the propagation environment and antenna design, ν is the propagation loss factor, and $D_{s,d}$ represents the distance between node s and node d. The noise term $z_{s,d}(n)$ is modeled as a complex Gaussian random variable with zero mean and variance N_0. Since different users transmit via orthogonal channels, no multiple access interference is considered in the signal model. From (2.7), the channel frequency response $H_{s,d}(n)$ is given by

$$H_{s,d}(n) = \sum_{c=0}^{C}\sum_{l=0}^{L}\alpha_{s,d}(c,l)e^{-\mathbf{j}2\pi n\Delta f[T_{s,d}(c)+\tau_{s,d}(c,l)]}, \qquad (7.3)$$

where the subscript $\{s,d\}$ indicates the channel link from the source to the destination. We assume that the nodes are spatially well separated such that the channel fades for for different propagation links are statistically mutually independent, i.e., $H_{i,j}(n)$ are independent for different transmit-receive links.

Note that the information can be jointly encoded across time or frequency to achieve diversities. For instance, in the multiband OFDM approach [19], the frequency-domain spreading is obtained by choosing conjugate symmetric inputs

to the IFFT, while the time-domain spreading is achieved by repeating the same information in an OFDM symbol on two different subbands [19]. When the frequency spreading is performed, the same information can be transmitted in more than one subcarrier. For subsequent performance evaluation, we denote Φ_n as a set of subcarriers that carry the information $x_s(n)$. The case when time spreading is performed is not considered here due to space limitation.

At the destination, the same information transmitted via different subcarriers is combined using the MRC. Assume that each transmitted symbol has unit energy, then the SNR of the MRC output is [81]

$$\zeta_{s,d} = \frac{P_{NC} k D_{s,d}^{-\nu}}{N_0} \sum_{n \in \Phi_n} |H_{s,d}(n)|^2. \tag{7.4}$$

In this paper, we characterize the system performance in terms of outage probability [81], which is defined as the probability that the combined SNR, ζ, falls below a specified threshold, ζ_o:

$$P_{\text{out}} = P\left(\zeta \leq \zeta_o\right). \tag{7.5}$$

If the combined SNR of any subcarrier symbol is larger than the given threshold ζ_o, the symbol is assumed to be decoded correctly. Otherwise, an outage occurs, and the symbol is considered lost.

7.2 Proposed Cooperative Protocol and Relay-Assignment Scheme

In this section, we first describe the proposed cooperative protocol, and then provide a practical relay-assignment scheme.

7.2.1 Proposed Cooperative Protocol

Consider a cooperation scenario where a source can employ another node (relay) to forward its information to the destination. The proposed cooperative protocol is based on the incremental relaying protocols [60], which exploit a bit feedback from the destination that indicates the success or failure of the direct transmission. The proposed protocol consists of two phases.

In Phase 1, each user transmits its packet to the destination (central node) and the packets are also received at the relay. After receiving the user's packet, the destination performs channel estimation using the OFDM pilot symbols in the packet header. Based on the estimated channel coefficients, the destination is able to specify which subcarrier symbols are not received successfully (i.e., those in the subcarriers of which the combined SNRs fall below the SNR threshold), and then broadcasts the indexes of the subcarriers carrying those symbols.

In Phase 2, the relay forwards the source symbols that are unsuccessfully transmitted in Phase 1 to the destination. Since it is unlikely that all subcarrier symbols are sent unsuccessfully, the proposed protocol makes efficient use of the available bandwidth by allowing the relay to help forward the information of multiple users in one OFDM block. The users' data to be forwarded by the relay can be arranged such that the destination can specify which subcarriers carry information of which users. For instance, if ω_i subcarriers of user i are in outage, then in Phase 2, the relay can use the first ω_1 subcarriers to transmit the data of user 1, the next ω_2 subcarriers to transmit the data of user 2, and so on. Before transmission, the relay can also perform subcarrier permutation (see [29] and references therein) to alleviate the effect of burst error.

(a) Phase 1

(b) Phase 2
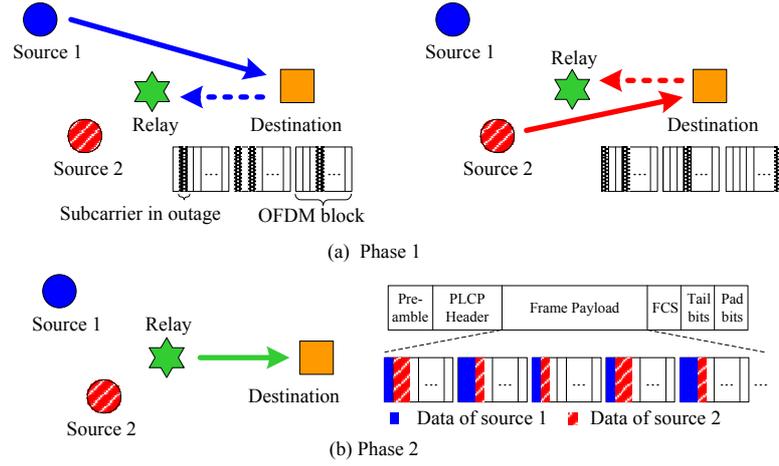
Figure 7.1: Illustrations of the proposed cooperative protocol for UWB multiband OFDM system with 2 users and 1 relay.

As an example, Fig. 7.1 illustrates the proposed protocol for a UWB multiband OFDM system with 2 source users and 1 relay. The multiple access is based on TDMA, and the first three subbands are used [19]. Figs. 7.1(a) and 7.1(b) depicts transmission in Phase 1 and Phase 2, respectively.

In Phase 1, the received signals at the destination and the relay are

$$y_{s,d}(n) = \sqrt{P_{CO}kD_{s,d}^{-\nu}}H_{s,d}(n)x_s(n) + z_{s,d}(n); \tag{7.6}$$

$$y_{s,r}(n) = \sqrt{P_{CO}kD_{s,r}^{-\nu}}H_{s,r}(n)x_s(n) + z_{s,r}(n), \tag{7.7}$$

where P_{CO} is the transmitted power in the cooperative mode. As we will show in Section 7.4, P_{CO} can be determined rigourously to ensure the same average transmitted power of both non-cooperative and cooperative protocols. In Phase 2, the signal received at the destination from the relay is given by

$$y_{r,d}(n) = \sqrt{P_{CO}kD_{r,d}^{-\nu}}H_{r,d}(n)\tilde{x}_s(n) + z_{r,d}(n), \tag{7.8}$$

174

(a) A cell with 3 sectors   (b) One sector
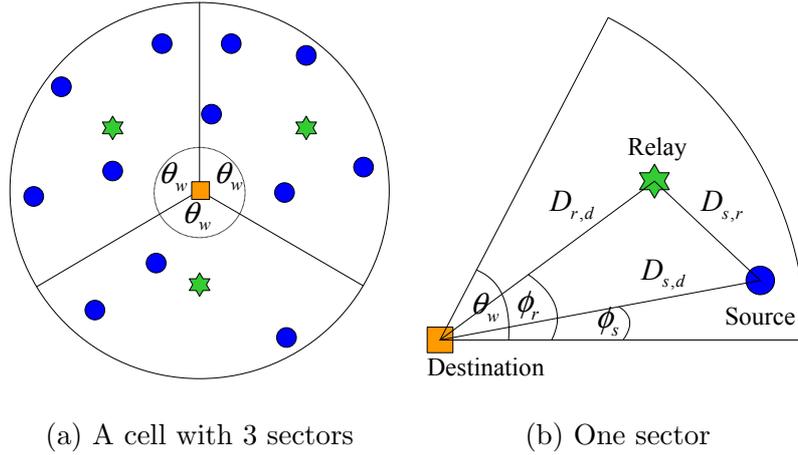
Figure 7.2: An example of relay assignment for a multiuser OFDM system.

where $\tilde{x}_s(n)$ denotes the source symbols that are not captured by the destination in Phase 1.

7.2.2 Relay Assignment Scheme

We propose in this subsection a practical relay assignment scheme for cooperative OFDM networks. In the proposed scheme, the cell is equally divided into w sectors, each with central angle $2\pi/w$; one relay is assigned to help users within each sector, as illustrated in Fig. 7.2(a) for a cell with $w = 3$ sectors.

In each sector, one relay is placed at an optimum relay location which minimizes the outage probability for all possible source-destination pairs within the sector. This scheme requires that the locations of all users in the cell is known. This can be done via network aid position techniques (see [92] and references therein). Once the relays are assigned, they continue helping the users. The relay assignment can be updated when the network topology changes considerably.

7.3 Performance Analysis

In this section, we first derive outage probability of the non-cooperative and the proposed cooperative protocols. Next, we provide a lower bound on the outage performance. Finally, we analyze performance of the proposed relay-assignment scheme.

7.3.1 Non-Cooperative and Cooperative Protocols

Given a distance $D_{i,j}$ of a transmit-receive link (i,j), the probability that the link (i,j) is in outage can be obtained from (7.4) and (7.5) as

$$\mathrm{P}_{\mathrm{out}}(D_{i,j}) = \mathrm{P}\left(\sum_{n\in\Phi_n} |H_{i,j}(n)|^2 \leq \frac{N_0\zeta_o D_{i,j}^\nu}{kP}\right), \tag{7.9}$$

where P is the transmitted power at node i. The outage probability in (7.9) can be determined from the PDF of $\xi_{i,j} \triangleq \sum_{n\in\Phi_n} |H_{i,j}(n)|^2$, which in turn can be obtained from the MGF of $\xi_{i,j}$ (denoted by $\mathcal{M}_{\xi_{i,j}}(s)$). If the data is jointly encoded across multiple subcarriers, it is difficult, if not impossible, to obtain closed-form formulations of the MGF $\mathcal{M}_{\xi_{i,j}}(s)$. In the sequel, we exploit an approximation approach in Chapter 5 which allows us to approximate $\mathcal{M}_{\xi_{i,j}}(s)$ as

$$\mathcal{M}_{\xi_{i,j}}(s) \approx \prod_{n=1}^M \frac{1}{1 - s\beta_{i,j}(n)} = \sum_{n=1}^M \frac{A_{i,j}(n)}{1 - s\beta_{i,j}(n)}, \tag{7.10}$$

where M is the cardinality of the set Φ_n, and $A_{i,j}(n)$ is

$$A_{i,j}(n) = \prod_{n'=1,n'\neq n}^M \frac{\beta_{i,j}(n)}{\beta_{i,j}(n) - \beta_{i,j}(n')}. \tag{7.11}$$

Here, $\beta_{i,j}(n)$ denote the eigenvalues of an $M \times M$ correlation matrix $\mathbf{R}_{i,j}$ whose diagonal component is one and the $(p,q)^{th}$ $(p \neq q)$ component is given by

$$R_{p,q} = \Omega(0,0)g_{p,q}(\Lambda, \Gamma^{-1})g_{p,q}(\lambda, \gamma^{-1}), \tag{7.12}$$

where $g_{p,q}(a,b) \triangleq (a + b + \mathbf{j}2\pi(n_p - n_q)\Delta f)/(b + \mathbf{j}2\pi(n_p - n_q)\Delta f)$ in which n_p denotes the pth element in the set Φ_n. By applying the inverse Laplace transform to the MGF in (7.10), and then substituting the obtained PDF into (7.9), we have

$$\mathrm{P_{out}}(D_{i,j}) \approx \sum_{n=1}^{M} A_{i,j}(n)\Big(1 - \exp\big(-\frac{N_0\zeta_o D_{i,j}^{\nu}}{kP\beta_{i,j}(n)}\big)\Big). \tag{7.13}$$

Note that the outage probability in (7.13) is exact in case of no jointly encoding across subcarriers.

The conditional outage probability of the non-cooperative protocol can be obtained from (7.4) and (7.13) as

$$\mathrm{P_{out}^{NC}}(D_{s,d}) \approx \sum_{n=1}^{M} A_{s,d}(n)\Big(1 - \exp\big(-\frac{N_0\zeta_o D_{s,d}^{\nu}}{kP_{NC}\beta_{s,d}(n)}\big)\Big). \tag{7.14}$$

The eigenvalues $\beta_{s,d}(n)$ depend on the channel model parameters of the source-destination link. For mathematical tractability, we assume that the channel parameters of all source-destination links are the same. By averaging (7.14) over the user distribution in (7.1), we obtain the average outage probability

$$\begin{aligned}
\mathrm{P_{out}^{NC}} &= \int_0^\rho \mathrm{P_{out}^{NC}}(D_{s,d})p_{D_{s,d}}(D_{s,d})dD_{s,d} \\
&\approx \sum_{n=1}^{M} A_{s,d}(n)\left(1 - \frac{2\Upsilon(2/\nu, B_{s,d}(n)\rho^\nu)}{\nu\rho^2 B_{s,d}^{2/\nu}(n)}\right),
\end{aligned} \tag{7.15}$$

where $B_{s,d}(n) = N_0\zeta_o/(kP_{NC}\beta_{s,d}(n))$ and $\Upsilon(a,x) \triangleq \int_0^x e^{-t}t^{a-1}dt$ is the incomplete Gamma function.

Under the proposed cooperative protocol, the destination broadcasts the indexes of the subcarriers of which the combined SNR falls below the SNR threshold, and the assigned relay re-transmits the information conveyed in those subcarriers. Given locations of the source user and the relay, the conditional outage probability

can be calculated as

$$P_{\text{out}}^{CO}(D_{s,d}) = P\big((\zeta_{s,d} \leq \zeta_o) \cap (\zeta_{r,d} \leq \zeta_o) \cap (\zeta_{s,r} > \zeta_o) \big)$$

$$+ P\big((\zeta_{s,d} \leq \zeta_o) \cap (\zeta_{s,r} \leq \zeta_o) \big), \qquad (7.16)$$

where the first term corresponds to the event that both the source-destination link and relay-destination link are in outage while the source-relay link is not, and the the second term corresponds to the event that both the source-destination link and source-relay link are in outage. Using the signal models in (7.6)-(7.8), the outage probability in (7.13), and the assumption of independent channel links among all nodes, the conditional outage probability in (7.16) can be calculated as

$$P_{\text{out}}^{CO}(D_{s,d}) = \big(1 - F_{s,d}(D_{s,d})\big)\big(1 - F_{s,r}(D_{s,r})F_{r,d}(D_{r,d})\big); \qquad (7.17)$$

$$F_{i,j}(D_{i,j}) = \sum_{n=1}^{M} A_{i,j}(n) e^{-\frac{N_0 \zeta_o D_{i,j}^{\nu}}{kP_{CO}\ \beta_{i,j}(n)}}. \qquad (7.18)$$

Finally, given specific relay locations, the average outage probability of the proposed cooperative protocol can be obtained as

$$P_{\text{out}}^{CO} = \frac{2}{\rho^2} \int_0^{\rho} D_{s,d} P_{\text{out}}^{CO}(D_{s,d}) dD_{s,d}, \qquad (7.19)$$

where $P_{\text{out}}^{CO}(D_{s,d})$ is given in (7.17). From (7.19), we can clearly see that the performance of the proposed cooperative protocol depends on how the relays are assigned to help the source users. To get more insights of the cooperation systems, we provide the performance lower bound and the performance of the proposed relay-assignment scheme in the following subsections.

7.3.2   Performance Lower Bound

To obtain a lower bound on the outage probability of the proposed cooperative protocol, we first determine an optimum relay location that minimizes the outage

probability for a fixed source-destination pair. Then, the lower bound can be determined as the outage performance of a network in which the assigned relay for every source is located in the optimum location.

It is obvious that if the relay can be placed anywhere in the cell, the optimum relay location must be on the line joining the source and the destination. In this case, the distance between the source and the relay can be written as $D_{s,r} = D_{s,d} - D_{r,d}$. Consequently, from the conditional outage probability in (7.17), the optimum relay location for a source-destination pair can be obtained by solving $\hat{D}_{r,d} = \arg\min_{D_{r,d}} \mathrm{P}^{CO}_{\mathrm{out}}(D_{s,d})$, which is equivalent to

$$\hat{D}_{r,d} = \arg\max_{D_{r,d}} \; F_{s,r}(D_{s,d} - D_{r,d})F_{r,d}(D_{r,d}) \tag{7.20}$$

$$\text{subject to } 0 \leq D_{r,d} \leq D_{s,d}.$$

For simplicity, we resort to the scenario that the channel model parameters of the source-relay links and relay-destination link are the same. In this case, (7.20) can be written as

$$\hat{D}_{r,d} = \arg\max_{D_{r,d}} \sum_{n=1}^{M} A_n e^{-B_n(D_{s,d}-D_{r,d})^\nu} \sum_{n=1}^{M} A_n e^{-B_n D^\nu_{r,d}}, \tag{7.21}$$

where $A_n = A_{s,r}(n) = A_{r,d}(n)$, and $B_n = N_0\zeta_o/(kP_{CO}\beta_n)$ in which $\beta_n = \beta_{s,r}(n) = \beta_{r,d}(n)$. By taking the derivatives of the right hand side of (7.21) with respect to $D_{r,d}$, we can show that the optimum relay location is $\hat{D}_{r,d} = D_{s,d}/2$. Finally, replacing $D_{r,d}$ in (7.19) with $\hat{D}_{r,d} = D_{s,d}/2$, we have

$$\mathrm{P}^{LB}_{\mathrm{out}} = \frac{2}{\rho^2} \int_0^\rho D_{s,d}\Big(1 - \sum_{n=1}^{M}\sum_{n'=1}^{M} A_n A_{n'} e^{-\frac{N_0\zeta_o D^\nu_{s,d}}{2^\nu kP_{CO}}\left(\frac{1}{\beta_n}+\frac{1}{\beta_{n'}}\right)}\Big)$$

$$\times \Big(1 - \sum_{n=1}^{M} A_{s,d}(n)e^{-\frac{N_0\zeta_o D^\nu_{s,d}}{kP_{CO}\;\beta_{s,d}(n)}}\Big)dD_{s,d}. \tag{7.22}$$

The outage probability in (7.22) serves as a lower bound on the outage probability of the proposed cooperative protocol. The performance of the proposed protocol employing any practical relay-assignment schemes can be lower bounded as

$$\mathrm{P}_{\mathrm{out}}^{CO} \geq \mathrm{P}_{\mathrm{out}}^{LB}. \tag{7.23}$$

7.3.3 Proposed Relay-Assignment Scheme

In this subsection, we derive an outage probability of the proposed cooperative protocol with the relay-assignment scheme presented in the previous section. In the proposed relay-assignment scheme, the cell is divided into w sectors, each containing one relay which is assigned to help all users in the sector. Without loss of generality, we consider the sector as shown in Fig. 7.2(b), in which the relay is located at $D_{r,d}e^{\mathbf{j}\phi_r}$ and a source user is located at $D_{s,d}e^{\mathbf{j}\phi_s}$ ($0 \leq \phi_r, \phi_s \leq \theta_w$). The distance between the source and the relay can be expressed as

$$D_{s,r} = [D_{s,d}^2 + D_{r,d}^2 - 2D_{s,d}D_{r,d}\cos(\phi_r - \phi_s)]^{\frac{1}{2}} \triangleq f(\phi_s, \phi_r).$$

Assuming that users are uniformly distributed within the cell, the PDF of the user's distance D from the destination conditioned that the user is located in the sector can be given by

$$p_D(D \mid 0 \leq \phi_s \leq \theta_w) = 2D/(w\rho^2), \quad 0 \leq D \leq \rho. \tag{7.24}$$

Given a fixed relay location within each sector, the average outage probability of the proposed relay-assignment scheme can be determined by averaging (7.17) over the user distribution in (7.24) as

$$\mathrm{P}_{\mathrm{out}}^{CO} = \frac{2}{w\rho^2} \int_0^\rho D_{sd}[1 - F_{s,d}(D_{s,d})][1 - G(D_{s,d})]dD_{s,d} \tag{7.25}$$

where $G(D_{s,d}) = w/(2\pi) \int_0^{\theta_w} F_{s,r}(f(\phi_s, \phi_r)) F_{r,d}(D_{r,d}) d\phi_s$.

Based on the average outage probability in (7.25), we can determine the optimum relay location as follows. Since the users are uniformly located in the cell, one can show that the optimum relay angle is $\hat{\phi}_r = \theta_w/2$. Substitute $\hat{\phi}_r$ into (7.25) and take the first derivative of P_{out}^{CO} with respect to $D_{r,d}$, then the optimum relay distance $\hat{D}_{r,d}$ can be obtained by solving

$$\int_0^\rho D_{s,d}\big(1 - F_{s,d}(D_{s,d})\big) \int_0^{\theta_w} \mathcal{G}(D_{s,d}) d\phi_s dD_{s,d} = 0; \tag{7.26}$$

$$\mathcal{G}(D_{s,d}) = CF_{r,d}(D_{r,d})\tilde{D}_{s,r}^{\nu-1} \sum A_{s,r}(n)B_{s,r}(n)e^{-B_{s,r}(n)\tilde{D}_{s,r}^\nu}$$
$$+ F_{s,r}(\tilde{D}_{s,r})D_{r,d}^{\nu-1} \sum A_{r,d}(n)B_{r,d}(n)e^{-B_{r,d}(n)D_{r,d}^\nu},$$

in which $\tilde{D}_{s,r} = f(\phi_s, \pi/w)$, $C = (D_{r,d} - D_{s,d}\cos(\pi/w - \phi_s))$ and $B_{i,j}(n) = N_0\zeta_o/(kP_{CO}\beta_{i,j}(n))$.

To get more insightful understanding, we also provide here an explicit relay location that achieves close performance to that of optimum relay location. First, we calculate the average value of the user location as

$$\bar{D}_{s,d} = \int_0^\rho D_{s,d}p_{D_{s,d}}(D_{s,d})dD_{s,d} = 2\rho/3. \tag{7.27}$$

Then, an approximate relay location can be determined as

$$\bar{D}_{r,d} = \arg \min_{0 \le D_{r,d} \le \bar{D}_{s,d}} P_{out}^{CO}(\bar{D}_{s,d}|D_{s,r} = \bar{D}_{s,d} - D_{r,d}), \tag{7.28}$$

where $P_{out}^{CO}(D_{s,d})$ is evaluated in (7.17). Using the results from Section 7.3.2, we can approximate the relay location by

$$\bar{D}_{r,d} = \bar{D}_{s,d}/2 = \rho/3. \tag{7.29}$$

As will be shown in the next section, the relay location obtained from this approximation leads to almost the same performance as that of optimum relay location.
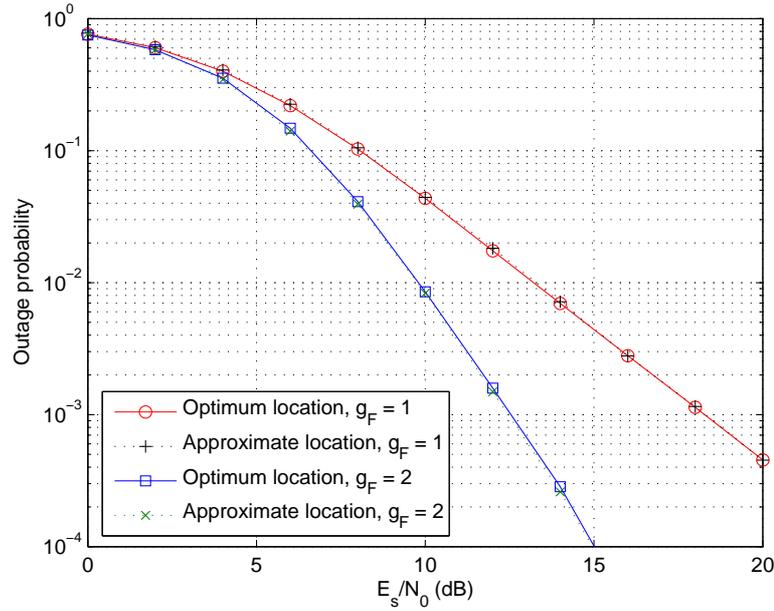
Figure 7.3: Outage probability of two proposed relay assignment schemes.

7.4 Simulation Results

We perform computer simulations to compare performance of the proposed relay-assignment scheme and to validate the above theoretical analysis. All simulations are based on UWB multiband OFDM systems with 128 subcarriers and the subband bandwidth of 528 MHz. The channel model parameters of every link follow those for CM4 [68], the path loss exponent is $\nu = 2$, and the number of users in the cell is set at 10 users. Unless stated otherwise, the cell radius is fixed at 10 meters.

In Figs. 7.3 and 7.4, we show the outage probability of the proposed relay-assignment scheme. Fig. 7.3 depicts the outage performance versus the SNR per subcarrier symbol (E_s/N_0) in case of $w = 2$ relays. For the relay-assignment scheme, the approximate relay location $\bar{D}_{r,d}$ results in very close performance to
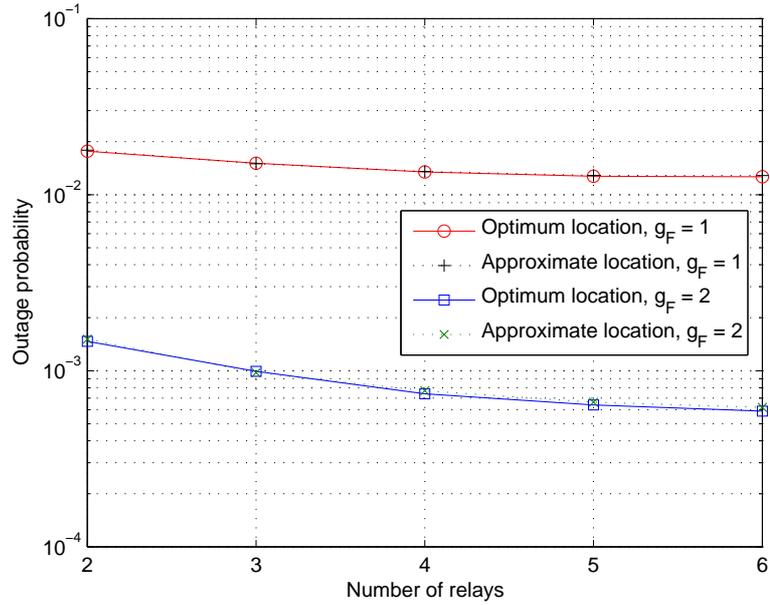
Figure 7.4: Outage probability of two proposed relay assignment schemes versus the number of relays.

that of the optimum relay location. In Fig. 7.4, the outage probability is plotted as a function of the number of relays. Notice that the outage probability slightly decreases with the number of relays. This implies that less than two relays are necessary for practical implementation of UWB system.

In Figs. 7.5-7.7, we compare the performance of the proposed cooperative protocol with that of non-cooperative protocol and the lower bound. Along with the simulation curves, we also plot the theoretical outage performance that is derived in the previous sections. For fair comparison between the non-cooperative and cooperative protocols, we use the same average transmitted power in both protocols. The average transmitted power of cooperative protocol is

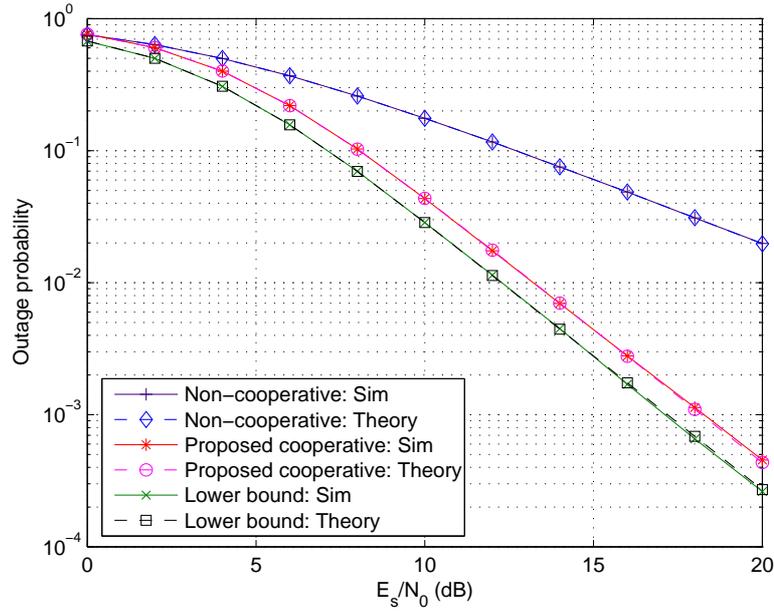$$\bar{P}_{CO} = P_{CO}\text{P(Source transmits only)} + 2P_{CO}\text{P(Source and relay transmit)},$$

Figure 7.5: Outage probability versus E_s/N_0 in case of no encoding across subcarriers.

which can be determined as

$$\bar{P}_{CO} = P_{CO}(1 + \mathrm{P}^{s,d}_{\mathrm{out}}(P_{CO}) - \mathrm{P}^{s,d}_{\mathrm{out}}(P_{CO})\mathrm{P}^{s,r}_{\mathrm{out}}(P_{CO})), \qquad (7.30)$$

where $\mathrm{P}^{i,j}_{\mathrm{out}}(P_{CO})$ denotes the outage probability of the direct transmission for the link $i-j$ when transmitted power P_{CO} is used. We set $P_{NC} = P_{CO}(1 + \mathrm{P}^{s,d}_{\mathrm{out}}(P_{CO}))$ which is in favor of the non-cooperative protocol. With the power in (7.30), the bandwidth efficiency of the proposed cooperative protocol is approximately the same as that of non-cooperative protocol. Figs. 7.5 and 7.6 depicts the outage probability versus E_s/N_0 for the case of no coding and jointly coding across 2 subcarriers, respectively. Clearly, the theoretical results match with the simulation results in all cases. In case of no coding, the proposed cooperative protocol achieves 6dB performance improvement compared to the non-cooperative protocol at an outage probability of 0.05; in other words, 75% power saving is achieved. Also,
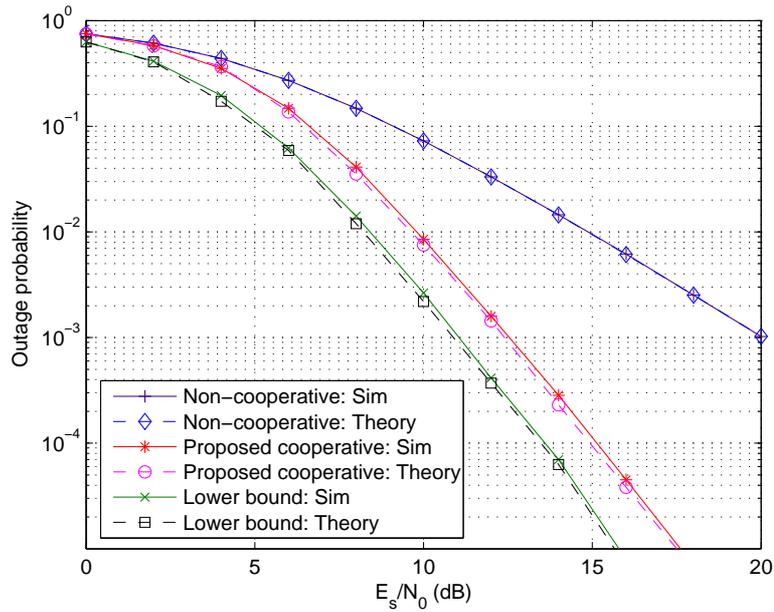
Figure 7.6: Outage probability versus E_s/N_0 in case of jointly encoding across two subcarriers.

there is only about 1dB performance gap between the proposed scheme and the lower bound. The same tendencies of the performance curves can be observed in case of jointly coding across subcarriers.

Fig. 7.7 depicts the outage probability as a function of the cell radius. The average SNR per symbol is fixed at $E_s/N_0 = 10$ dB. Again, the theoretical results closely match with the simulation results. If the outage probability is required to be at most 0.01, then the cell radius can be at most 3 meters. By employing the proposed cooperative protocol with 2 relays, the cell radius can be improved to 9m, i.e., 200% increase. Also, the cell radius of the proposed scheme is only 1m less than that of the lower bound.
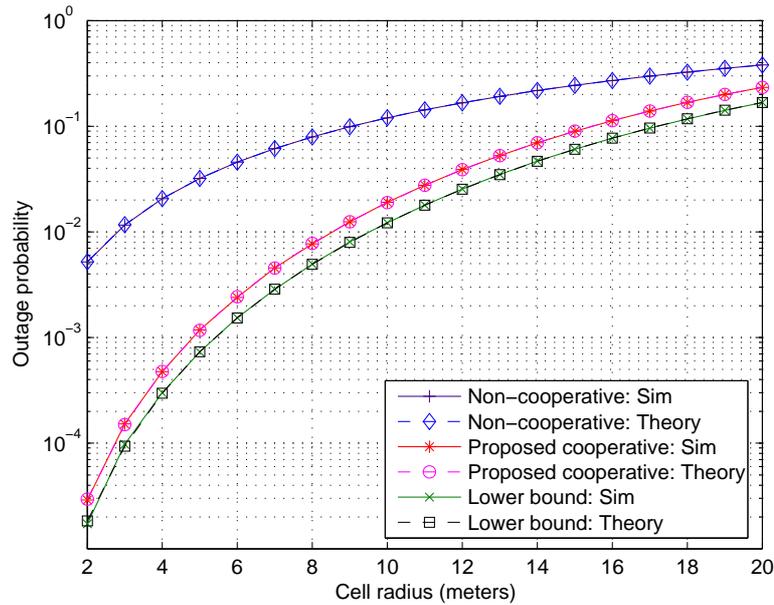
Figure 7.7: Outage probability versus cell radius.

7.5 Chapter Summary

We propose in this chapter a bandwidth-efficient cooperative protocol for OFDM systems. In the proposed protocol, the destination broadcasts subcarriers indexes of which the received SNR falls below a specific SNR threshold, and the relay forwards only the source symbols carried in those subcarriers. In this way, the relay can help forward the data of multiple sources in one OFDM symbol, and the proposed protocol greatly improves the spectral efficiency, while still achieving full diversity. For practical implementation of the proposed cooperative protocol in OFDM networks, we proposed a relay-assignment scheme in which each relay is placed in the optimum location. Performance analysis in terms of outage probability is provided. Furthermore, we investigate the application of the proposed protocol to enhance the performance of UWB communications. Both analytical

186

and theoretical results show that the proposed cooperative protocol can achieve 75% power saving and 200% coverage extension compared to the non-cooperative UWB multiband OFDM at the same data rate.

Chapter 8

Conclusions and Future Research

8.1 Conclusions

In this thesis, we provide the performance analysis of UWB systems and develop various techniques to enhance the performance and transmission range of UWB systems.

We first propose a multiband MIMO coding framework for UWB systems. By a technique of band hopping in combination with jointly coding across spatial, temporal and frequency domains, our scheme is able to exploit all available spatial and multipath diversities, richly inherent in UWB environments. We show that the maximum achievable diversity advantage of our proposed system is KLN_tN_r regardless of the temporal correlation of the channel. An interesting result is that the diversity advantage obtained under Nakagami fading with arbitrary m parameter is almost the same as that obtained in Rayleigh fading channels. Simulation results show that the employment of STF coding and band hopping techniques is able to increase the diversity order significantly, thereby considerably improving

system performance. In case of single-antenna system, increasing the number of jointly encoded OFDM blocks from one to two yields the performance improvement of 6 dB at a BER of 10^{-4}. By increasing also the number of transmit antennas from one to two, the proposed STF coded multiband UWB system has a total gain of 9 dB at a BER of 10^{-4}.

We then provide the pairwise error probability and outage probability analysis that captures the unique multipath-rich and random-clustering characteristics of UWB channels. Both theoretical and simulation results reveal that the performances of uncoded multiband UWB systems do not depend on the clustering property, while the performances of coded multiband systems depend heavily the multipath arrival rates and decay factors. In case of jointly coding across two sub-carriers, we obtain the following results. When the product of the cluster arrival rate and cluster decay factor is small, e.g., in a short-range (0-4 meters) line-of-sight scenario, the effect of the first cluster will dominate and the UWB performance can be well approximated by taking into consideration only the first cluster. In contrast, when the product of the ray arrival rate and ray decay factor is much less than one, the performance seriously depends only on the first path in each cluster. We also provide the performance analysis of UWB-MIMO systems. Our results show disclose that the coding gain strongly relates to the channel model parameters; the diversity gain on the other hand, can be improved by increasing the number of jointly encoded subcarriers, the number of jointly encoded OFDM symbols, or the number of antennas, regardless of the random-clustering behavior of UWB channels.

Low power consumption is one of the key elements to make UWB technology be the solution for future indoor wireless communications. We also present in this

189

thesis our proposed efficient cross-layer algorithm for allocating subband and power among users in UWB multiband OFDM systems. The proposed scheme aims to reduce power consumption without compromising performance, resulting in much lower co-channel interference and a substantial increase in battery life. We propose a general framework to minimize the overall transmit power under the practical implementation constraints. The formulated problem is NP hard; however, with the proposed fast suboptimal algorithm, we can reduce the computational complexity to only $O(K^2S)$, where K is the number of users and S is the number of subbands. Simulation results show that the proposed algorithm achieves comparable performances to those of complex optimal full search algorithm, and can save up to 61% of power consumption compared to the standard multiband scheme.

We next propose to enhance UWB system performance by employing cooperative diversity. We analyze the symbol error rate performance and provide optimum power allocation of cooperative UWB multiband OFDM systems with decode-and-forward protocol. Both non-cooperative and cooperative schemes achieve the same diversity order of twice the frequency spreading gain for every channel environment. The cooperation gain, on the other hand, depends on the clustering property of UWB channels. By taking advantage of the relay location and properly allocating the transmitted power, the cooperation gain can be improved such that the cooperative UWB achieves superior performance to the non-cooperative scheme with the same data rate. It turns out that at low SNR, the coverage is maximized if the relay is located farthest away from the source, and almost all of the transmitted power is allocated at the source; at high SNR, the coverage is maximized if the relay is located in the midpoint between source and destination, and equal power allocation is used. We also propose to further improve the cooperative UWB

190

scheme by allowing the source and the relay nodes to simultaneously retransmit the information. Simulation results confirm the theoretical analysis that the cooperative UWB scheme can achieve 43% power saving and 85% coverage extension compared to the non-cooperative scheme, while the improved cooperative UWB scheme can achieve 52% power saving and 100% coverage extension.

We further develop a bandwidth-efficient cooperative protocol for OFDM wireless networks, and analyze the performance of the proposed protocol in multiuser systems with randomly distributed users. The proposed protocol exploits limited feedback from the destination terminal (central node) such that each relay is able to help forward information of multiple sources in one OFDM symbol. In this way, the proposed protocol not only achieves full diversity but also efficiently utilizes available bandwidth. To specify how relay-source pairs should be assigned, we propose a practical relay-assignment scheme in which the relays are fixed at optimum locations. We provide outage probability analysis of the proposed protocol in wireless indoor environment. Moreover, a lower bound on the outage probability of any relay-assignment schemes is established, and the performance of the proposed relay-assignment scheme is analyzed. We also investigate the application of the proposed protocol to enhance the performance of UWB systems. In UWB wireless indoor scenarios, both theoretical and simulation results show that the proposed cooperative protocol can achieve 75% power saving and 200% coverage extension compared to the non-cooperative UWB system proposed in the IEEE 802.15.3a standard.

8.2 Future Research

There are a variety of fruitful areas for future research on UWB communications and related topics. We present in what follows some of interesting research directions that need to be further investigated.

Our current work on the performance analysis of UWB systems is based on the assumption of perfect channel estimation as well as no interference. In practice, the system performance will be degraded due to the channel estimation error and the following interference:

- Intersymbol interference

- Multiple access interference

- Narrowband interference

Due to the scattering nature of indoor scenarios and the narrow duration of UWB signals, the long delay spread can be observed in UWB channels. When the delay spread is longer than the length of the cyclic prefix, it can cause various deleterious effects, such as intersymbol interference and channel estimation errors, both of which can degrade system performance. Furthermore, when more than one piconet is simultaneously operating in the same proximity, it can cause multiple access interference. Similarly, if the UWB device shares the same frequency band as a narrowband devices, the narrowband interference can cause significant performance degradation. It is important to investigate the UWB performance under the present of such interference, and study efficient techniques to mitigate these interference and further improve UWB performance.

In addition, our current work focuses on error probability and outage probability analysis of UWB systems. Another important measure that has not been investigated is the capacity of single-antenna UWB and UWB-MIMO systems. It is essential to determine the capacity of UWB systems under the realistic UWB channels and investigate how the random clustering characteristic of UWB channels affect the system capacity. Also, as mentioned in Chapter 1, there are two main approaches to generate UWB signals: single band approach and multiband approach. Both approaches have their advantages and drawbacks. Our current research work focus on multiband OFDM approach. It is interesting to also investigate the single band approach, e.g., time hopping UWB and direct sequence UWB. Particularly, the performance of single band UWB systems under realistic channel scenario should be analyzed, and the effect of clustering property of UWB channels on the system performance should be investigated.

In the decode-and-forward cooperative scheme, our current work assumes that the relay is able to make correct judgement whether the decoded symbol is correct or not. In practice, this knowledge is not available at the relay. However, the relay can apply a threshold test to the received signal from the source or the measured channel between the source and the relay. The interesting question is how to decide when to cooperate. It is crucial to investigate the decision criteria as well as the optimum threshold that leads to superior performance of the decode-and-forward cooperative systems.

BIBLIOGRAPHY

[1] G. F. Ross *The transient analysis of multiple beam feed networks for array systems*, Ph.D. dissertation, Polytechnic Institute of Brooklyn, Brooklyn, NY, 1963.

[2] G. F. Ross *Transmission and reception system for generating and receiving base-band duration pulse signals for short base-band pulse communication system*, U.S. Patent no. 3728632 dated April 17, 1973.

[3] T. W. Barrett "History of UltraWideband (UWB) radar and communications: Pioneers and innovators," *Proc. of Progress in Electromagnetics Symposium*, Cambridge, MA, Jul. 5-14, 2000.

[4] Federal Communications Commission Report "Revision of Part 15 of the Commission's Rules Regarding Ultra-Wideband Transmission Systems, First Report and Order ", Federal Communications Commission, Washington DC, ET-Docket 98-153, Feb. 2002.

[5] D. Porcino, and W. Hirt, "Ultra-Wideband Radio Technology: Potential and Challenges Ahead", *IEEE Commun. Magazine*, vol. 41, no. 7, pp. 66-74, Jul. 2003.

[6] T. Kaiser, Ed., *UWB Communications Systems - A Comprehensive Overview*, EURASIP Series on Signal Processing and Communications, Hindawi, 2005.

[7] J. G. Proakis, *Digital Communications*, 4th Ed., McGraw-Hill, New York, 2001.

[8] IEEE 802.15WPAN High Rate Alternative PHY Task Group 3a (TG3a). Internet: www.ieee802.org/15/pub/TG3a.html

[9] I. Oppermann, et. al, "UWB Wireless Sensor Networks: UWEN - A Practical Example," *IEEE Communications Magazine*, vol. 42, no. 12, pp. 27-32, Dec. 2004.

[10] R. A. Scholtz "Multiple Access with Time-Hopping Impulse Modulation," *Proc. of MILCOM Conf.*, Boston, MA, USA, pp. 447-450, Oct. 1993.

[11] M. Z. Win and R. A. Scholtz, "Impulse Radio: How It Works," *IEEE Commun. Letters*, vol. 2, no. 2, pp. 36-38, Feb. 1998.

[12] M. L. Welborn, "System Considerations for Ultra-Wideband Wireless Networks," *IEEE Radio and Wireless Conf.*, pp. 5-8, Aug. 2001.

[13] J. R. Foerster, "The Performance of a Direct-Sequence Spread UltraWideband System in the Presence of Multipath, Narrowband Interference, and Multiuser Interference," *IEEE Conf. on Ultra Wideband Systems and Tech.*, pp. 87-91, May 2002.

[14] R. Roberts, "XtremeSpectrum CFP Document," IEEE P802.15-03/154r1. March 3, 2003.

[15] N. Boubaker and K. B. Letaief, "Ultra Wideband DSSS for Multiple Access Communications Using Antipodal Signaling," *IEEE Int. Conf. on Commun.*, vol. 3, pp. 11-15, May 2003.

[16] E. Saberinia and A. H. Tewfik, "Pulsed and Non-Pulsed OFDM Ultra Wideband Wireless Personal Area Networks *IEEE Conf. on Ultra Wideband Systems and Tech.*, pp. 275-279, Nov. 2003.

[17] J. R. Foerster, et. al, "Intel CFP Presentation for a UWB PHY," IEEE P802.15-03/109r1, Mar. 3, 2003.

[18] A. Batra, et. al, "Multi-band OFDM Physical Layer Proposal for IEEE 802.15 Task Group 3a", IEEE P802.15-03/268r3, Mar. 2004.

[19] A. Batra, et. al, "Design of a Multiband OFDM System for Realistic UWB Channel Environments," *IEEE Trans. on Microwave Theory and Techniques*, vol. 52, no. 9, pp. 2123-2138, Sep. 2004.

[20] J.-C. Guey, M. P. Fitz, M. R. Bell, and W.-Y. Kuo, "Signal Design for Transmitter Diversity Wireless Communication Systems over Rayleigh Fading Channels," *IEEE Trans. on Commun.*, vol. 47, pp. 527-537, Apr. 1999.

[21] V. Tarokh, N. Seshadri and A. R. Calderbank, "Space-Time Codes for High Data Rate Wireless Communication: Performance Criterion and Code Construction," *IEEE Trans. on Inform. Theory*, vol. 44, no. 2, pp. 744-765, Mar. 1998.

[22] S. Alamouti, "A Simple Transmit Diversity Technique for Wireless Communications," *IEEE J. on Selected Areas in Commun.*, vol. 16, no. 8, pp. 1451-1458, Oct. 1998.

[23] V. Tarokh, H. Jafarkhani and A. R. Calderbank, "Space-Time Block Codes from Orthogonal Designs," *IEEE Trans. on Inform. Theory*, vol. 45, no. 5, pp. 1456-1467, Jul. 1999.

[24] B. M. Hochwald and T. L. Marzetta, "Unitary Space-Time Modulation for Multiple-Antenna Communication in Rayleigh Flat Fading," *IEEE Trans. on Inform. Theory*, vol. 46, pp. 543-564, Feb. 2000.

[25] D. Agrawal, V. Tarokh, A. Naguib, and N. Seshadri, "Space-Time Coded OFDM for High Data-Rate Wireless Communication over Wideband Channels," *IEEE Conf. on Vehicular Tech.*, vol. 3, pp. 2232-2236, 1998.

[26] R. Blum, Y. Li, J.Winters, and Q. Yan, "Improved Space-time Coding for MIMO-OFDM Wireless Communications," *IEEE Trans. on Commun.*, vol. 49, pp. 1873-1878, Nov. 2001.

[27] H. Bölcskei and A. J. Paulraj, "Space-Frequency Coded Broadband OFDM Systems," *IEEE Wireless Commun. Networking Conf.*, pp. 1-6, Sep. 2000.

[28] W. Su, Z. Safar, M. Olfat, and K. J. R. Liu, "Obtaining Full-Diversity Space-Frequency Codes from Space-Time Codes via Mapping," *IEEE Trans. on Signal Proc.*, vol. 51, no. 11, pp. 2905-2916, Nov. 2003.

[29] W. Su, Z. Safar, and K. J. R. Liu, "Full-Rate Full-Diversity Space-Frequency Codes with Optimum Coding Advantage," *IEEE Trans. on Inform. Theory*, vol. 51, no. 1, pp. 229-249, Jan. 2005.

[30] W. Su, Z. Safar, and K. J. R. Liu, "Systematic Design of Space-Frequency Codes with Full Rate and Full Diversity," *IEEE Wireless Commun. and Networking Conf.*, vol. 3, pp. 1436-1441, Mar. 2004.

[31] Y. Gong and K. B. Letaief, "Space-Frequency-Time Coded OFDM for Broadband Wireless Communications," *IEEE Global Telecommun. Conf.*, vol. 1, pp. 519-523, Nov. 2001.

[32] A. F. Molisch, M. Z. Win, and J. H. Winters, "Space-Time-Frequency (STF) Coding for MIMO-OFDM Systems," *IEEE Commun. Letters*, vol. 6, no. 9, pp. 370-372, Sep. 2002.

[33] Z. Liu, Y. Xin, and G. Giannakis, "Space-Time-Frequency Coded OFDM over Frequency Selective Fading Channels," *IEEE Trans. on Signal Processing*, vol. 50, no. 10, pp. 2465-2476, Oct. 2002.

[34] W. Su, Z. Safar, and K. J. R. Liu, "Towards Maximum Achievable Diversity in Space, Time and Frequency: Performance Analysis and Code Design," *IEEE Trans. on Wireless Commun.*, vol. 4, no. 4, pp. 1847-1857, Jul. 2005.

[35] J. D. Choi and W. E. Stark, "Performance of Ultra-Wideband Communications with Suboptimal Receivers in Multipath Channels," *IEEE J. on Selected Areas in Commun.*, vol. 20, no. 9, pp. 1754-1766, Dec. 2002.

[36] G. Durisi, and S. Benedetto, "Performance Evaluation of TH-PPM UWB Systems in the Presence of Multiuser Interference," *IEEE Commun. Letters*, vol. 7, no. 5, pp. 224-226, May 2003.

[37] J. Zhang, R. A. Kennedy and T. D. Abhayapala, "Performance of RAKE Reception for Ultra Wideband signals in a Lognormal fading Channel," *Inter. Workshop on UWB Systems*, Oulo, Finland, Jun. 2003.

[38] H. Liu "Performance of a Pulse Amplitude and Position Modulated Ultra-Wideband System Over Lognormal Fading Channels," *IEEE Commun. Letters.*, vol. 7, no. 11, pp. 531-533, Nov. 2003.

[39] N. Boubaker and K. B. Letaief, "Performance Analysis of DS-UWB Multiple Access Under Imperfect Power Control," *IEEE Trans. on Commun.*, vol. 52, no. 9, pp. 1459-1463, Sep. 2004.

[40] Y.-L. Chao and R. A. Scholtz "Weighted Correlation Receivers for Ultra-Wideband Transmitted Reference Systems," *IEEE Global Telecommun. Conf.*, vol. 1, pp. 66-70, Dec. 2004.

[41] W. Zhuang, X. Shen, and Q. Bi, "Ultra-Wideband Wireless Communications," *Wireless Commun. and Mobile Computing - Special Issue on Ultra-Broadband Wireless Communications for the Future, Invited paper*, vol. 3, no. 6, pp. 663 - 685, 2003.

[42] F. Cuomo, C. Martello, A. Baiocchi, and F. Capriotti "Radio Resource Sharing for Ad Hoc Networking with UWB," *IEEE J. on Selected Areas in Commun.*, vol. 20, no. 9, pp. 1722-1732, Dec. 2002.

[43] F. Cuomo and C. Martello "MAC Principles for an Ultra Wide Band Wireless Access," *IEEE Global Telecommun. Conf.*, vol. 6, pp. 3548-3552, Nov. 2001.

[44] H. Xu and A. Ganz, "A Radio Resource Control Method in UWB MAC Protocol Design," *IEEE Military Commun. Conf.* vol. 2, pp. 886-891, Oct. 2003.

[45] G. Giancola, L. De Nardis, M.-G. Di Benedetto, and E. Dubuis, "Dynamic Resource Allocation in Time-Varying Ultra Wide Band Channels," "IEEE International Conf. on Commun.," vol. 6, pp. 3581-3585, Jun. 2004.

[46] B. Radunovic and J.-Y. Le Boudec, "Optimal Power Control, Scheduling, and Routing in UWB Networks," *IEEE J. Selected Areas in Commun.*, vol. 22, no. 7, pp. 1252-1270, Sep. 2004.

[47] Y. Chu and A. Ganz, "Joint Scheduling and Resource Control for QoS Support in UWB-Based Wireless Networks," *IEEE Military Commun. Conf.*, vol. 2, pp. 1100-1106, 31 Oct.-3 Nov. 2004

[48] E. Saberinia, J. Tang, A. H. Tewfik, and K. K. Parhi, "Design and Implementation of Multi-Band Pulsed-OFDM System for Wireless Personal Area Networks," *IEEE Int. Conf. on Commun.*, vol. 2, pp. 862-866, Jun. 20-24, 2004.

[49] Y. Nakache, et. al, "Low-Complexity Ultrawideband Transceiver with Compatibility to Multiband-OFDM," Technical Report, A Mitsubishi Electronic Research Laboratory. Internet: www.merl.com/reports/docs/TR2004-051.pdf.

[50] L. Yang and G. B. Giannakis, "Space-Time Coding for Impulse Radio", *IEEE Conf. on Ultra Wideband Systems and Technologies*, pp. 235-239, May 2002.

[51] M. Weisenhorn and W. Hirt, "Performance of Binary Antipodal Signaling over the Indoor UWB MIMO Channel", *IEEE Int. Conf. on Commun.*, vol. 4, pp. 2872 - 2878, May 2003.

[52] W. P. Siriwongpairat, M. Olfat, and K. J. R. Liu, "On the Performance Evaluation of TH and DS UWB MIMO Systems", *IEEE Wireless Commun. and Networking Conf.*, pp. 1800-1805, Mar. 2004.

[53] W. P. Siriwongpairat, M. Olfat, and K. J. R. Liu, "Performance Analysis of Time Hopping and Direct Sequence UWB Space-Time Systems", *IEEE Global Telecommun. Conf.*, vol. 6, pp. 3526-3530, 29 Nov.-Dec. 3, 2004.

[54] E. Baccarelli, M. Biagi, and C. Pelizzoni "A Simple Multi-Antenna Transceiver for Ultra Wide Band Based 4GWLANs," *IEEE Wireless Commun. and Networking Conf.*, vol. 3, pp. 1436-1441, Mar. 2004.

[55] W. P. Siriwongpairat, M. Olfat, and K. J. R. Liu, "Performance Analysis and Comparison of Time Hopping and Direct Sequence UWB-MIMO Systems", *EURASIP J. on Applied Signal Proc. Special Issue on "UWB-State of the Art"*, 2004 (to appear).

[56] Z. Feng and T. Kaiser, "On Channel Capacity of Multi-Antenna UWB Indoor Wireless Systems", *IEEE Int. Symposium on Spread Spectrum Techniques and Applications*, Sydney, Australia, Aug. 30 - Sep. 2, 2004.

[57] W. P. Siriwongpairat, W. Su, M. Olfat, and K. J. R. Liu, "Multiband Space-Time-Frequency Coding for UWB Communication Systems", *IEEE Trans. on Signal Proc.*, to appear.

[58] W. P. Siriwongpairat, W. Su, M. Olfat, and K. J. R. Liu "Space-Time-Frequency Coded Multiband UWB Communication Systems," *IEEE Wireless Commun. and Networking Conf.*, vol. 1, pp. 426-431, Mar. 2005.

[59] J. N. Laneman and G. W. Wornell, "Distributed Space-Time Coded Protocols for Exploiting Cooperative Diversity in Wireless Networks," *IEEE Trans. Inform. Theory*, vol. 49, pp. 2415-2525, Oct. 2003.

[60] J. N. Laneman, D. N. C. Tse, and G. W. Wornell, "Cooperative Diversity in Wireless Networks: Efficient Protocols and Outage Behavior," *IEEE Trans. on Inform. Theory*, vol. 50, no. 12, pp. 3062-3080, Dec. 2004.

[61] A. Sendonaris, E. Erkip, and B. Aazhang, "User Cooperation Diversity, Part I: System Description," *IEEE Trans. on Commun.*, vol. 51, no. 11, pp. 1927-1938, Nov. 2003.

[62] A. Sendonaris, E. Erkip, and B. Aazhang, "User Cooperation Diversity, Part II: Implementation Aspects and Performance Analysis," *IEEE Trans. on Commun.*, vol. 51, no. 11, pp. 1939-1948, Nov. 2003.

[63] M. Janani, et. al, "Coded Cooperation in Wireless Communications: Space-Time Transmission and Iterative Decoding," *IEEE Trans. Signal Processing*, vol. 52, pp. 362-370, Feb. 2004.

[64] J. Boyer, D. D. Falconer, and H. Yanikomeroglu, "Multihop Diversity in Wireless Relaying Channels," *IEEE Trans. on Commun.*, vol. 52, no. 10, pp. 1820-1830, Oct. 2004.

[65] W. Su, A. K. Sadek, and K. J. R. Liu, "SER Performance Analysis and Optimum Power Allocation for Decode-and-Forward Cooperation Protocol in Wireless Networks," *IEEE Wireless Commun. and Networking Conf.*, vol. 2, pp. 984-989, Mar. 2005.

[66] A. K. Sadek, W. Su, and K. J. R. Liu, "Performance analysis for multi-node decode-and-forward relaying in cooperative wireless networks," *in Proc. IEEE Inter. Conf. on Acoustics, Speech, and Signal Proc.*, vol. 3, pp. 521-524, Mar. 2005.

[67] D. Cassioli, M. Z. Win, and A. F. Molisch, 'The Ultra-Wide Bandwidth Indoor Channel From Statistical Model to Simulations," *IEEE J. on Selected Areas in Commun.*, vol. 20, pp. 1247-1257, Aug. 2002.

[68] J. R. Foerster, et. al, "Channel Modeling Sub-committee Report Final," IEEE802.15-02/490, Nov. 18, 2003.

[69] J. R. Foerster and Q. Li, "UWB Channel Modeling Contribution from Intel," *Technical Report P802.15 02/279SG3a*, Intel Corporation, Hillboro, OR, Jun. 2002.

[70] S. S. Ghassemzadeh, et. al, "A Statistical Path Loss Model for In-Home UWB Channels," *IEEE Conf. on Ultra Wideband Systems and Tech.*, pp. 5964, 2002.

[71] M. Nakagami, "The m-Distribution: A General Formula of Intensity Distribution of Rapid Fading," *Statistical Methods in Radio Wave Propagation*, W. G. Hoffman, Ed. Oxford, England: Pergamon, 1960.

[72] H. Hashemi, "Impulse Response Modeling of Indoor Radio Propagation Channels," *IEEE J. on Selected Areas in Commun.*, vol. 11, no. 7, pp. 967-978, Sep. 1993.

[73] A. A. M. Saleh and R. A. Valenzuela, "A Statistical Model for Indoor Multipath Propagation," *IEEE J. on Selected Areas in Commun.*, vol. 5, no. 2, pp. 128-137, Feb. 1987.

[74] M. Pendergrass and W.C. Beeler, "Empirically based Statistical Ultra-Wideband (UWB) Channel Model," *Technical Report P802.15 02/240SG3a*, Time-Domain Corporation, Jun. 2002.

[75] F. Zhu, Z. Wu, and C. R. Nassar, "Generalized Fading Channel Model with Applications to UWB," *IEEE Conf.on Ultra Wideband Systems and Tech.*, pp 1317, 2002.

[76] R. A. Horn and C. R. Johnson, *Matrix Analysis*, Cambridge Univ. Press, New York, 1985.

[77] IEEE 802.15WPAN High Rate Task Group 3 (TG3). Internet: www.ieee802.org/15/pub/TG3.html.

[78] M. K. Simon and M.-S. Alouini, *Digital Communication over Fading Channels*, 2nd Ed., John Wiley and Sons, New Jersey, 2004.

[79] S. S. Ghassemzadeh, L. J. Greenstein, T. Sveinsson, and V. Tarokh, "A Multipath Intensity Profile Model for Residential Environments," *IEEE Wireless Commun. and Networking Conf.*, vol. 1, pp. 150-155, Mar. 2003.

[80] R. J. Cramer, R. A. Scholtz, and M. Z. Win, "Evaluation of an Ultra-Wide-Band Propagation Channel," *IEEE Trans. on Antennas and Propagation*, vol. 50, pp. 561-570, May 2002.

1985.

[81] M. K. Simon and M. S. Alouini, *Digital Communication over Fading Channels: A Unified Approach to Performance Analysis*, John Wiley and Sons, New York, 2000.

[82] A. M. Mathai and S. B. Provost, *Quadratic Forms in Random Variables: Theory and Applications*, Marcel Dekker Inc., New York, 1992.

[83] A. F. Molisch, J. R. Foerster, and M. Pendergrass, "Channel Models for Ultrawideband Personal Area Networks," *IEEE Wireless Commun.*, vol. 10, no. 6, pp. 14 - 21, Dec. 2003.

[84] W. P. Siriwongpairat, Z. Han, and K. J. R. Liu, "Energy-Efficient Channel Allocation for Multiuser Multiband UWB System," *IEEE Wireless Commun. and Networking Conf.*, New Orleans, LA, Mar. 2005.

[85] H. Kellerer, U. Pferschy, and D. Pisinger, *Knapsack problems*, Springer, New York, 2004.

[86] C. Y. Wong, R. S. Cheng, K. B. Letaief, and R. D. Murch, "Multiuser OFDM with Adaptive Subcarrier, Bit, and Power Allocation," *IEEE J. on Sel. Areas in Commun.*, vol.17, no.10, pp. 1747-1758, Oct. 1999.

[87] F. Kelly, "Charging and Rate Control for Elastic Traffic," *European Trans. on Telecommun.*, vol. 8, no.1, pp. 33 - 37, Jan. 1997.

[88] C. Cho, H. Zhang, and M. Nakagawa "A UWB Repeater with a Short Relaying-delay for Range Extension," *IEEE Wireless Commun. and Networking Conf.*, vol. 3, pp. 1436-1441, Mar. 2004.

[89] A. Bletsas and A. Lippman, "Efficient Collaborative (Viral) Communication in OFDM Based WLANs," *Inter. Symposium on Advanced Radio Technologies (ISART 2003)*, Boulder Colorado, March 4-7, 2003.

[90] S. Yatawatta and A. P. Petropulu, "A Multiuser OFDM System with User Cooperation," *38th Asilomar Asilomar Conf. on Signals, Systems, and Computers*, vol. 1, pp. 319-323, Nov. 2004.

[91] Z. Han, T. Himsoon, W. P. Siriwongpairat, and K. J. R. Liu, "Energy-Efficient Cooperative Transmission over Multiuser OFDM Networks: Who Helps Whom and How to Cooperate," *IEEE Wireless Commun. and Networking Conf.*, vol. 2, pp. 1030-1035, Mar. 2005.

[92] G. Sun, J. Chen, W. Guo, and K. J. R. Liu, "Signal Processing Techniques in Network-Aided Positioning: A Survey Of State-Of-The-Art Positioning Designs," submitted to *IEEE Signal Processing Magazine*, vol. 22, no. 4, pp. 12-23, Jul. 2005.